The role of co-stimulatory molecules CD40/CD40L during the immune response after acute myocardial infarction

Inaugural-Dissertation

zur Erlangung des Doktorgrades
der Mathematisch-Naturwissenschaftlichen Fakultät
der Heinrich-Heine-Universität Düsseldorf

vorgelegt von

Sven Witkowski
aus Duisburg

Düsseldorf, Dezember 2023

aus der Klinik für Kardiologie, Pneumologie und Angiologie
der Heinrich-Heine-Universität Düsseldorf
Klinikdirektor: Univ.-Prof. Dr. med. Malte Kelm

Gedruckt mit der Genehmigung der
Mathematisch-Naturwissenschaftlichen Fakultät der
Heinrich-Heine-Universität Düsseldorf

Berichterstatter:

1. Prof. Dr. rer. nat. Norbert Gerdes

2. Jun.-Prof. Dr. rer. nat. Mathias Beller

Tag der mündlichen Prüfung: 05.06.2024

Parts of this dissertation were already presented as poster on a scientific conference:

12.-15.04.2023 | 89. Annual Meeting of the German Cardiac Society (DGK):

Witkowski, S., Ampem, G., Lang, A., Du Plessis, A., Kaldirim, M., Fiegenbaum, P., Wernet, C., Pfeiler, S., Becher, S., Elster, C., Barcik; M., Benkhoff, M., Bönner, F., Polzin, A., Jung, C., Winkels, H., Lutgens, E., Kelm, M., Gerdes, N.

“Inhibition of CD40-TRAF6 signaling in the subacute phase following acute myocardial infarction improves left ventricular function and alters cardiac immune cell infiltration”

Abstract

Cardiovascular diseases (CVD) are the most common cause of death worldwide and the number of cases has increased steadily in recent years. Acute myocardial infarction (AMI) represents one of these CVDs and contributes to the majority of annual deaths. During the course of AMI, the blood flow in coronary arteries is blocked, usually due to atherosclerotic plaque formation and subsequent rupture, erosion and thrombus formation, leading to ischemia. Under these ischemic conditions, apoptotic and necrotic processes lead to myocardial cell damage and death, which in turn will deteriorate the heart function and negatively affect survival of the patient. Therefore, rapid reperfusion of the occluded arteries is indispensable to protect cardiac cells, prevent further damage and initiate healing mechanisms. Immune regulation is mediated by various factors including cytokines, cell-cell interactions, as well as pro- and anti-inflammatory signaling pathways. These regulatory processes play a crucial role to promote healing after AMI, as they control the remodeling of the left ventricle (LV). However, a decisive factor of activating the immune response is its duration, because prolonged inflammation can adversely alter cardiac remodeling, eventually leading to heart failure. One possible approach is the modulation of pro-inflammatory signaling pathways or more precisely their associated co-stimulatory molecules. In this context, the co-stimulatory molecules CD40 and its ligand CD40L are of particular interest, since they can be found on a variety of immune cells, where they are responsible to regulate pro- and anti-inflammatory processes, as well as differentiation, proliferation and survival of immune cells. Therefore, the better understanding of CD40/CD40L signaling is a prerequisite to explore this promising target for future medical therapies of AMI. Accordingly, this thesis focuses on the interaction of CD40 and CD40L and the effects of modulating CD40 signaling on the cardiac outcome, as well as the immune cell composition after experimental AMI in a mouse model. To cover the widest practicable spectrum, the modulation of CD40 signaling was performed in three different ways: inhibition, activation and cell type-specific genetic depletion. While activation of CD40 signaling via an agonistic CD40 antibody resulted in an impaired cardiac function coinciding with larger infarct sizes, blocking of CD40 signaling using a small molecule inhibitor called TRAF-STOP revealed a beneficial impact by reducing scar size and improving LV heart function in a time-dependent manner. Additionally, the T cell-specific genetic depletion of CD40L also showed great potential by achieving similar effects in the acute phase comparable to the blocking of CD40 signaling. Thus, these findings collectively provide a first step for a better understanding of the regulatory processes and mechanisms driven by CD40 and CD40L during the injury and healing phases after AMI. Moreover, the results highlight CD40 signaling as a potential target for a future pharmacological treatment to improve cardiac outcome after AMI and overcome the morbidity and mortality associated with this disease.

Zusammenfassung

Herz-Kreislauf-Erkrankungen stellen weltweit die häufigste Todesursache dar und die Zahl der Fälle ist in den letzten Jahren stetig gestiegen. Innerhalb der Herz-Kreislauf-Erkrankungen ist der akute Myokardinfarkt für die Mehrzahl der jährlichen Todesfälle verantwortlich. Während des Myokardinfarkts wird der Blutfluss in den Koronararterien blockiert, was vorwiegend auf die Bildung atherosklerotischer Plaques, deren Ruptur und Erosion sowie der anschließenden Thrombusbildung zurückzuführen ist, welche letztendlich eine Ischämie verursacht. Unter diesen ischämischen Bedingungen kommt es durch apoptotische und nekrotische Prozesse zur Schädigung sowie zum Absterben von Herzmuskelzellen, wodurch sich die Herzfunktion verschlechtert und das Überleben der Patienten negativ beeinflusst wird. Daher ist eine schnelle Reperfusion der verschlossenen Arterien unerlässlich, um die Herzzellen zu schützen, weitere Schäden zu verhindern und Heilungsmechanismen zu aktivieren. Die dafür notwendige Immunregulation wird durch verschiedene Faktoren wie Zytokine, Zell-Zell-Interaktionen sowie pro- und antiinflammatorische Signalwege vermittelt. Des Weiteren sind diese immunregulatorischen Prozesse entscheidend für den Verlauf der Heilung nach dem akuten Myokardinfarkt, da sie den Umbau des linken Ventrikels koordinieren. Ein wesentlicher Faktor für die Aktivierung der Immunreaktion ist jedoch ihre Dauer, denn eine anhaltende Entzündung kann die kardiale Remodellierung nachteilig beeinflussen und sogar langfristig zu Herzversagen führen. Ein möglicher Lösungsansatz ist die Modulation proinflammatorischer Signalwege oder vielmehr der damit assoziierten kostimulatorischen Moleküle. Von besonderem Interesse sind dabei die kostimulatorischen Moleküle CD40 und der entsprechende Ligand CD40L, da sie auf einer Vielzahl von Immunzellen zu finden sind, wo sie entzündungsfördernde und entzündungshemmende Prozesse sowie die Differenzierung, Proliferation und das Überleben von Immunzellen regulieren. Folglich ist ein besseres Verständnis des CD40/CD40L-Signalweges eine grundlegende Voraussetzung, um das vielversprechende Ziel von zukünftigen medizinischen Therapien nach einem akuten Myokardinfarkt zu erreichen. Dementsprechend konzentriert sich diese Dissertation auf die Interaktion von CD40 und CD40L und die Auswirkungen verschiedener Modulationen des CD40-Signalweges auf die Herzfunktion sowie die Zusammensetzung der Immunzellen nach einem experimentell induzierten Myokardinfarkt im Mausmodell. Um ein möglichst breites Spektrum abzudecken, wurde die Modulation des CD40-Signalweges auf drei verschiedene Arten durchgeführt: Inhibierung, Aktivierung und zelltypspezifische genetische Depletion. Während die Aktivierung des CD40-Signalweges durch einen agonistischen CD40-Antikörper zu einer Beeinträchtigung der Herzfunktion führte, die mit einem größeren Infarkt einherging, zeigte die Inhibierung des CD40-Signalweges mittels des Moleküls TRAF-STOP eine positive, vom Behandlungszeitpunkt abhängige Wirkung, bei der es zu einer Verringerung der Narbengröße und einer Verbesserung der Herzfunktion kam. Darüber hinaus wies die T-Zell-

spezifische genetische Depletion von CD40L ebenfalls großes Potenzial auf, da sie in der akuten Phase ähnliche Wirkungen erzielte wie das Blockieren des CD40-Signalweges. Diese Ergebnisse sind ein erster wichtiger Schritt für ein besseres Verständnis der regulatorischen Prozesse und Mechanismen, die von CD40 und CD40L während der Entzündungs- und Heilungsphase nach einem akuten Myokardinfarkt gesteuert werden. Außerdem verdeutlichen die Resultate, dass der CD40-Signalweg ein vielversprechendes Ziel für eine künftige pharmakologische Behandlung ist, um das Therapieergebnis nach einem Herzinfarkt zu verbessern und die mit dieser Krankheit verbundene Morbidität und Mortalität zu verringern.

Table of contents

Table of figures

Abbreviations

±dP/dt	First negative/positive derivate of left ventricular-derived pressure
αCD40	Agonistic anti-CD40 antibody with clone FGK45
γδT	Gamma delta T cells
AAR	Area at risk
Akt	Thymoma viral proto-oncogene 1
AMI	Acute myocardial infarction
APC	Allophycocyanin
APCs	Antigen presenting cells
APC-Cy7	Allophycocyanin cyanine 7
Apoe	Apolipoprotein E-deficient
BPM	Beats per minute
BW	Body weight
CD	Cluster of differentiation
CVD	Cardiovascular disease
CO	Cardiac output
DAMPs	Danger-associated molecular patterns
DCs	Dendritic cells
DMSO	Dimethyl sulfoxide
ECG	Electrocardiogram
EDTA	Ethylenediaminetetraacetic acid
EDV	End-diastolic volume
EF	Ejection fraction
ESV	End-systolic volume
FITC	Fluorescein isothiocyanate
FoxP3	Forkhead box P3
FSC	Forward scatter
HR	Heart rate
HW	Heart weight
IR	Ischemia reperfusion
IFN	Interferon
IgG2a	Immunoglobulin G 2a

IL	Interleukin
INF	Infarct area
Jak3	Janus family kinase 3
JNK	Jun N-terminal protein kinase
KHB	Krebs-Henseleit buffer
LAD	Left anterior descending coronary artery
LD	Langendorff
LV	Left ventricular
LVDP	Left ventricular derived pressure
Ly6C	Lymphocyte antigen 6 family member C
$Ly6C^{int}$	$Ly6C^{intermediate}$
MAPKs	Mitogen-activated protein kinases
MFI	Mean fluorescence intensity
mRNA	Messenger RNA
NFκB	Nuclear factor kappa B
NGS	Next generation sequencing
PBS	Phosphate-buffered saline
PC	Principal components
PE	Phycoerythrin
PerCP-Cy5	Peridinin chlorophyll-Cyanine 5
PI3K	Phosphoinositide 3-kinase
PLCγ	Phospholipase Cγ
PRRs	Pattern recognition receptors
qPCR	Quantitative polymerase chain reaction
ROS	Reactive oxygen species
RT	Room temperature
sCD40L	soluble CD40 ligand
scRNASeq	Single cell RNA Sequencing
SEM	Standard error of the mean
SSC	Side scatter
STAT5	Signal transducer and activator of transcription 5
SV	Stroke volume

SW	Spleen weight
TGFβ	Transforming growth factor beta
Th	T helper cell
TLRs	Toll-like receptors
TNFα	Tumor necrosis factor alpha
TRAF	Tumor necrosis factor receptor-associated factor
T_{reg}	regulatory T cell
TTC	2,3,5-Triphenyltetrazolium chloride
UMAP	Uniform Manifold Approximation and Projection
WGA	Wheat germ agglutinin

1 Introduction

1.1 Cardiovascular diseases

Cardiovascular disease (CVD) is defined as a group of acute and chronic disorders affecting the heart and blood vessels, including diseases like acute coronary syndrome, atherosclerosis, hypertension, cardiomyopathy, and acute myocardial infarction (AMI).[1] Despite significant advancements in diagnosis and therapy, CVD repeatedly take the global lead as most common cause of mortality among non-communicable diseases.[2, 3] According to the World Health Organization, an estimated 17.9 million people died from CVD in 2019, accounting for approximately 32 % of all deaths worldwide with heart attacks and strokes responsible for 85 % of these deaths.[1] The prevalence of CVD-related deaths is still increasing and predicted to reach about 24 million by 2030, making advances regarding prevention and treatment of CVD essential to counteract this development.[2, 3]

For a functional prevention, it is crucial to know which factors can predict the risk of establishing CVD. However, the pathophysiology of CVD involves a complex interaction of environmental influences, genetic predisposition and lifestyle factors.[4-6] Age, sex, race, obesity, hypertension, diabetes mellitus, smoking, physical activity, psychosocial stress and unhealthy nutrition are all recognized, partly interrelated risk factors for CVD that are important for risk assessment.[7] These risk factors can be classified into adjustable conditions, which can be changed via behavior, like smoking, diet and physical activity, whereas the non-adjustable determinants including sex and age are non-modifiable.[5] Hence, mostly changes regarding the adjustable risk factors, which nearly stayed the same over the past 30 years, provide a perspective to reduce the occurrence of CVD (**Fig. 1**).[4] For that reason, guidelines based on a variety of studies concerning these risk factors were compiled to identify and support amendments in human behavior.[8, 9] Overall, early adaptation of modifiable risk factors, beginning from childhood, is the preferred way to prevent or minimize CVD in adult age.[10]

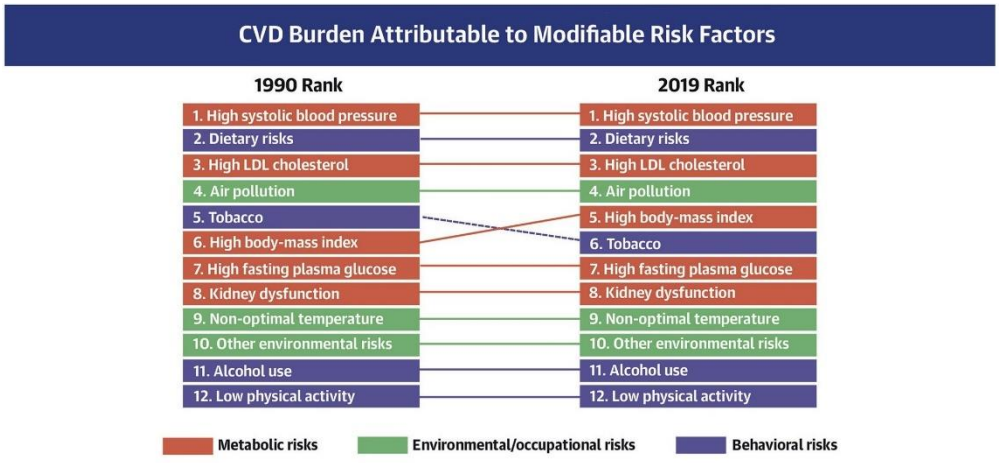

Figure 1: CVD burden attributable to modifiable risk factors. Comparison of the rankings of CVD DALYs attributable to modifiable risk factors in 1990 and 2019. CVD = cardiovascular disease; DALYs = disability-adjusted life years; LDL = low-density lipoprotein. Adjusted after Roth et al.[4]

Up to 90 % of CVD, such as heart attacks and stroke, could be avoided in the future with the help of adjustments to variable risk factors in combination with monitoring and medical treatment of developing CVD symptoms.[11, 12] However, receiving medical care early on is typically not possible or at least challenging because the symptoms throughout the often long-term development of CVD cover a wide spectrum and typically go unreported until ultimately leading to an acute event, such as a heart attack.[12] Therefore, monitoring via regular checkups and screenings are crucial for early detection and appropriate treatments. The most typical signs and warning signals of an AMI, including chest discomfort, pain in the left arm or shoulder, shortness of breath, fatigue, nausea, and cold sweats, can individually differ in occurrence and severeness depending on the sex.[13, 14] Nevertheless, these symptoms are only a first indication of an AMI and since time is crucial for the outcome, further fast and reliable diagnosis is essential to ensure the occurrence of AMI beyond any doubt, enabling immediate therapy through appropriate treatments.[15]

Diagnosis of AMI is based on a number of characteristics, either appearing separately or in combination[16]. One common criterion for diagnosis is the rise or fall of certain biomarkers associated with the heart, whereby cardiac troponins take a crucial role, as they feature a high sensitivity and specificity.[12, 17] Assays for troponin T and I molecules are highly specific, as their amino acid sequences are only found in cardiac tissue. In combination with an increasing sensitivity over the last years, this makes troponin assays the preferred biomarker tool to detect cardiac damage.[18] However, the elevation of cardiac troponins alone is not sufficient and needs to emerge with at least one of the following criteria: symptoms of ischemia, changes on electrocardiogram regarding ST-segment or Q waves, loss of viable myocardium or wall motion abnormalities evidenced via imaging or the discovery of an intracoronary thrombus by angiography.[19] Following confirmed diagnosis of AMI a rapid and suitable therapy is required to reduce morbidity and mortality. Therapy approaches encompass reperfusion strategies, via percutaneous coronary intervention or thrombolytic therapy, as well as pharmacological treatments.[20, 21] While these treatments focus on the ischemic phase of AMI, the handling after reperfusion during the healing phase remains mostly incomplete. Thereby, medications or other treatments could potentially rescue injured tissue and restore myocardial function, leading to beneficial cardiac outcome and reducing the possibility of chronic heart failure.[22]

Since CVD cannot entirely be prevented and as in an increasingly aging society, more people are projected to die from these diseases in the coming years, it is even more important to think about how treatment for CVD might be improved. Considering AMI as one of the major precipitations of CVD, this thesis will address immune-associated treatment strategies and their effects on cardiac outcome post AMI.

1.2 Acute myocardial infarction

AMI is pathologically defined as necrosis of myocardial cells due to a sustained ischemic condition caused by the blockage or severe narrowing of coronary vessels.[21] While at the same time clinical characterization is based on the detection of alterations in cardiac biomarker levels, preferably measurements of troponins, combined with evidences of acute myocardial ischemia.[19, 23] Ischemia in the myocardium is indicated by shortage of oxygen for cardiac cells due to occlusion of coronary vessels. As a result of this critical loss of oxygen and nutrients supply via blood flow, myocardial cells first start to take damage and finally die when the blockage persists for longer.[21, 24] Numerous factors may contribute to blood vessel obstruction or narrowing. In most cases, atherosclerotic changes at the vessel walls with associated plaques formation are responsible, while spasms and allergic reactions are rather rare reasons (**Fig. 2**).[24, 25] While narrowing of coronary blood vessels is a long-term phenomenon, caused by accumulation of lipid deposits, inflammation and vascular injury, the rupture or erosion of atherosclerotic plaques is an acute event resulting in a thrombus formation, being the most frequent cause of obstruction and AMI.[26, 27]

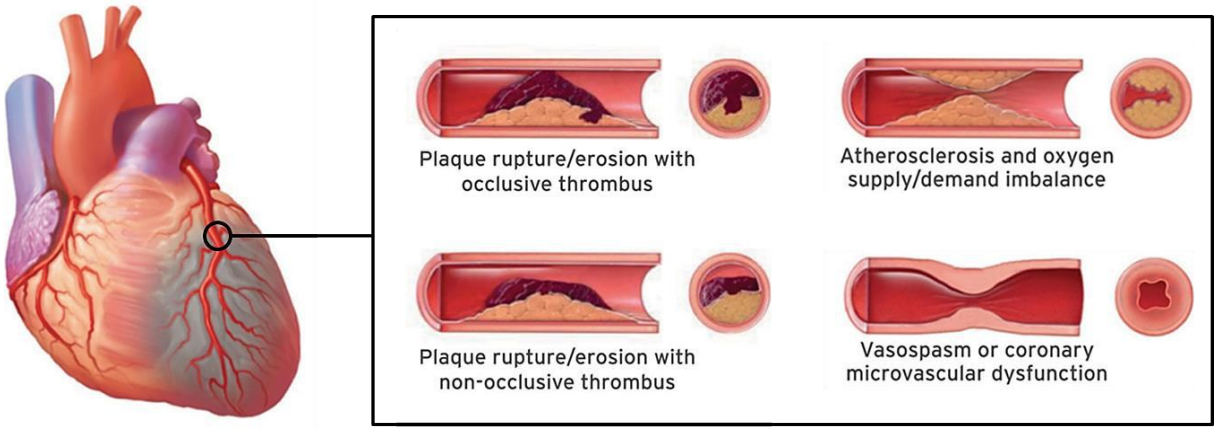

Figure 2: Types of myocardial infarction based on the physiological causes that lead to narrowing or occlusion of coronary artery resulting in myocardial ischemia, modified from Thygesen et al.[23]

As myocardial cell death occurs relatively fast after thrombosis, prolonged occlusion contributes to more necrosis correlating with increased infarct sizes and a severe outcome following AMI.[28] Therefore, the quicker the blockage is resolved via thrombolysis or catheter-based therapy the better the outcome and survival prospects for patients.[29, 30] As time is the most critical factor, reperfusion should be accomplished before reaching six hours after diagnosis of AMI and is usually achieved in highly-developed countries.[31] However, coronary angioplasty and thrombolysis are exclusive methods for early and direct treatment to allow reperfusion of blood into affected infarct area, there are still several complications that can occur after reperfusion therapy of AMI.[32, 33] Interestingly the reperfusion process itself can paradoxically induce death of cardiomyocytes, which is known under the term ‘myocardial

reperfusion injury' or 'ischemia reperfusion (IR) injury'.[34] Thereby, IR injury is either induced over mechanical mechanisms such as hemorrhage and interstitial pressure or the contribution of different signaling pathways like oxidative stress or inflammation that lead to apoptosis and necrosis of myocardial tissue.[31, 35] Granting the fact that reperfusion therapy is necessary to limit damage to the heart after AMI, understanding the processes that promote IR injury is a promising therapeutical target to reduce the degeneration of cardiomyocytes and heart function even more.[36, 37]

Depending on the duration of myocardial ischemia, necrosis of cardiomyocytes aggravates pathological damage to the heart, thereby deteriorating its function and potentially resulting in chronic heart failure and finally death.[38] Scar formation and unfavorable remodeling of the left ventricle (LV), that is characterized by complicated short- and long-term alterations in LV size, shape, function, as well as in cellular and molecular composition, are major factors in the development of chronic heart failure following AMI.[38] Major drivers of LV remodeling are infiltrating immune cells, contributing to acute inflammation and healing of affected myocardium.[39] Hence, prevention of adverse LV remodeling leading to scar size reduction, restored heart function and improved clinical outcome post AMI, could be achieved by vaster investigation of the procedures during the immune response following AMI. Novel therapeutical strategies aiming at the alteration of immune cell composition and function, are a potential instrument to overcome the burden of high AMI-associated mortality.

1.3 Function of the immune response and inflammatory processes after AMI

Regenerative processes differ in mammals depending on their age, exemplified by the decaying regenerative capacity of cardiomyocytes over time, exacerbating repair mechanisms in adult mammals.[40] Given the limited proliferative ability of cardiomyocytes, the profound loss of these cells due to necrosis in AMI cannot be entirely intercepted by regeneration of cardiac cells.[41] Instead LV remodelling and fibrotic scar formation take place causing functional impairment ultimately promoting heart failure and death.[42] Pro- and anti-inflammatory pathways of the immune response drive these processes after AMI, making further insight into underlying mechanisms essential for improved resolving and healing of affected cardiac area, ultimately improving the outcome post AMI.[43]

The death of cardiac cells due to ischemic conditions or IR injury after AMI initiates a reparative process that can be divided into three overlapping phases: the inflammatory phase, the proliferative phase, and the maturation phase.[44, 45] All phases are characterized by infiltration of explicit immune cells as well as tissue remodelling processes (**Fig. 3**). The inflammatory reaction, covers an acute pro-inflammatory phase followed by an anti-inflammatory response.[39] While the pro-inflammatory reaction is responsible for recruitment of immune cells

into the infarct and remote area for clearing damaged and dead cells, the anti-inflammatory reaction commences the reparative phase including tissue healing and fibrotic scar formation.[46] The pro-inflammatory response is initiated via signals of the dying myocardial cells and activated fibroblasts triggering several systems and pathways.[39] These processes include generation of reactive oxygen species (ROS)[47], release of danger-associated molecular patterns (DAMPs)[48], signaling via pattern recognition receptors (PRRs) like Toll-like receptors (TLRs)[49] or the receptor for advanced glycosylation end products (RAGE)[50], and activation of the complement system.[51] Finally, the interconnection of all these mechanisms leads to release of pro-inflammatory cytokines like interleukin (IL)-1β, IL-6, tumor necrosis factor (TNF)-α and chemokines, that activate resident leukocytes and attract distinct immune cells into the myocardium.[39, 45]

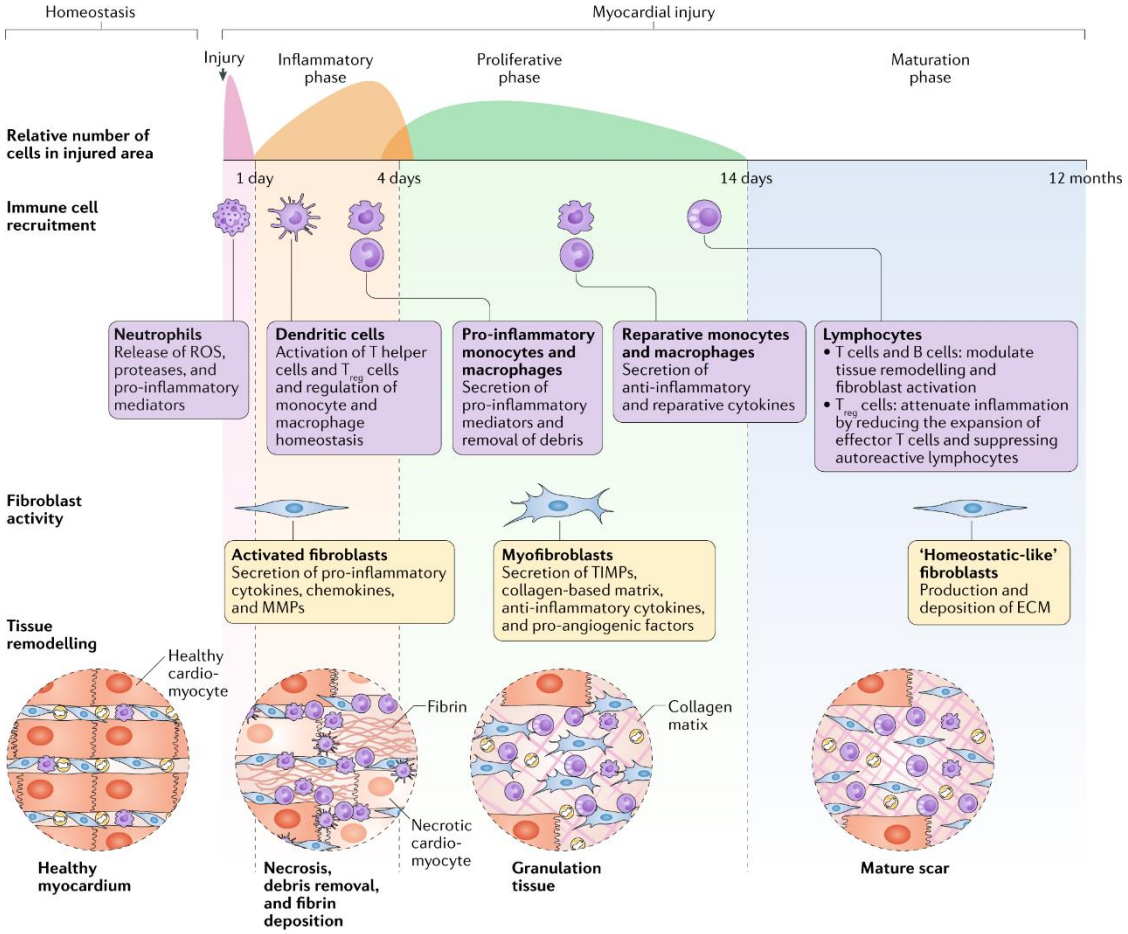

Figure 3: Immune cell and fibroblast functions during the three phases of cardiac repair after myocardial injury. AMI leads to damage and death of cardiomyocytes that initiates cardiac repair mechanisms, which can be divided into three phases: inflammatory, proliferative, and healing or maturation. Each phase is characterized by time dependent infiltration and recruitment of specific immune cells, driving the main processes of cell debris clearance, fibrin deposition, tissue remodeling and scar formation. Adapted from Forte et al.[45]

Neutrophils are the first cells that infiltrate the myocardium, reaching their peak at 1-3 days and decline by 5-7 days.[52] Besides the release of ROS and matrix-degrading enzymes they

start to attract additional cells of the innate immune response, including circulating monocytes and dendritic cells (DCs), to the infarcted area via chemokine gradients.[53] The interaction of these cells is important for the clearance of dead cardiomyocytes and other cellular debris. Neutrophils phagocytose the cellular debris and undergo apoptosis, which in turn produces signals to attract pro-inflammatory monocytes and that can give rise to macrophages to enforce removal.[54] Even though, macrophages are capable to phagocytose dead cardiomyocytes and cell debris directly, neutrophils are essential for their recruitment and only the interplay between both cell populations results in accurate clearance.[53] DCs infiltrate the infarct and remote area during the inflammatory phase and function as regulators of monocyte and macrophage homeostasis keeping a balance between pro- and anti-inflammatory monocytes and macrophages.[55] The healing process following AMI requires an accurate balance of monocytes and macrophages, making DCs of protective value. Additionally, DCs function as activators of the adaptive immunity via their role as antigen presenting cells (APCs).[56] When the antigens have been processed by the DCs, they migrate into the draining lymph nodes, where naïve T cells recognize the presented antigens.[57] Thus, DCs initiate the antigen-specific immunity via activation of T helper (Th) cells and regulatory T (T_{reg}) cells that are needed during the proliferative phase.[45, 58]

The end of the inflammatory phase and beginning of the proliferative phase typically occur at day 4-7 after reperfusion and are overlapping, because the aforementioned cell types not only induce their specific mechanisms, but at the same time initiate the adaptive immune response, which is certain for resolution of inflammation and contributes to regeneration.[59] For example the resolving macrophages release anti-inflammatory and pro-fibrotic cytokines, like IL-10 and transforming growth factor (TGF)β to overcome pro-inflammatory response and set off the reparative development.[60] Thereby TGFβ is a key factor for the differentiation of activated fibroblasts into myofibroblasts that are the main modulators of the scar via collagen accumulation and synthesis of extracellular matrix proteins inside the infarct area.[61] Moreover, myofibroblasts contribute to angiogenesis via secretion of the vascular endothelial growth factor (VEGF)-A, facilitating novel routes for the supply of oxygen and nutrients.[62] Instead of pro-inflammatory monocytes and macrophages the proliferative phase is characterized by an abundant increase of anti-inflammatory monocytes and macrophages, reaching its peak around day 7 after AMI.[63] This shift is mostly caused by infiltration of circulating anti-inflammatory monocytes into the myocardium, where they differentiate into macrophages.[64] These monocytes and macrophages express anti-inflammatory and reparative cytokines, as well as profibrotic and angiogenic factors (IL-10, TGF-β, VEGF).[46] DCs contribute to the reparative phase by downregulating pro-inflammatory cytokines, preventing accumulation of pro-inflammatory monocytes, stimulating scar formation and finally initiating the adaptive immune response.[65] T cells and B cells are part of the adaptive immune response and

therefore recruited to the heart during the proliferative phase, where they modulate wound healing and tissue LV remodelling.[66] Both populations peak around day 7 inside the myocardium.[67] B cell infiltration is attributable to circulating mature B cells[68], while T cells, including cluster of differentiation (CD)4^+ helper and $CD8^+$ cytotoxic T cells, predominantly emerge from heart-draining lymph nodes.[66] The subsets of $CD4^+$ T cells persist mostly of Th1 and T_{reg} cells, whilst Th2 and Th17 cells only make up a minor proportion.[67] The function of T cells in cardiac repair is complex, because depletion of T cell subtypes reveals contrary results in tissue remodelling making investigation of T cell dynamics in the proliferative phase even more important.[69] Thus, understanding the role of T_{reg} cells is a promising approach, as this cell type can terminate pro-inflammatory signaling by shifting it towards an anti-inflammatory response and regulating effector activities of other T cells and also B cells.[70]

Once all these processes contributing to the proliferative or healing phase are completed, the majority of all infiltrated immune cells and myofibroblasts are deactivated and emigrate or undergo apoptosis, marking the begin of the maturation phase. At this point, the extracellular matrix is cross-linked via collagen fibers forming the scar area of the infarct.[71] Even though scar formation inside the myocardium leads to stiffness that compromises heart function, potentially causing arrhythmias or contraction deficits, it is required to maintain the structure and overall function of the heart.[72] Scar maturation can take several days or even weeks. During the maturation phase, late post infarction remodelling of the remote area of the heart takes place, which is again reflected by inflammation and fibrosis resulting in prolonged inflammatory activity that can impair contractility and LV remodelling.[46]

Understanding the underlying connections and pathways of the different processes that are involved in cardiac repair after AMI is a promising strategy to develop appropriate therapy and to improve cardiac outcome, function and survival of patients. Considering the complex mechanisms of all three phases, a variety of topics for further investigation appears promising indeed. However, the role of immune cells and their manifold influence over the entire process of cardiac repair surely resembles one of the predominant targets. Hence, this thesis focuses on investigation of immune cell function, mechanisms and signaling pathways across the different phases of cardiac repair post AMI.

1.4 Co-stimulatory molecules CD40 and CD40L in the immune response

The interaction of immune cells during immune responses leading to pro- and anti-inflammatory processes is a key regulator of the outcome after AMI, since alterations in immune cell composition can shift the balance between these two polarizations.[46] Several signals and molecules including proteins, cytokines, chemokines, hormones and cell-cell interactions drive the communication and binding of immune cells to trigger activation and

effector function.[73] An example for this is the activation of T cells via APCs like DCs, macrophages or B cells during the adaptive immune response, as it requires the combination of three signals: antigen-specific interactions, co-stimulatory molecules, and instructive cytokines (**Fig. 4**).[74, 75] The primary signal is the presentation of an antigen, generally via the major histocompatibility complex (MHC) class II to the T cell receptor (TCR).[76] To support the antigen presentation a second signal induced by co-stimulatory molecules is necessary, since the absence of this signal results in T cell anergy and ineffective response onto the particular antigen.[77] Ultimately, a third signal is needed for functional T cell activation, which is provided by cytokine expression and recognition.[75] Depending on the secreted cytokines T cells undergo polarization into their various subpopulations.[78] As a consequence, the immune response and healing after AMI could be driven into favorable directions, e.g. by modifying the signal of co-stimulatory molecules.

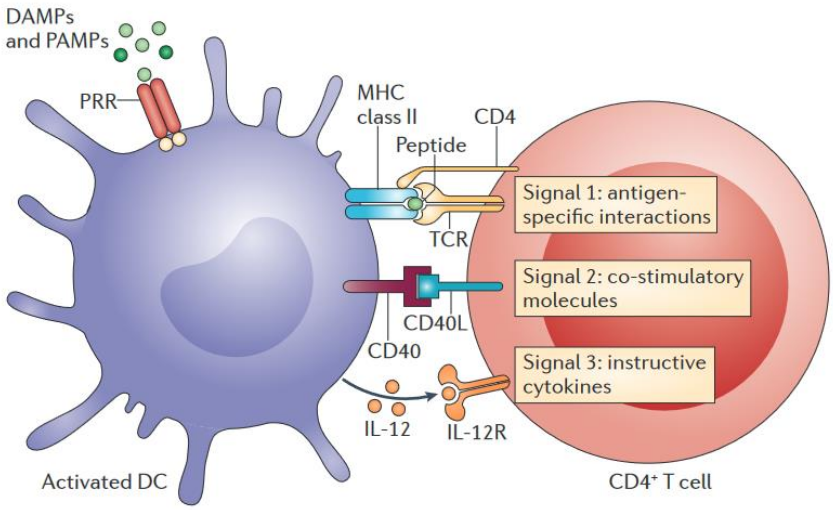

Figure 4: Overview of T cell activation via antigen presentation and three-signal model. Dendritic cells (DC) are activated via danger-associated molecular patterns (DAMPs) and pathogen associated molecular patterns (PAMPs) that bind to pattern recognition receptors (PRRs). For sufficient T cell activation, the combination of three signals is essential. Main signal is the antigen presentation via the major histocompatibility complex (MHC)-II to the T cell receptor (TCR). This initial activation is supported by a secondary signal via co-stimulatory molecules, here CD40 and CD40L, and a third signal administrated by cytokine production and recognition, e.g. interleukin (IL)-12 and IL-12 receptor. Adapted from Kambayashi and Laufer.[75]

One prominent pair of co-stimulatory molecules is CD40 and its ligand CD40L, that belong to the TNF (receptor) (TNF(R)) super family.[79] CD40 resembles the receptor and is a type I transmembrane protein, forming a trimer for optimal signaling.[80] B cells were the first immune cells on which CD40 expression was discovered.[81] Furthermore, numerous other immune cells including monocytes, macrophages, DCs and neutrophils are known to express CD40.[82, 83] However, not only cells of the immune system feature expression of CD40, since it is also found on non-hematopoietic cells like fibroblasts, smooth muscle cells, endothelial, and epithelial cells.[81, 82, 84] The ligand of CD40 is a type II transmembrane protein, known as

CD40L or CD154 and also a member of the TNF family.[79] Similar to its receptor, CD40L occurs as trimer on the cell surface.[85] Nevertheless, CD40L can maintain a second form, were the membrane bound CD40L is shed due to proteolytic cleavage or alternative splicing and released into the plasma as soluble CD40L (sCD40L).[86] While first discovery of CD40L mostly linked its expression to activated T cells during B cell activation, the cellular pattern of CD40L expression gradually increased throughout the years, which includes platelets, activated B cells, natural killer cells, mast cells, endothelial, and epithelial cells.[87, 88] Besides the previously described activation of T cells via antigen presentation and cell-mediated innate immune response, CD40 and CD40L play a role in the humoral immune response of adaptive immunity. Thereby CD40 and CD40L support the activation of B cells that is triggered by binding of activated Th cells.[84] Signaling of the CD40/CD40L dyad initiates proliferation, differentiation, antibody isotype switching, maturation, germinal center formation, survival and immunoglobulin production of B cells.[84, 89, 90]

After binding of CD40L to CD40, activation of CD40 induces the recruitment of up to five different adaptor proteins termed TNF receptor-associated factors (TRAFs) towards its cytoplasmic domain, since CD40 itself has no direct kinase activity.[79, 91] These TRAFs, including TRAF1, -2, -3, -5, and -6, are essential for further signal transduction and can be divided into two groups depending on their binding site. While TRAF1, -2, -3, and -5 are located at the distal part at which TRAF1 and -2 form a heterotrimer, TRAF6 binds to a proximal section of the cytosolic CD40.[92, 93] Upon TRAF recruitment, several downstream signaling pathways are activated including the canonical and non-canonical nuclear factor κB (NFκB), the phosphoinositide 3-kinase (PI3K), the mitogen-activated protein kinases (MAPKs), Jun N-terminal protein kinase (JNK), and the phospholipase Cγ (PLCγ) pathway (**Fig. 5**).[94]

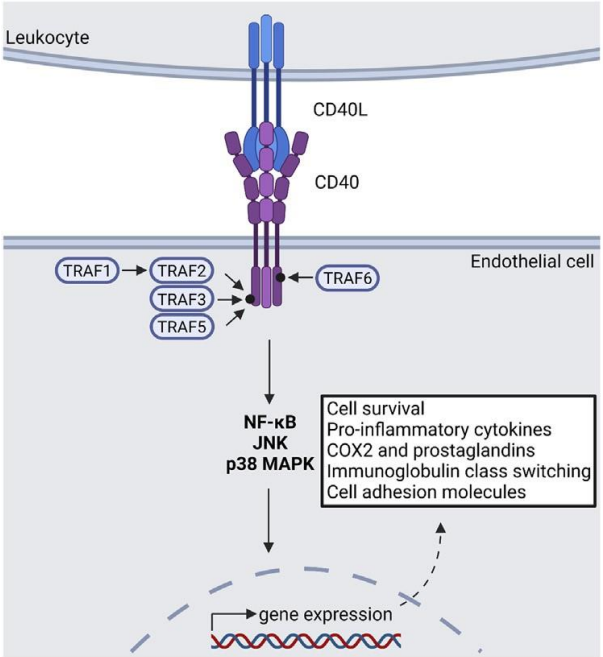

Figure 5: CD40/CD40L signaling pathway. Binding of CD40 and CD40L results in recruitment of different TNF receptor-associated factors (TRAFs) towards the cytoplasmic part of CD40. Each TRAF has its specific role during the downstream signaling and specifically activates a subset out of a variety of signaling pathways, like nuclear factor κB (NFκB), Jun N-terminal protein kinase (JNK) or p38/mitogen-activated protein kinases (MAPKs). These pathways further transduce the signal and lead to distinct gene expression, finally resulting in mechanisms that control cell survival, inflammation and immune response. COX2 = Cyclooxygenase 2. Modified from Strohm et al.[93]

These pathways are all linked to particular kinds of TRAF binding to CD40, whereby several pathways are not only activated by one TRAF alone. In fact, TRAF2 is a mediator of JNK, p38/MAPK and thymoma viral proto-oncogene 1 (Akt) pathways, while TRAF3 and TRAF5 in combination control the canonical and non-canonical NFκB pathway.[84] Moreover, TRAF1 and TRAF3 are capable to function as negative regulators of signaling, by interaction with other TRAFs and inhibiting their activation.[95, 96] Given the characteristic of its own binding site, TRAF6 signaling is relatively unique. It mostly drives NFκB, JNK, and p38/MAPK pathway activation.[97] Interestingly, TRAF6 interacts with TRAF2 making downstream signaling possible even when its original binding site is blocked.[98] Besides all these pathways relying on TRAF binding, there is one independent pathway that can be activated via direct binding of the Janus family kinase 3 (Jak3), which induces phosphorylation of signal transducer and activator of transcription 5 (STAT5).[99] CD40/CD40L signaling via all of these TRAFs and induced pathways contributes to gene expression that is dependent on involved cell types and triggers multiple mechanisms including cell survival, cytokine production, and immune and inflammatory responses.[93]

1.5 CD40/CD40L function and therapeutical potential in CVD

Excessive and prolonged immune cell infiltration is linked with long lasting and exaggerated pro-inflammatory activities that promote adverse cardiac remodelling.[46, 100] The broad variety of hematopoietic and non-hematopoietic cells expressing the co-stimulatory molecules CD40 and CD40L and their contribution to inflammation and healing makes this signaling dyad a promising target for therapeutical treatment towards a beneficial outcome in CVD.[101] Therefore, a range of potential interventions, either attenuating pro-inflammatory or advancing anti-inflammatory processes, by activation or inhibition of the CD40/CD40L dyad, regarding its cell type-specific function, are possible in context of CVD.

Platelet activation during inflammatory responses is considered the predominant source for release of sCD40L.[102] High levels of sCD40L in the plasma are associated with some forms of CVD like acute coronary syndromes[103], hypertension[104] or chronic heart failure[105] and function as biomarkers for inflammation.[106] Even risk factors or comorbidities (e.g., diabetes) can account for high levels of sCD40L[107]. Furthermore, elevated sCD40L in serum of patients after AMI alludes a higher incidence of all-cause and cardiovascular mortality, as well as increased risk of recurrent cardiovascular events.[108] Accordingly, high levels of sCD40L are of predictive character for future cardiovascular events, especially in women.[109] In atherosclerosis, one of the major causes of AMI, sCD40L and membrane-bound CD40L of activated platelets are responsible for initial formation of atherosclerotic plaques by stimulating endothelial cells promoting adhesion of leukocytes to the vessel wall.[110] In addition, platelet

CD40 signaling contributes to leukocyte recruitment and activation of endothelial cells advancing plaque formation.[111] However, high levels of CD40 and CD40L expression were also found in the late phase of atherosclerosis, precisely in rupture-prone and ruptured lesions, displaying a substantial function of the CD40/CD40L dyad during atherosclerotic plaque formation, rupture and thrombosis.[112, 113] Targeting CD40/CD40L interaction in atherosclerosis by genetic deficiency or inhibition via antibody led to smaller and more stable atherosclerotic plaque phenotype, by increasing the collagen amount, reducing lipid content and limit adhesion of immune cells.[114, 115] Even a late antibody-based inhibition of CD40 in established plaque formation was able to stabilize plaques and prevent rupture.[116] Therefore, inhibition of CD40L seemed to have great potential to overcome the burden of atherosclerosis and associated CVD, with the exception, that clinical studies of unrestricted CD40L inhibition revealed a high risk of thrombosis, causing severe thrombo-embolic events.[117, 118] Hence, a more directed approach of interrupting CD40/CD40L signaling in atherosclerosis appears necessary[119]. One experimental approach to test the cell type-specific contribution of CD40 on DCs and CD40L on T cells was performed by using the Cre/loxP system. In an atherosclerotic model, both cell type-specific deficient mice showed a reduction of lesion size and inflammation alongside with a more stable plaque phenotype.[120] Interestingly, CD40L deficiency on platelets was associated with limiting atherothrombosis and revealed the platelet-specific expression of CD40L as a mediator of pro-inflammatory and thrombotic processes in atherosclerosis.[120, 121] Another study examined the role of CD40 deficient macrophages, uncovering reduced atherosclerosis and less inflammation, due to an impaired transition of macrophages towards a pro-inflammatory state. These genetic modifications unveiled the role of different immune cells during atherosclerosis and an important role of CD40-TRAF6 signaling regarding the anti-inflammatory immune response.[122] Lutgens et al. investigated the function of the different TRAF molecules in terms of CD40 signaling in atherosclerosis via deficient mice for TRAF2, -3, -5, and -6, revealing that only the deficiency of CD40-TRAF6 signaling abrogated atherosclerosis, emphasizing the importance of this signaling interaction.[123] Despite their invaluable contribution to decipher the molecular and cellular mechanisms in experimental models, this technology is not practical in terms of clinical application.

Yet another alternative target-orientated strategy is to inhibit CD40 function by specifically suppressing downstream signaling. Upon the relevance of CD40-TRAF6 signaling during atherosclerosis a small molecule called TRAF-STOP, that exclusively targets the interaction of CD40 and TRAF6 was designed.[124] TRAF-STOP is packed in high density lipoprotein based nanoparticles allowing targeted delivery in myeloid cells like monocytes an macrophages for specific inhibition of CD40-TRAF6 interaction.[124] TRAF-STOP treatment of apolipoprotein E-deficient ($Apoe^{-/-}$) mice resulted in less atherosclerosis by reducing monocyte and macrophage recruitment, while CD40-mediated immunity through TRAF2, -3, and -5 signaling

was maintained.[125] Thus, treatment with TRAF-STOP slowed progression and even inhibited established atherosclerosis, due to restrained leukocyte recruitment, predominantly neutrophils and monocytes, to the vessel wall and transition to a stable plaque phenotype.[125] Underlying mechanisms of these findings were reduced macrophage activation and altered cytokine and chemokine secretion.[125] Most of these effects were successfully reproduced in a translational study of non-human primates when treated with the high density lipoprotein based TRAF-STOP.[124, 126] In context of other CVD, here in a model of non-ischemic heart failure in mice, the inhibition of CD40-TRAF6 signaling resulted in an improved cardiac function, due to reduced cardiac remodelling and fibrosis following diminished infiltration of macrophages and T cells.[127] However, little is known about the role of CD40-TRAF6 interaction in AMI and whether targeting this signaling pathway could confer a more favorable morphological and functional outcome.

These findings of TRAF-STOP treatment in heart failure and atherosclerosis indicate a promising approach for direct transfer into a model of AMI. Understanding CD40/CD40L signaling in AMI will introduce new insights to inflammatory processes, cardiac function and outcome after AMI and set the stage for possible therapies of AMI patients in the future.

2 Aim of the study

The CD40/CD40L axis plays a crucial role during immune response by regulating inflammatory processes, and therefore provides a potential target to influence cardiac outcome post AMI. This study aims to investigate the impact of modulating CD40 signaling and its resulting effects on immunological and functional cardiac outcome using an experimental murine model of AMI. For this purpose, this study is divided into three major parts, based on individual hypotheses, each focusing on a specific aspect of the CD40/CD40L axis and its modulation. The first section investigates the specific blocking of CD40 signaling in macrophages using TRAF-STOP (**Fig. 6 A**), while the second segment sets the focus on the activation of CD40 signaling via an agonistic CD40 antibody (**Fig. 6 B**). Lastly, a cell type-specific genetic modification of CD40L is used to better understand the role of CD40L during CD40 signaling after AMI (**Fig. 6 C**). The central methods to analyze the resulting effects in all three approaches are echocardiography to assess cardiac function, measurements of infarct sizes by TTC and estimating the immune cell composition via flow cytometry.

Blocking of CD40 signaling is induced via time-dependent administration of TRAF-STOP before and after AMI. We hypothesize that blocking CD40/TRAF6 signaling using TRAF-STOP in AMI leads to less inflammation by altering immune cell distribution that results in an improved overall cardiac outcome (**Fig. 6 A**).

Given the increased levels of sCD40L in diabetic patients, resulting in enhanced CD40 activation and inflammation, we thus hypothesize that mimicking exaggerated CD40 activation via an agonistic CD40 antibody that simulates high levels of sCD40L in normo-glycemic mice results in increased inflammation causing an impaired outcome after AMI (**Fig. 6 B**).

To survey which CD40L-expressing cells are relevant after AMI, mouse lines with a cell-type specific deficiency for CD40L on either T cells or platelets are generated and tested in an experimental AMI model. We hypothesize that a deletion of CD40L on the most common CD40L-expressing cells including T cells and platelets reduces the activation of CD40 signaling and therefore results in less inflammation and positively affecting the cardiac outcome after AMI (**Fig. 6 C**).

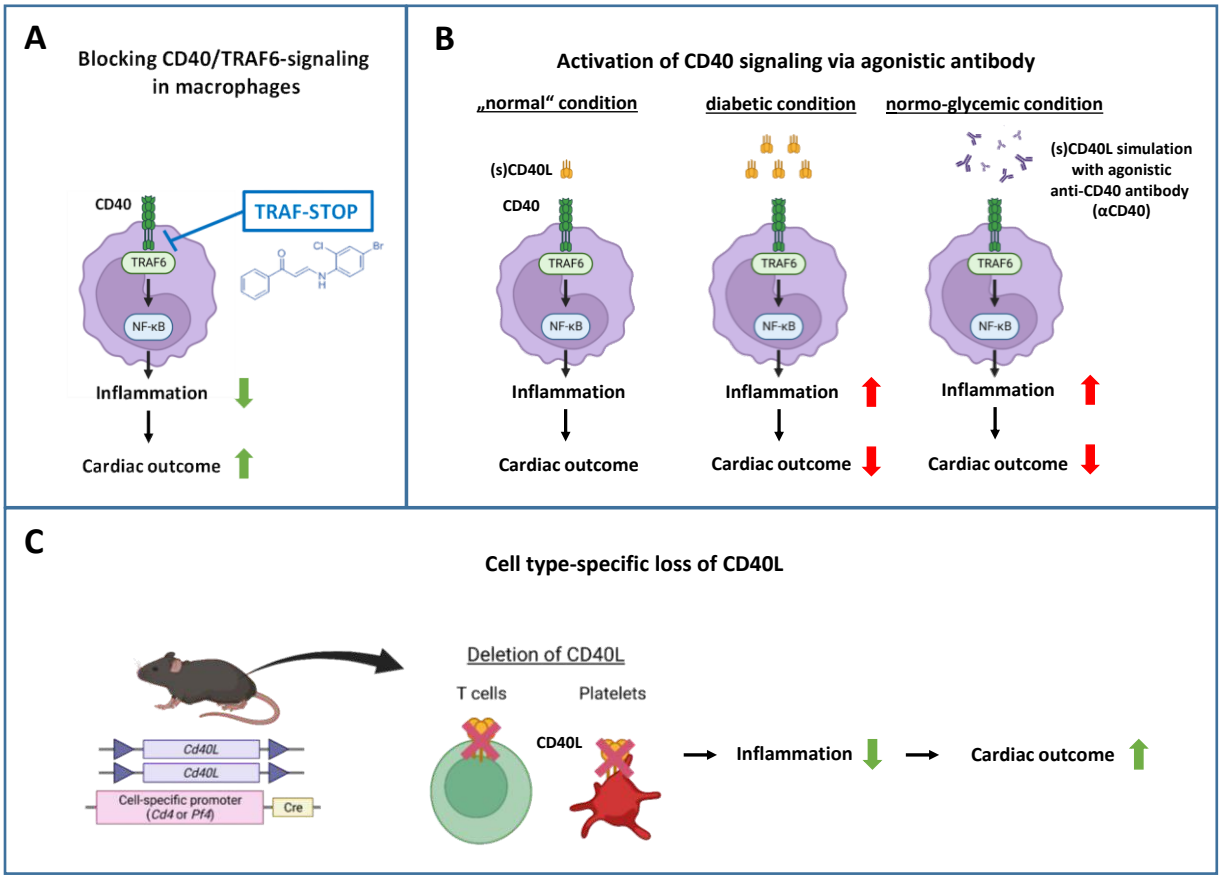

Figure 6: Graphical abstract of the three main hypotheses of this study. (A) Inhibition of CD40/TRAF6 signaling via a small molecule inhibitor TRAF-STOP in monocytes and macrophages expected to reduce inflammation resulting in a better cardiac outcome after AMI. **(B)** sCD40L is increased under diabetic conditions enhancing the activation of CD40 signaling causing an impaired cardiac outcome. Treatment with an agonistic CD40 antibody is hypothesized to mimic this situation under normo-glycemic conditions after AMI. **(C)** A cell type-specific deficiency of CD40L on T cells and platelets is supposed to reveal the role of these cell types in terms of CD40 signaling and their beneficial effect on cardiac outcome after AMI.

Investigating these three hypotheses will shed novel light on understanding CD40/CD40L signaling and how its modulation could alter pro- and anti-inflammatory processes post AMI. Whether and how modulating the CD40/CD40L dyad can affect infarct size and immune cell distribution and in the end benefit heart function in mice will reveal its value as a potential target for therapeutic approaches in future treatments of AMI patients.

3 Materials and Methods

3.1 Mouse studies

All animal procedures were performed in accordance with the European convention for the protection of vertebrate animals used for experimental and other scientific purposes and were approved by LANUV (Landesamt für Natur-, Umwelt- und Verbraucherschutz Nordrhein-Westfalen) under the file numbers 81-02.04.2020.A225. Mice were kept according to the "Guide for the Care and Use of Laboratory Animals", the ARRIVE (Animal Research: Reporting of In Vivo Experiments) II guidelines and the German "Tierschutzgesetz".

Male C57BL/6J mice, aged 10-12 weeks at the beginning of the experiments, were purchased from Janvier Labs (53940 Le Genest-Saint-Isle, France). Additional studies were performed on cell type-specific gene deficient mice using the Cre/loxP system.[128] Herein, the *Cd40lg*$^{fl/fl}$*Cd4-Cre* line with a specific gene deficiency of *CD40l* on T cells and the *Cd40lg*$^{fl/fl}$*Pf4-Cre* line with a gene deficiency of *CD40l* on platelets were used. All animals were housed in standard cages at constant room temperature and humidity, with a 12 hours light/dark cycle, in the central facility premises for animal research and scientific animal protection tasks (ZETT) at Heinrich Heine University Düsseldorf. Animals received standard chow diet and drinking water *ad libitum*.

3.2 *In vivo* studies

3.2.1 Ischemia reperfusion surgery

Prior to the induction of AMI via ischemia reperfusion (IR) surgery, mice were injected subcutaneously with buprenorphine (0.1 mg/kg body weight, Temgesic©; Indivior Europe, Dublin, Ireland). After 30 minutes, mice were anesthetized in an inhalation chamber with 3 % isoflurane in room air. Next, mice were intubated using an indwelling venous cannula (Vasofix Safety Kanüle 20 G 1,1x25 mm, B. Braun, Melsungen, Germany) and placed on a heated small animal surgery table, where temperature was continuously checked via rectal probe. Furthermore, a surface ECG (Powerlab 8/35, Software: LabChart, ADInstruments, Sydney, Australia) was used as control and mice received eye ointment (Bepanthen Augensalbe, Bayer, Leverkusen, Germany) on their eyes as protection from drying out. Anesthesia was maintained via a murine respirator (MiniVent Type 845, Hugo Sachs, March-Hugstetten, Germany) at a respiratory volume of 0.2-0.25 mL and a respiratory rate of 140 breaths per minute with isoflurane (2 %) and oxygenated (40 %) air. Surgery started by opening the thorax between third and fourth rip and carefully preparing the heart free from surrounding tissue. The left anterior descending artery (LAD) was identified and tied using a 7-0 prolene thread (Ethicon, Raritan, United States) and a small piece of plastic hose. Subsequently, mice underwent either a 45 min occlusion of the LAD to induce AMI or sham surgery without the occlusion of the LAD as previously described. Following 45 min of ischemia controlled by visual

inspections and changes in electrocardiogram with regular monitoring of body temperature (37°C), the occlusion was resolved. The thread was removed, except for mice that were used to determine infarct size at d1 post AMI. Ribs were closed with a 4-0 silk thread (Ethicon), skin sewed up using a 5-0 prolene thread (Ethicon) and suture was disinfected with “Octenisept” (Schülke & Mayr, Norderstedt, Germany). Finally, mice were extubated and put into a cage under a heating lamp until they woke up. Following the IR surgery to induce AMI, animals received further buprenorphine in drinking water 24 h post-surgery for 3 days where necessary and were monitored regularly until the end of the experiment. The surgical procedures were performed by Stefanie Becher und Pia Fiegenbaum.

3.2.2 Echocardiography

Analysis of cardiac function was assessed by ultrasound using a Fujifilm VisualSonics Vevo 3100 Ultra High Frequency Imaging Platform (18–38 MHz linear array micro scan transducer; VisualSonics, Toronto, Canada). First, mice were placed in an induction chamber with 2.5-3 % isoflurane with oxygen-enriched room air. Next, the anesthetized mice were placed on a heated examination table with constant monitoring of electrocardiogram, respiratory rate, heart rate and body temperature. Anesthesia was maintained through a respiratory mask with 1.5-2 % isoflurane. A chemical hair remover (Veet, Heidelberg, Germany) was used to scrape off the fur from the chest of mice to improve cardiac image quality. Next, preheated Aquasonic 100 Gel (Parker Laboratories, Fairfield, United States) was applied onto the mice chest. Imaging was performed in the parasternal long-axis (**Fig. 7**). Cardiac parameters such as left ventricular (LV) chamber volume in end-diastole (EDV) and end-systole (ESV), stroke volume (SV), ejection fraction (EF), cardiac output (CO) and heart rate (HR) were measured in B-Mode using the Vevo LV-Trace function and Strain. Imaging was performed on baseline mice prior to surgery and at various time points post-surgery. Data analysis was carried out with Vevo Lab software (Visual Sonics, Fujifilm, Japan) in collaboration with Dr. Grace Ampem.

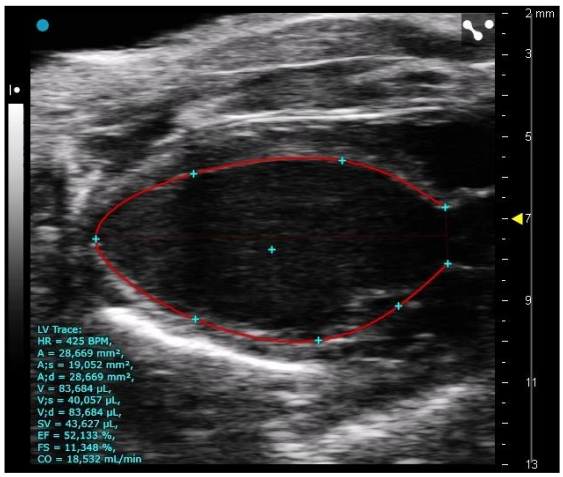

Figure 7: Parasternal long axis ultrasound image of the LV from a mouse heart.

3.2.3 *In vivo* treatment protocols

The small molecule inhibitor TRAF-STOP 6860766 (provided by the laboratory of Prof. Dr. Ester Lutgens), henceforth TRAF-STOP, was used to block CD40 signaling (**Fig. 8**).[124]

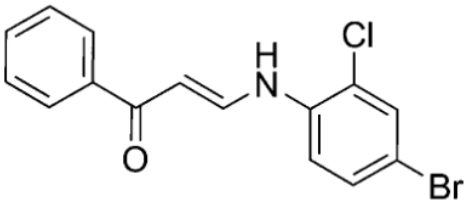

Figure 8: Structure of TRAF-STOP 6860766, modified from Zarzycka et al.[124]

Mice were injected intraperitoneally with either TRAF-STOP at a final concentration of 10 µmol/kg/injection or 2.5 % dimethyl sulfoxide (DMSO) (Carl Roth, Karlsruhe, Germany) as vehicle control according to the different experimental setups (**Fig. 9**). First the preconditional and continuous treatment with TRAF-STOP before, during and after IR surgery was investigated for end points day 1 and day 28 (**Fig. 9 A**). The second approach was to apply TRAF-STOP starting at day 5 until the end points of day 14 and 28 after IR (**Fig. 9 B**).

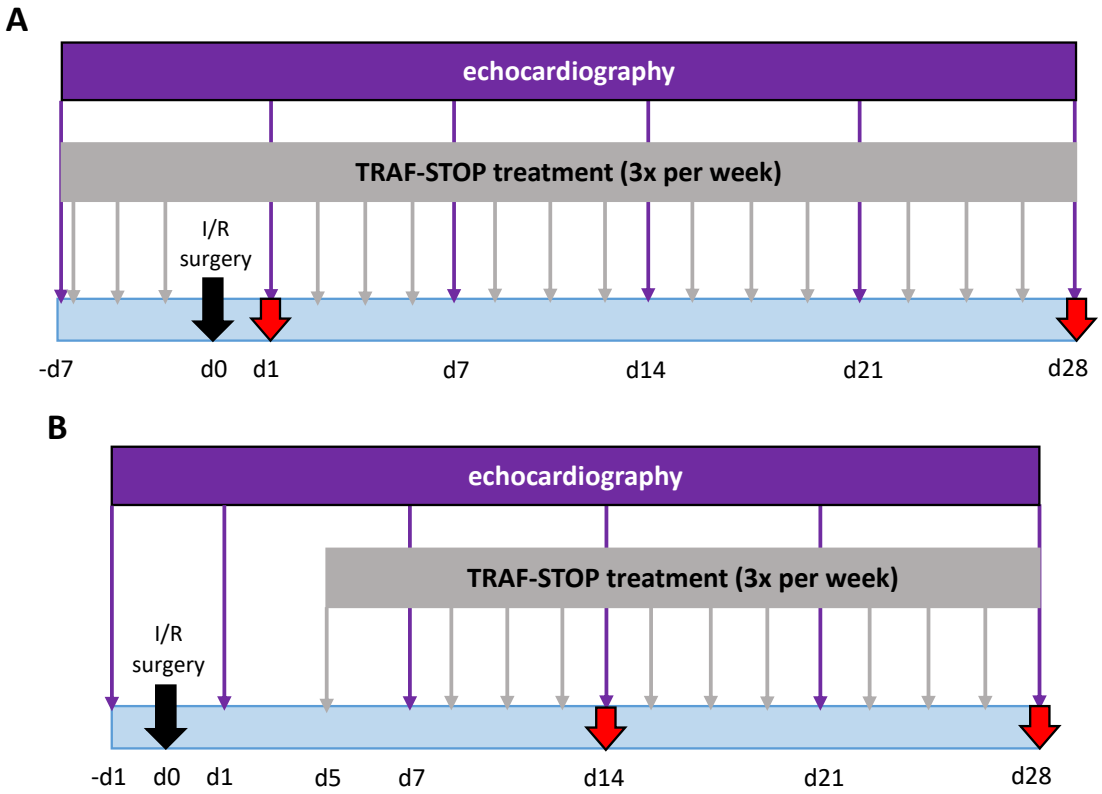

Figure 9: Schematic illustration of experimental procedure with TRAF-STOP treatment. (A) After baseline echocardiography, mice were either continuously treated with TRAF-STOP or vehicle control (DMSO) for three times per week, starting 7 days before IR surgery. Following IR, mice were monitored by echocardiography at day 1, 7, 14, 21 and 28. End points for following analyses were day 1 and day 28 after AMI induction. **(B)** Mice underwent baseline echocardiography one day before IR surgery and further echocardiography analysis at day 1, 7, 14, 21, 28 after AMI. TRAF-STOP or DMSO treatment started at day 5 after AMI and maintained for three times per week until end points at day 14 or 28.

To activate CD40 signaling the agonistic anti-CD40 antibody with clone FGK45 (αCD40) was applied to the mice. Mice were injected intraperitoneally with either αCD40 (BioXCell, Lebanon, United States) at a final concentration of 100 µg/30 g body weight or IgG2a isotype control (BioXCell) with the same final concentration as vehicle control according to the different experimental setups (**Fig. 10**). The first treatment protocol was used to investigate the basal effects of a treatment with agonistic CD40 antibody onto immune cell composition (**Fig. 10 A**). The second setup should implement whether short-term CD40 activation directly after AMI induction, mimicking high levels of CD40L during the acute phase, alters cardiac outcome at end points day 1 and 7 post AMI (**Fig. 10 B**).

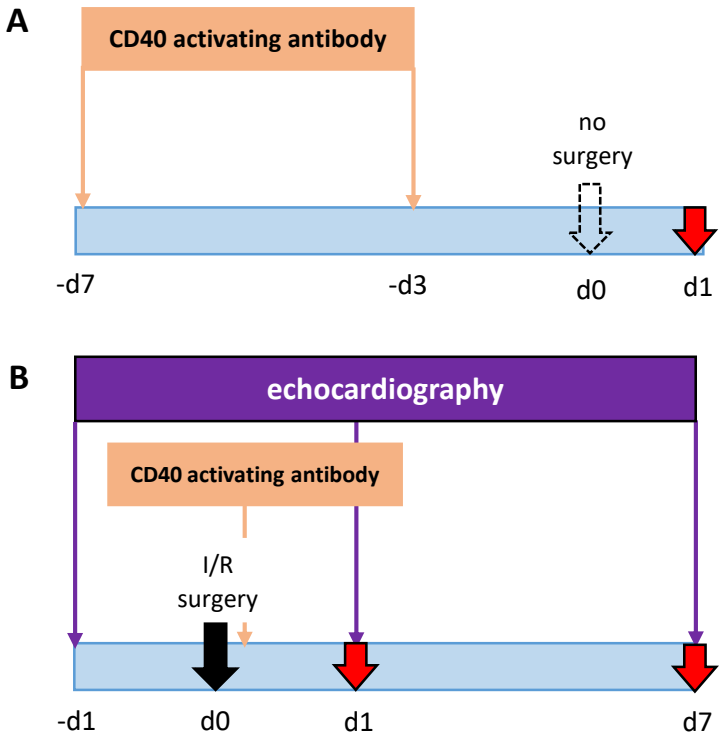

Figure 10: Schematic illustration of experimental procedure with CD40 activating antibody (αCD40). (A) Following baseline echocardiography mice underwent a 45 min IR surgery, after which they were directly treated with either one dose of αCD40 or control IgG2a. Before sacrificing mice at end points day 1 or 7 after AMI, mice were again analyzed by echocardiography. **(B)** After baseline measurement of echocardiographic parameters, mice were treated with either αCD40 or IgG2a at day 7 and 3 prior to IR surgery. One day after IR surgery mice underwent echocardiography and were either sacrificed or kept until end point day 7. During this time, they received further treatment at day 1 and 3.

3.3 *In vitro* studies

3.3.1 Organ harvesting

At the individual end points of all experiments, mice were anesthetized by intraperitoneal injection with ketamine (Ketaset®; Zoetis, Parsippany-Troy Hills Township, United States) (100 mg/kg body weight) and xylazine (Rompun®; Serumwerk Bernburg, Bernburg, Germany) (10 mg/kg body weight). After checking that mice were fully anesthetized, by loss of “toe pinch

reflex", they were placed and fixated with tape onto a surgery table. Mice were killed by final blood taking via heart puncture using a 1 ml syringe (B. Braun). About 50 µl of blood was filled into a tube coated with ethylenediaminetetraacetic acid (EDTA) and later measured by using the blood count meter VETSCAN® HM5 Hematology Analyzer (Zoetis). The remaining blood was transferred into 1.5 ml tubes (Eppendorf, Hamburg, Germany) and centrifuged at 800 x g, 10 min, RT. The upper layer, containing the plasma, was carefully pipetted into cryotubes (VWR, Radnor, United Sates), which were put into liquid nitrogen and later stored in -80°C freezers. The thorax was opened and the vena cava inferior severed, to allow flushing out the residual blood using cold phosphate-buffered saline (PBS; Sigma-Aldrich, St. Louis, United States) injected into the heart via a syringe with a 25 G needle (Becton Dickinson, Franklin Lakes, United States). Afterwards, the heart was removed and placed in a petri dish (Greiner bio-one, Kremsmünster, Austria) with cold PBS. Next, all otiose fat and tissue were cut off and the heart stored in a tube with cold PBS on ice until further processing. Finally, the spleen was removed and stored in a tube with cold PBS until further processing.

3.3.2 Flow Cytometry

First, hearts were dried on a sheet of paper and then weighed. For isolation of viable leukocytes, hearts were minced into small pieces and digested using a digestion solution consisting of RPMI-1640 (Merck, Darmstadt, Germany) and three different enzymes (Multi Tissue Dissociation Kit 1, Miltenyi Biotec, Bergisch Gladbach, Germany) for 15-20 min at 37°C with agitation. Cell suspension was passed through a 100 µm (Miltenyi Biotec) and a 40 µm strainer (pluriSelect Life Science, Leipzig, Germany), after which RPMI-1640 was added and centrifuged for 5 min at 450 × g at 4°C. For lysis of erythrocytes, the supernatant was removed and the pellet was resuspended in red blood cell lysis buffer, containing ammonium chloride, potassium hydrogen carbonate, sodium edetate and water at a pH of 7.4. Following an incubation for 5 min, the cell suspension was centrifuged for 5 min at 450 × g at 4°C. The pellet was resuspended in 3 ml of cold PBS and 1 ml of a debris removal solution (Miltenyi Biotec) was carefully added. To remove debris the cell suspension was overlaid with 4 ml of cold PBS and centrifuged for 10 min at 3000 × g at 4°C. After centrifugation three phases had formed, of which the two upper phases, consisting of PBS and debris, were removed leaving the lowest phase, which included the immune cells. The pellet of the lower phase was resuspended in cold PBS and again centrifuged for 10 min at 3000 × g at 4°C. Thereafter, the supernatant was removed and cardiac cells were resuspended in 0.5-1 ml of cold PBS. For each staining 100 µl of this cell solution were pipetted into a 96-well V-bottom plate and a distinct number of counting beads (CountBright™ Absolute Counting Beads, Thermo Fisher Scientific, Waltham, United States) was added to wells of the "Differential leukocyte panel" to assess absolute cell numbers after processing. After centrifugation for 5 min at 450 × g at 4°C, cells were incubated

with a mixture of Fc receptor blocker (TruStain FcX™ anti-mouse CD16/32, BioLegend, San Diego, United States) and viability stain (Zombie AquaTM Fixable Viability Kit, BioLegend) in the dark for 10 min at RT. Flow cytometric buffer (1× PBS and 0.5 % bovine serum albumin; Merck) was added and cells were centrifuged for 5 min at 450 × g at 4°C. Subsequently, cells were resuspended in flow cytometric buffer and stained for 20 min in the dark at RT with the following conjugated antibodies: CD45-V450, Ly6G-PerCP-Cy5.5, CD19-FITC, CD11b-APC-Cy7, Ly6C-PE, CD3-APC or CD40-APC (all BioLegend). Cells were centrifuged again for 5 min at 450 × g at 4°C and cell pellet was resuspended in flow cytometric buffer.

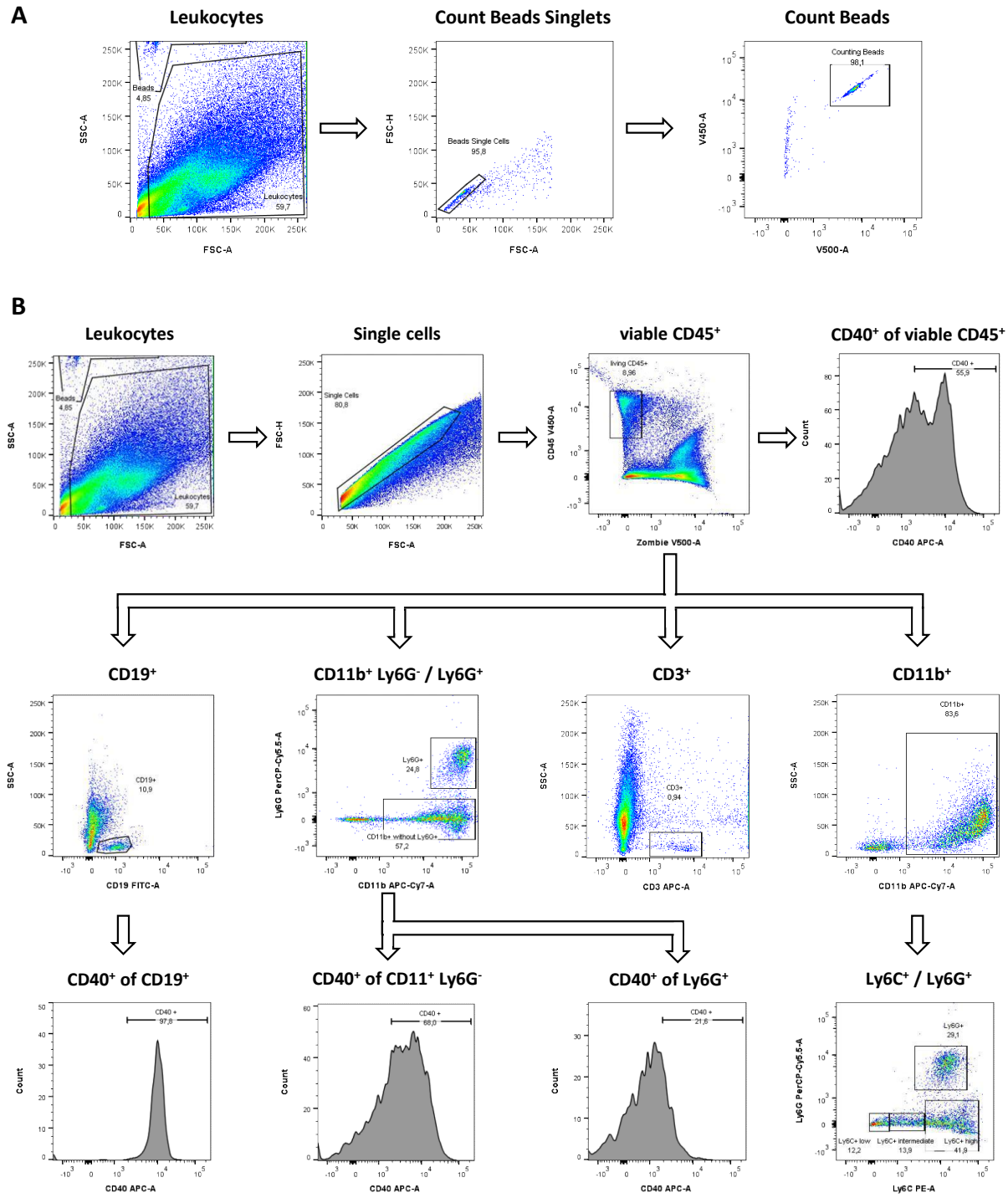

C

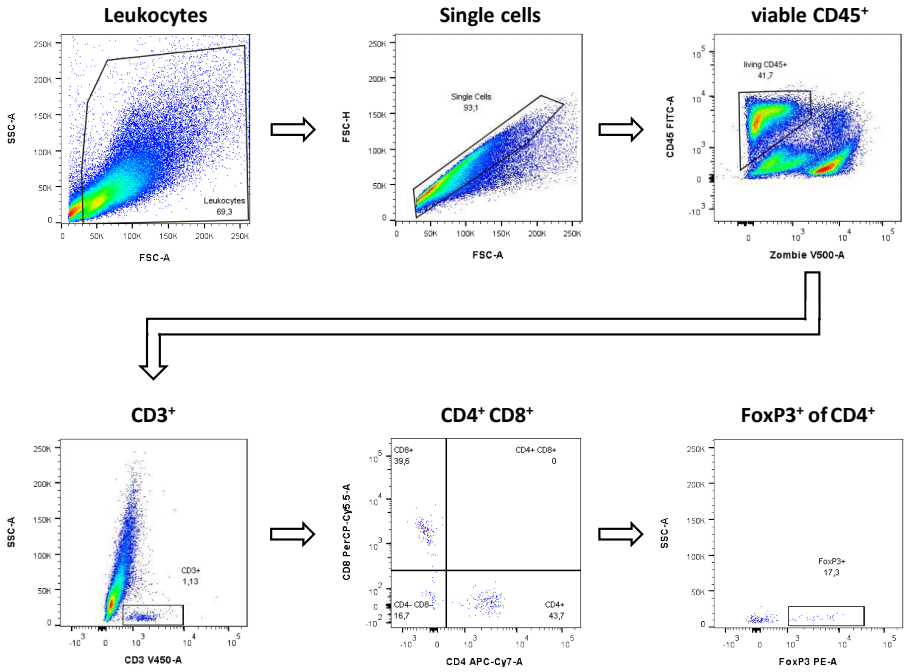

Figure 11: Flow cytometric gating strategies for selecting counting beads and cardiac immune cells. (A) Counting beads were determined according to their forward- and side scatter-area (FSC-A and SSC-A). Single cells were gated from counting beads via forward scatter-height (FSC-H) and forward scatter-area (FSC-A) and were positive for V450 and V500. Gated counting beads were used for calculation of absolute cell numbers. **(B)** Leukocytes were determined according to their forward- and side scatter-area (FSC-A and SSC-A), respectively. Single cells were gated from leukocyte population via forward scatter-height (FSC-H) and forward scatter-area (FSC-A). A viability marker (Zombie) was used to exclude dead leukocytes. Viable $CD45^+$ leukocytes were used to identify neutrophils ($Ly6G^+$), B cells ($CD19^+$), T cells ($CD3^+$) and monocytes/macrophages ($CD11b^+/Ly6G^-$). Finally, Ly6C was used to separate monocytes/macrophages into $Ly6C^{low}$, $Ly6C^{intermediate}$ ($Ly6C^{int}$) and $Ly6C^{high}$ subtypes. Thereafter, CD40 expression of these populations was determined. **(C)** Leukocytes, single cells and viable $CD45^+$ leukocytes were gated the same way as previously described. T cells ($CD3^+$) were gated out of the viable leukocytes and then further divided into subpopulations of Th cells ($CD4^+$) and cytotoxic T cells ($CD8^+$). Finally, FoxP3 was used on $CD4^+$ population to detect T_{reg} cells.

Surface staining for T cell based panel was performed in the same way as described before using the following antibodies: CD4-APC-Cy7, CD8-PerCP-Cy5.5 (BioLegend) and CD45-FITC, CD3-V450 (Becton Dickinson). After centrifugation, cells were fixed and permeabilized according to the protocol of the FoxP3/Transcription Factor Staining Buffer Set (Thermo Fisher Scientific). Next, intracellular staining with FoxP3-PE (BioLegend) followed and finally cells were resuspended in flow cytometric buffer. Flow cytometric data were acquired using a BD FACSVerse™ Cell Analyzer (Becton Dickinson) and analyzed using FlowJo software v10.5.3 (**Fig. 11**). Final calculation of absolute cell numbers was performed using the corresponding formula from the user guide of the CountBright™ Absolute Counting Beads (**Fig. 12**).

$$Absolute\ Count\ \left(\frac{cells}{\mu l}\right) = \frac{(Cell\ Count\ \times Counting\ beads\ volume)}{(Counting\ beads\ count\ \times Cell\ volume)} \times Counting\ beads\ concentration\ \left(\frac{beads}{\mu l}\right)$$

Figure 12: Equation to calculate the absolute cell numbers using counting beads after flow cytometry.

3.3.3 Determination of infarct size via 2,3,5-Triphenyltetrazolium chloride

This staining method allows measuring of infarct size 24 h after IR surgery. Mice were anesthetized as described before (see 3.3.1 Organ harvesting) and killed via final blood draw. Hearts were removed quickly and transferred to cold, isotonic 0.9 % saline solution (Fresenius Kabi, Bad Homburg, Germany) supplemented with 1 ml heparin (5000 IU) (B. Braun). All otiose tissue and fat were removed, with the result that only a few millimeter long part of the aorta ascendens remained. Next, the heart was mounted onto a cannula by fixating it at the aorta and rinsed with isotonic 0.9 % saline solution to eliminate the blood inside. The remaining thread of the IR surgery, indicating the position where the LAD was occluded, was removed and the LAD occluded again at the same position using a 7-0 silk thread (Ethicon). A 1 % Evans blue dye solution (Merck) was injected into the heart through the aorta until the myocardium turned blue. Remaining solution was washed away with saline solution and the heart dried on a sheet of paper. To allow precise cutting of the stained heart was wrapped in cling film and frozen at -20°C for at least 1 h. Afterwards, hearts were sliced into 1 mm sections along the long axis, weighed and incubated in 1 % 2,3,5-triphenyltetrazolium chloride (TTC) solution for 5-7 min at 37°C. During this incubation, the viable tissue converts the TTC into a red dye, which allows the identification of viable and dead myocardium. Slices were photographed (Leica DM6B) and infarct area (INF, white), viable areas affected (red) or not (blue) by ischemia as well as area at risk (AAR, white + red) were assessed using a computer-assisted planimetry software called Diskus Viewer (Technisches Büro Hilgers, Königswinter, Germany), taking the slice weight into account (**Fig. 13**).

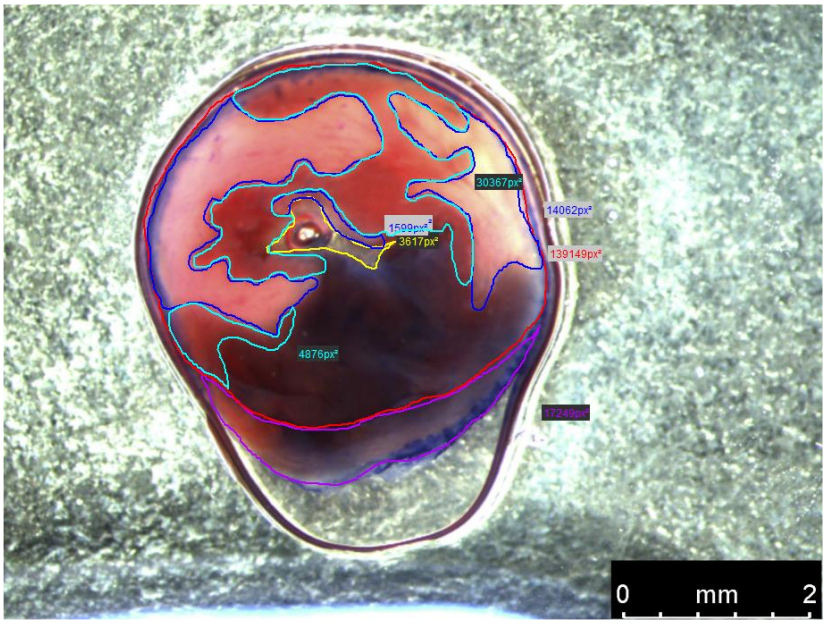

Figure 13: Infarct size determination of an exemplary heart slice after TTC staining procedure. Based on its anatomy and the stained colors after Evans blue and TTC procedure the heart can be divided into following areas: infarct area (white), viable areas affected (red) or not (blue) by ischemia as well as area at risk (white + red). These areas and anatomical characteristics are outlined by different colors using Diskus Viewer and stand for left ventricle (red line), right ventricle (violet line), left lumen (yellow line), infarct area (blue line) and area at risk (turquoise line).

3.3.4 Isolated mouse heart perfusion model

To investigate the role of CD40 inhibition via TRAF-STOP on the heart function ex vivo, a Langendorff model was used[129]. Mice were anesthetized as described before (see Organ harvesting). Furthermore, mice received an intraperitoneal injection of heparin (1000 IU). Hearts were removed quickly and transferred to cold, Krebs Henseleit buffer (KHB), containing 118 mM NaCl, 4.7 mM KCl, 0.8 mM $MgSO_4$, 25 mM $NaHCO_3$, 1.2 mM KH_2PO_4, 5 mM glucose, 110 mM Na-pyruvate, and 2.5 mM $CaCl_2$, supplemented with 1 ml of heparin (5000 IU). All otiose tissue and fat were removed, with the result that only a few millimeter long part of the aorta ascendens remained. Next, the heart was mounted onto a cannula by fixating it at the aorta and placed inside a Langendorff (LD)-apparatus (Hugo Sachs), where it was retrogradely perfused with KHB at 37°C and a constant pressure of 100 mm Hg. The whole procedure from heart removal to perfusion of the heart should not exceed six minutes to ensure accurate functionality of the heart. To measure left ventricular developed pressure (LVDP) and its positive and negative first derivate (+dP/dt and -dP/dt), a small balloon filled with water connected to a pressure transducer was inserted through the mitral valve into the left ventricle and hearts were paced to a constant rate of 600 beats/min. Hearts underwent a stabilization period of 20 minutes, followed by 20 seconds of global zero flow ischemia to test coronary reserve and 5 minutes of recovery. Before global ischemia, baseline parameters including LVPD, +dP/dt, -dP/dt and coronary flow were measured. At the beginning of the 40 min zero flow global ischemia, by stopping coronary flow, 400 µL of blood, taken from another donor mouse, enriched with or without TRAF-STOP (10 µmol) were loaded to the coronary system of the murine hearts via a side arm using a syringe driver set to 0.4 mL/min. During ischemia, hearts, still connected to the LD apparatus, were kept in a beaker with KHB at 37°C to prevent them from becoming hypothermic. After 40 min, flow was re-established, allowing restart of LV contractility. Hearts were monitored for the full recovery length of 120 min (**Fig. 14**).

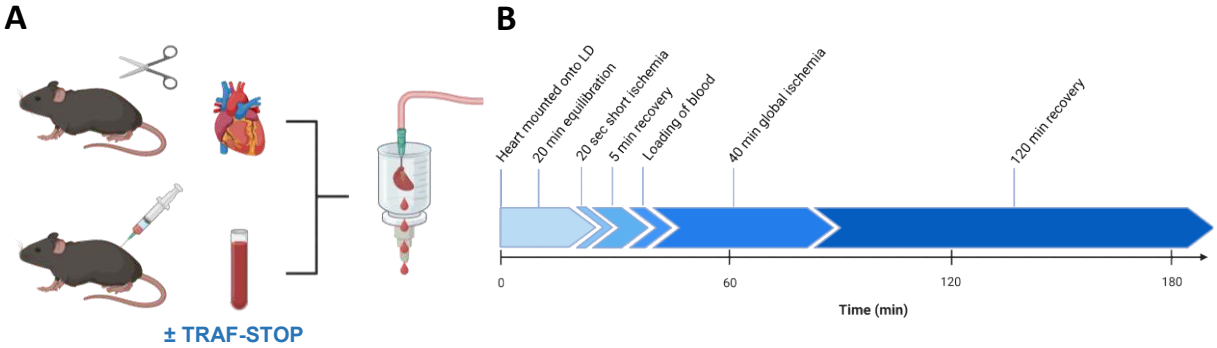

Figure 14: Isolated mouse heart perfusion model. (A) Schematic experimental setup of LD model. Explanted hearts were mounted onto a LD apparatus and loaded with blood enriched with either TRAF-STOP or control during global ischemia. **(B)** Timeline of the LD experiments.

3.3.5 Histology

Directly after removal, total hearts were fixed in 4 % paraformaldehyde (Thermo Fisher Scientific) for 1 hour at RT. After this, the hearts were transferred into a solution of 30 % sucrose (Sigma-Aldrich) in PBS and kept at 4°C for dehydration overnight. Next, hearts were embedded in the cryo-medium Tissue-Tek® (Sakura Finetek, Umkirch, Germany) and stored at -80°C for at least 24 hours until sectioning. According to a predefined scheme with ten different layers starting from the apex, 5 µm thin sections were made using a cryotome. Every layer consisted of 20 sections, while the trimmed distance between layers was 250 µm. Until further procession, the sections were stored at -20°C (**Fig. 15**).

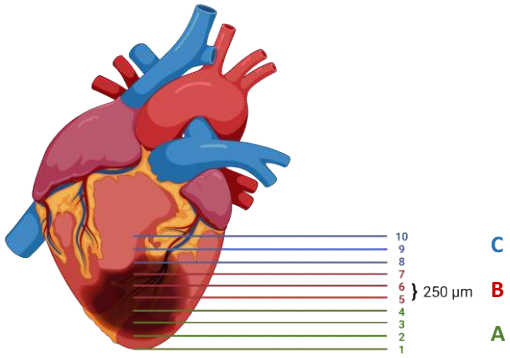

Figure 15: Scheme for cryosectioning of hearts. Hearts were divided into 10 different layers, consistent of 20 slices a 5 µm. Between each layer, 250 µm of tissue was trimmed.

For determination of scar sizes after AMI, slices were stained with wheat germ agglutinin (WGA) and phalloidin to allow the simultaneous visualization of fibrotic tissue with WGA and actin filaments on viable tissue with phalloidin. First, cryosections were defrosted for 30 min at RT and rehydrated in PBS for 5 min. The tissue was permeabilized with 0.5 % TritonX-100 (Sigma-Aldrich) in PBS for 10 min at RT. After washing the slices three times for 3 min in PBS, unspecific bindings were blocked by use of a blocking solution consisting of 0.1 % saponin (Sigma-Aldrich), 0.5 % BSA (Carl Roth GmbH) and 0.2 % fish gelatin (Sigma-Aldrich) for 1 hour at RT. After performing another wash step (3 x 3 min in PBS), heart slices were incubated with 1:80 diluted phalloidin-594 (BioLegend) for 20 min at RT in the dark. Next, slices were washed again (3 x 3 min in PBS) and incubated with a 1:200 dilution of WGA-FITC (Merck) for 1 h at RT in the dark. Following a last washing step (3 x 3 min in PBS), slides were mounted with Prolong Antifade Mountant (Thermo Fisher Scientific), which contains 4',6-diamidino-2-phenylindol (DAPI) for 3 min to stain nuclei before covering the slides with coverslips. For imaging a Leica fluorescence microscope camera DFC9000 (Leica, Wetzlar, Germany) supported by LASX software were used. Analyses were performed using ImageJ software and carried out by Chiara Wernet.

3.3.6 RNA extraction and quantitative polymerase chain reaction (qPCR)

Total ribonucleic acid (RNA) was isolated from hearts with the RNeasy Mini Kit (QIAGEN, Hilden, Germany) following the manufacturer's instructions. RNA integrity was analyzed with a fragment analyzer. Only non-degraded total RNA (500 ng/µl) with RNA integrity number between 8 and 10 was used for complementary DNA (cDNA) synthesis with SuperScript™ IV VILO™ Master Mix with ezDNase enzyme (Thermo Fisher Scientific, Schwerte, Germany) according to manufacturer's instructions. Gene expression analyses were performed with the QuantStudio™ 7 Flex Real-Time PCR System (Thermo Fisher Scientific). Amplifications were carried out in a reaction solution consisting of TaqMan™ Fast Advanced Mastermix (Thermo Fisher Scientific), first-stranded cDNA (diluted 1:10), specific TaqMan™ probes and water. Gene expression values were expressed as relative mRNA levels according to ΔCt and $\Delta\Delta$Ct methods, using *Gapdh* as reference gene. The following TaqMan™ probes were used: *Gapdh Mm99999915_g1; Cd40 Mm00441891_m1.*

3.3.7 Single cell RNA sequencing

Isolated cardiac immune cells were stained against CD45 (BioLegend) and one specific TotalSeq Hashtag (TotalSeq™-B, BioLegend) in MACS-Buffer (Miltenyi Biotec) for 15 min at room temperature. Cell viability and cell number were assessed via DAPI staining while sorting. Cell sorting was performed by Dipl. Ing. Katharina Raba on a MoFlo XDP (Beckman Coulter, Krefeld, Germany) in the 'Institute of Transplantation Diagnostics and Cell Therapeutics, University Hospital Düsseldorf'. In total, cells from six different mice (2 for each condition) were incubated with individual hashtags before pooling into one sequencing run. A total of 40,000 cells were loaded for single-cell droplet libraries generation on a 10× Chromium Controller system utilizing the Chromium Single Cell 3 Reagent Kit v3 according to manufacturer's instructions (10X Genomics, Leiden, The Netherlands). Sequencing was carried out on a NextSeq550 system (Illumina Inc. San Diego, USA) with a mean sequencing depth of ~50,000 reads/cell and 5,000 paired end reads/hashtag. The experiment was performed twice by Dr. Tobias Lautwein of the 'Genomics & Transcriptomics Lab, Düsseldorf'. Raw sequencing data was processed using the 10× Genomics CellRanger software (v6.0.0). Raw BCL-files were demultiplexed and processed to Fastq-files using the CellRanger mkfastq pipeline. Alignment of reads to the mm10 genome and unique molecular identifier counting was performed via the CellRanger count pipeline to generate a gene-barcode matrix.

Further analyses were carried out with the Seurat v4.0 R package. Initial quality control consisted of removal of cells with fewer than 300 detected genes and removal of genes expressed in fewer than three cells. Furthermore, cells with a mapping rate of >30% to the mitochondrial genome were removed, under the assumption that they represent dead or damaged cells. Normalization was carried out utilizing SCTransform. Dimensional reduction of

the data set was achieved by principal component analysis based on identified variable genes and subsequent Uniform Manifold Approximation and Projection (UMAP) embedding. The number of meaningful principal components (PC) was selected by ranking them according to the percentage of variance explained by each PC, plotting them in an “elbow plot” and manually determining the number of PCs that represent the majority of variance in the data set. Cells were clustered using the graph-based clustering approach implemented in Seurat v4.0. Markers defining each cluster and differential gene expression between different clusters were calculated using a Wilcoxon Rank Sum test, which was implemented in Seurat. The single cell RNA-sequencing data are available through the Zenodo data repository (https://doi.org/10.5281/zenodo.6334831). Procedure and analyses of single cell RNA sequencing were assisted by Dr. Alexander Lang.

3.4 Statistics

Statistical analyses and graphical illustrations were performed using GraphPad Prism 8.0.2 (Graphpad Prism Inc., La Jolla, California, USA). If not stated otherwise in figure legends, data are presented as mean ± standard error of the mean (SEM) of *N* individual samples. Data were considered statistically significant with a p-value ≤ 0.05. Significance level is further stated as *p≤ 0.05, **p≤ 0.01, p ***≤ 0.001, p ****≤ 0.0001 or as accurate value.

4 Results

4.1 Characterization of immune cells and cardiac function after AMI

The healing process after AMI is associated with a time- and cell type-specific immigration and emigration of immune cells into the myocardium and can be divided into an acute, subacute and late phase. To validate that the inducible AMI model reliably reproduces these changes in the immune cell distribution, the number of viable $CD45^+$ leukocytes per heart was measured at different time points (day 1, 3, 5 and 28) using a flow cytometric protocol. Mice that underwent a sham surgery, without occlusion of the LAD, served as control group while mice without any treatment were used as baseline group. The number of viable $CD45^+$ leukocytes of IR treated mice peaked on day 1 and declines over time until day 28 (**Fig. 16**). While the IR group exhibits higher numbers of leukocytes on day 1 and 3 compared to the sham group, this numbers remain unchanged in the long run for day 5 and 28 returning towards baseline level.

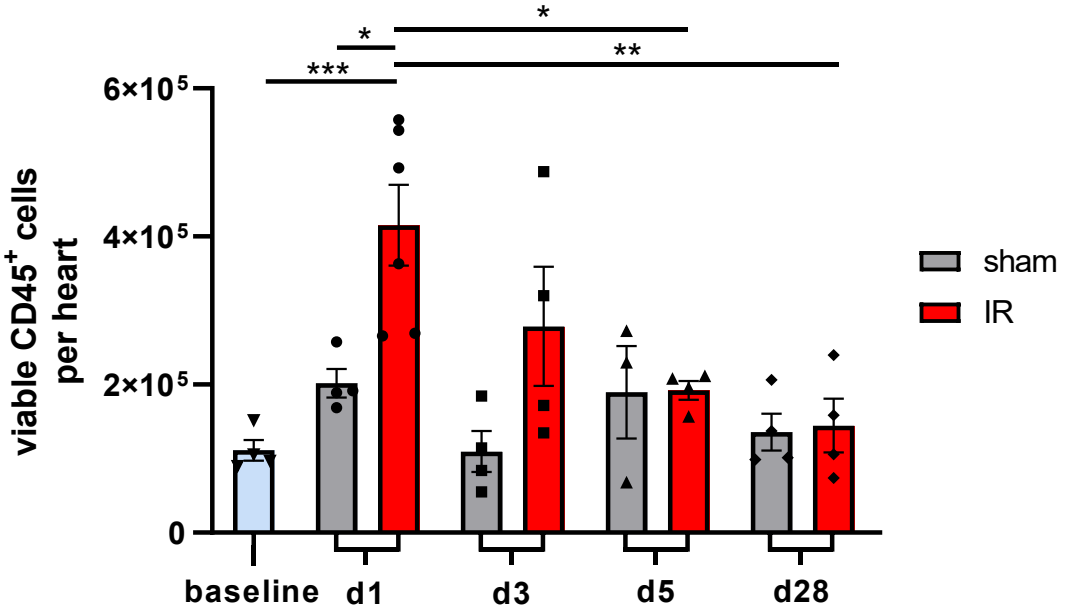

Figure 16: Time-dependent numbers of viable $CD45^+$ leukocytes in the heart after sham and IR surgery. Mice underwent either sham or IR surgery after which cardiac leukocyte numbers were assessed using flow cytometry at the distinct time points. Cardiac leukocyte numbers of mice without any surgery were used as baseline reference. N = 3-6. Data are presented as mean ± SEM. Statistical analyses were performed using 2-way ANOVA.

Besides the immunological changes caused by AMI, measurement of cardiac function is a major indicator to check for the functionality of our IR mice model. Mice were monitored via echocardiography before the induction of either sham or IR to set a baseline and one day afterwards. Comparison of cardiac parameters between baseline and data at day 1 showed, that there were no differences within the sham group, except for the heart rate (HR), while mice after IR displayed a significant decrease of ejection fraction (EF) and stroke volume (SV) leading to an impaired cardiac function (**Fig. 17**). Furthermore, HR of mice undergoing IR surgery was significantly increased, also indicating that AMI deteriorates cardiac function.

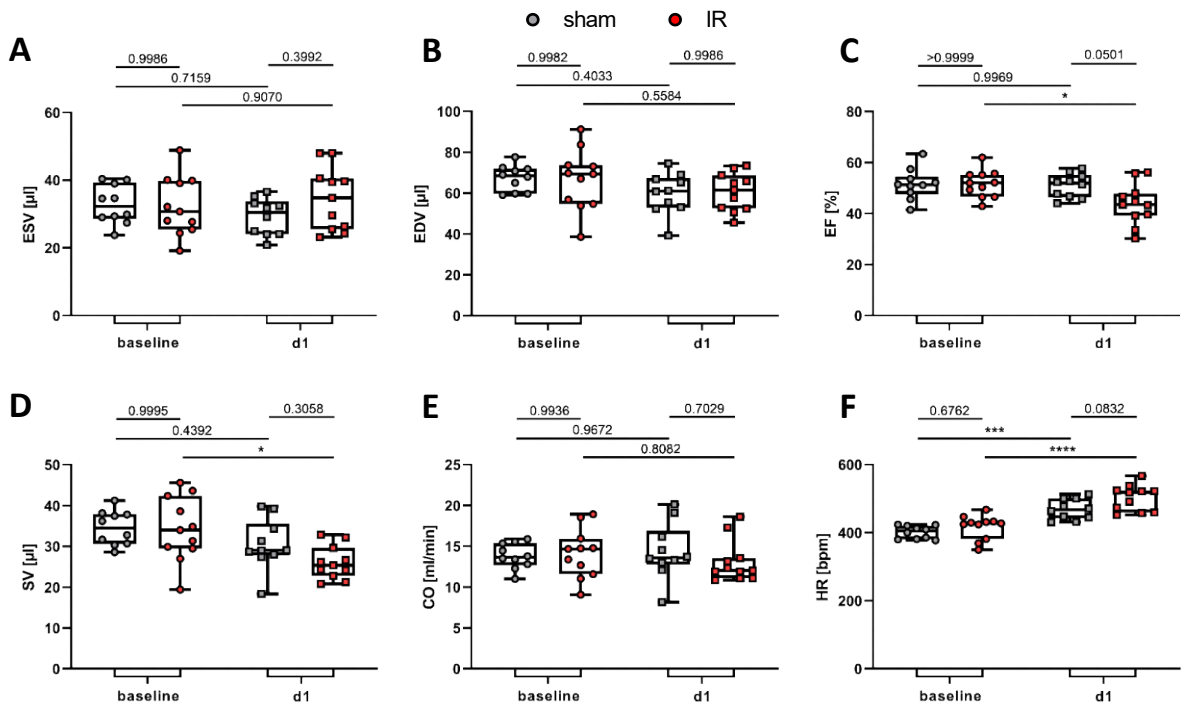

Figure 17: Cardiac function is impaired 24 h after IR surgery. Cardiac function was measured via echocardiography before and 24 h after sham or IR surgery. The following parameters were assessed: **(A)** End-systolic volume (ESV), **(B)** End-diastolic volume, **(C)** ejection fraction (EF), **(D)** stroke volume (SV), **(E)** cardiac output, **(F)** heart rate (HR). N = 10 (sham), 11 (IR). Data are presented as box and whiskers plot with minimum and maximum. Statistical analyses were performed using 2-way ANOVA.

4.2 CD40 expression during the acute phase following AMI

Since increased leukocyte numbers at day 1 and 3 after AMI indicated enhanced inflammatory processes in the heart (**Fig. 16**), the role of CD40, which is an important mediator of inflammation, was investigated by measurements of gene expression levels of CD40 in the infarct and remote area after AMI via qPCR. Sham-operated mice were used as control. *Cd40* mRNA is strongly upregulated in the infarct area 24 h and at day 3 after IR (**Fig. 18**), while the levels of *Cd40* mRNA in the remote area remain unchanged. Furthermore, *Cd40* mRNA in the infarct area is significantly higher compared to the remote area.

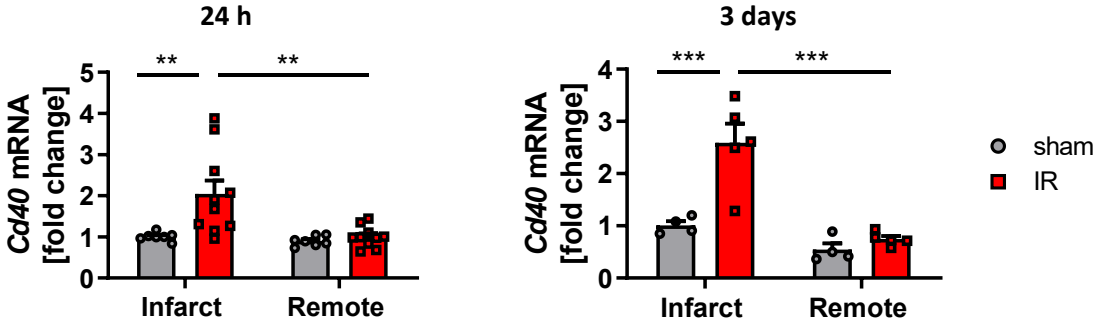

Figure 18: *Cd40* mRNA is strongly upregulated in the infarct area 24 h and 3 days after AMI. Following IR surgery infarct and remote area of the left ventricle were separated and used for qPCR analyses. *Cd40* mRNA levels are elevated in the infarct area 24 hours and 3 days after IR. No changes in remote area. N = 4-10 mice were assessed. Statistical analyses were performed using 2-way ANOVA.

The upregulation of *Cd40* expression in the infarct area raises the question, which immune cells are responsible for increment and if there are changes over time. One way to approach this was by single cell RNA sequencing (scRNASeq). After clustering the cells into specific immune cell populations by basis of their distinct RNA expression patterns, the level of CD40 expression on these immune cells was analyzed. After one day of reperfusion, the most common cells expressing high levels of CD40 were B1 and B2 cells, DCs and T cell-like macrophages (**Fig. 19 A**). However, 5 days after IR the clusters which were highly positive for CD40 shifted with the result that now CCR2^{-} or CCR2^{+} resident-like macrophages as well as Lgals3 macrophages became the most prominent clusters (**Fig. 19 B**). These findings indicate that B cells and certain subpopulations of macrophages are responsible for CD40 expression after AMI.

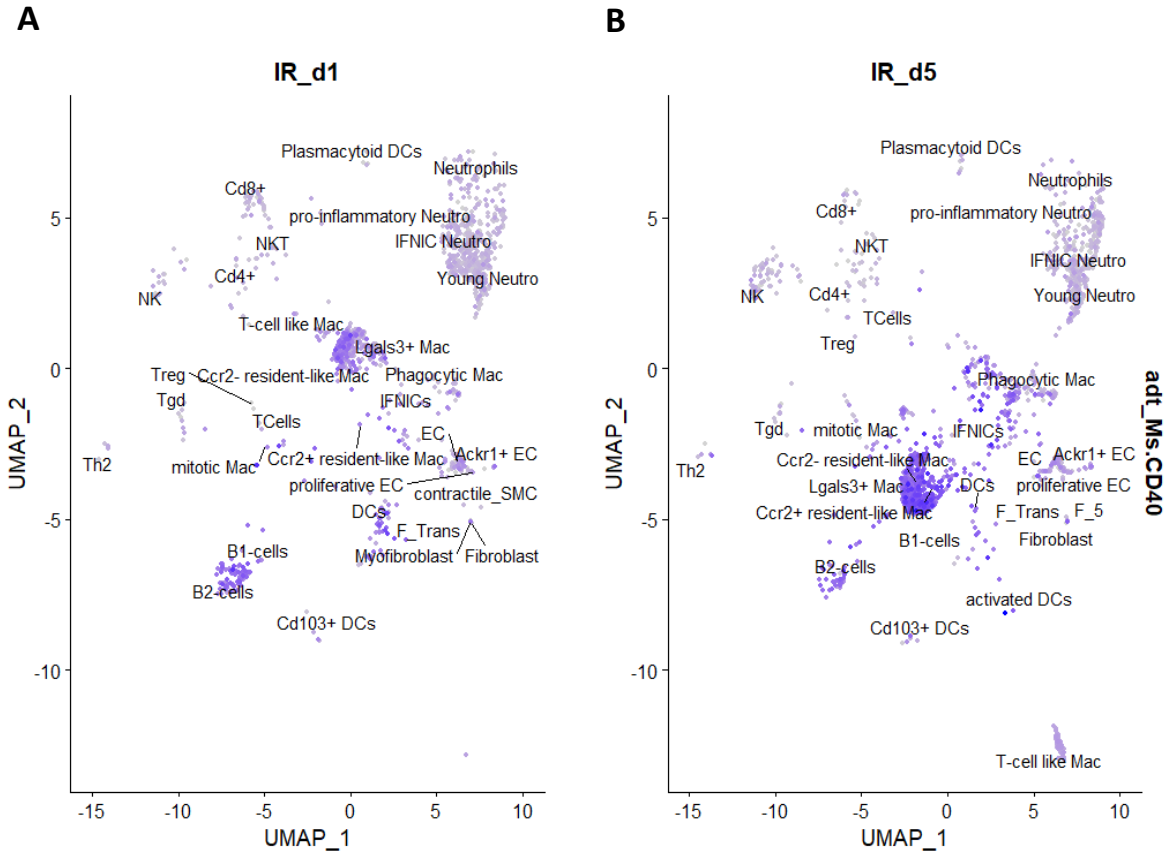

Figure 19: Single cell RNA sequencing reveals CD40 expression of immune cell populations 1 and 5 days after AMI. Hearts of two mice per condition were pooled for the analyses. Clustering CD45^{+} leukocytes at day 1 **(A)** or day 5 **(B)** by similar RNA expression patterns defines populations and subpopulations of immune cells. These clusters were than analyzed regarding their CD40 RNA expression levels.

To get a better insight about kinetics of CD40 expression on protein level during the acute healing phase, the mean fluorescence intensity (MFI) of CD40 on cardiac immune cells, especially on those expressing high levels of CD40 (**Fig.19**), including CD45^{+} leukocytes, CD11b^{+}/Ly6G^{-} monocytes and macrophages and CD19^{+} B cells, was measured at day 1, 3

and 5 after sham or AMI surgery. Sham-operated hearts contained less leukocytes compared to AMI, confirming the previous flow cytometry data, and showed an increase in CD40 MFI at day 3 that was reversed at day 5 to the level of day 1 (**Fig. 20 A**). In the leukocyte population of mice with AMI, a significant shift towards a higher CD40 MFI from day 1 to day 3 and day 1 to day 5 could be observed, while the level between day 3 and 5 remained mostly the same. Comparison between sham and AMI revealed a striking exaggeration of CD40 MFI following 5 days after AMI (**Fig. 20 A**). To get a closer look which subpopulations of immune cells, commonly expressing CD40, are responsible for this shift, the populations of $CD11b^{+}/Ly6G^{-}$ monocytes and macrophages (**Fig. 20 B**) and also $CD19^{+}$ B cells (**Fig. 20 C**) were analyzed.

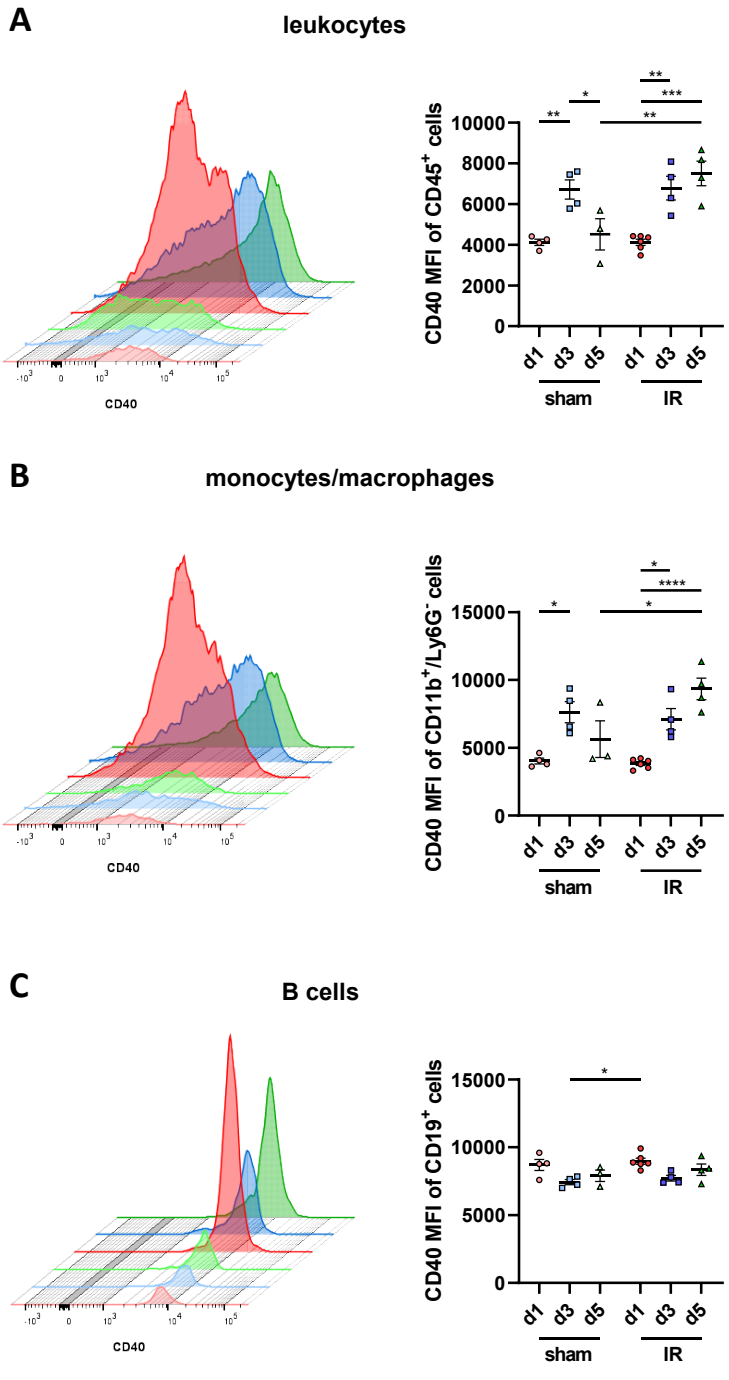

Figure 20: CD40 mean fluorescence intensity (MFI) of different immune cell populations at day 1, 3 and 5 after AMI. Expression of CD40 was measured using flow cytometry and displayed as MFI. Immune cell populations shown are **(A)** viable $CD45^{+}$ leukocytes; **(B)** $CD11b^{+}/Ly6G^{-}$ monocytes and macrophages; **(C)** B cells. For each population a representative histogram of CD40 expression for day 1 (red), day 3 (blue) and day 5 (green) is pointed out on the left side. First, three rows illustrating the sham and last three rows the AMI data. Detailed analysis of CD40 MFI for all mice over time is featured on the right side. N = 3-6. Data are presented as mean ± SEM. For statistical analysis, two-way ANOVA test with Tukey's multiple comparisons was used.

Monocytes and macrophages featured the same alterations in MFI of CD40 as the leukocyte population. Overall CD40 surface expression measured by flow cytometry on monocytes and macrophages increased steadily until day 5 after AMI, indicating that these cells are mostly responsible for the shift of CD40 positivity of all immune cells. In contrast, B cells did only change in overall numbers and the CD40 MFI remained the same in sham and AMI regarding day 1, 3 and 5.

4.3 Inhibition of CD40 signaling by TRAF-STOP in an *ex vivo* Langendorff model

Given the upregulated *Cd40* expression in the acute phase post AMI, we hypothesize that an inhibition of CD40 signaling has a beneficial effect on cardiac function and outcome after AMI. A first approach to investigate whether inhibiting CD40 signaling in an acute situation affects LV cardiac function was via an *ex-vivo* Langendorff model. This Langendorff model should provide information whether isolated mouse hearts respond to inhibition of CD40-TRAF6 signaling, via administration of TRAF-STOP, thus exhibiting an improved cardiac recovery. Therefore, hearts were mounted inside the LD apparatus and baseline parameters for LVPD, +dP/dt, -dP/dt and coronary flow were measured. Then hearts were loaded with blood from a littermate mouse either containing TRAF-STOP or corresponding vehicle control during 40 min global ischemia. Thereafter, hearts underwent one hour of reperfusion and functional parameters were assessed again, to calculate the percentage of recovery after global ischemia in relation to baseline values. Taking functional parameters into account, a treatment with TRAF-STOP during global ischemia had no effect on cardiac recovery (**Fig. 21**). These results may occur due to the relative short application time of TRAF-STOP or because of the *ex vivo* model, that excludes the influence of other components like immune response. Hence, following experiments concentrate on the effects of CD40 signaling modulation in an *in vivo* state to include and better understand the interactions of the whole organism.

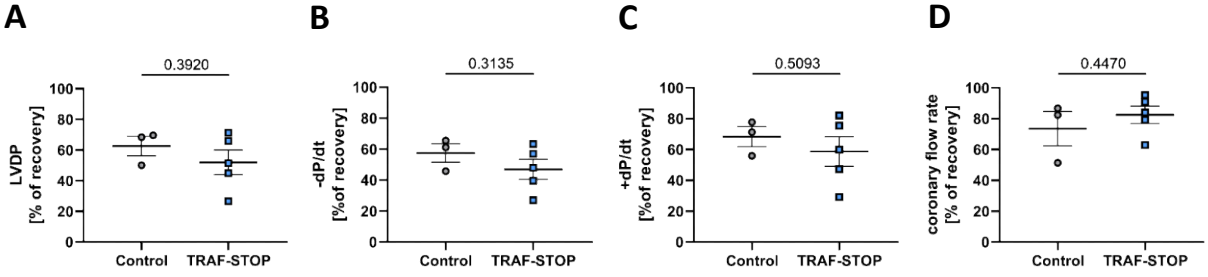

Figure 21: Inhibition of CD40-TRAF6 signaling does not alter cardiac function in an *ex vivo* Langendorff IR model. Isolated hearts were exposed to blood enriched with either TRAF-STOP or vehicle control during 40 min ischemia. **(A)** LVDP, **(B)** -dP/dt, **(C)** +dP/dt, and **(D)** coronary flow were assessed after 60 minutes of reperfusion and are expressed in percentage of the preischemic baseline values. N = 3 (control), 5 (TRAF-STOP). Data are presented as mean ± SEM. Statistical analyses were performed using unpaired t-test.

4.4 Preconditional inhibition of CD40 signaling by TRAF-STOP prior to AMI

4.4.1 Acute effects of TRAF-STOP treatment 24 h after AMI

Signaling of CD40/CD40L axis plays a major role during immune response by driving inflammation and healing processes. Nevertheless, prolonged inflammation after AMI can lead to a worsened outcome, making reduction of inflammation, by inhibition of CD40 signaling a potential target to overcome this aggravation. Therefore, CD40 inhibition, induced by injecting mice TRAF-STOP, was performed over a long-term treatment protocol including a preconditioning phase, starting 7 days before IR surgery and continued afterwards (**Fig. 9 A**). At first, the end point of 24 h after AMI induction was analyzed to see whether preconditional inhibition of CD40 itself effects cardiac function, immune cell distribution and infarct size. Cardiac function of control- and TRAF-STOP-treated mice was monitored by echocardiography 24 h after AMI induction. None of the assessed echocardiographic parameters displayed any changes comparing the control and TRAF-STOP group (**Fig. 22**). Hence, LV cardiac function appears not to be affected by preconditional CD40 inhibition.

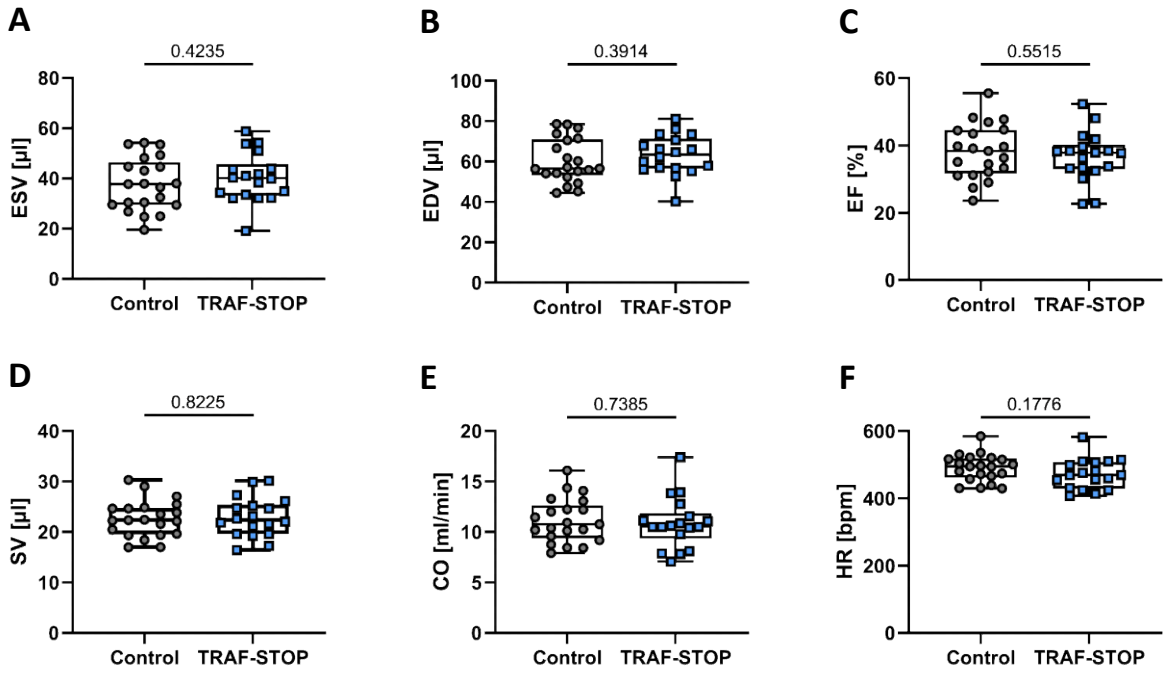

Figure 22: Preconditional TRAF-STOP treatment has no effect on LV function 24 h after AMI. Mice were either treated with TRAF-STOP or vehicle control starting 7 days before IR surgery. After 24 h of reperfusion, mice were subjected to echocardiography to analyze LV function by assessing following parameters: **(A)** End-systolic volume (ESV), **(B)** End-diastolic volume, **(C)** ejection fraction (EF), **(D)** stroke volume (SV), **(E)** cardiac output, **(F)** heart rate (HR). N = 18 (control), 21 (TRAF-STOP). Data are presented as box and whiskers plot with minimum and maximum. Statistical analyses were performed using unpaired t-test.

Given the fact, that TRAF-STOP inhibits CD40-TRAF6 interaction, which is the main CD40 signaling route in monocytes and macrophages, cardiac immune cell distribution was quantified using flow cytometry. The overall number of immune cells per heart was calculated and then divided by the heart weight to normalize it. Preconditional TRAF-STOP treatment did not affect numbers of cardiac $CD45^+$ leukocytes, $Ly6G^+$ neutrophils, $CD19^+$ B cells and $CD3^+$ T cells after 24 h of reperfusion (**Fig. 23 A-D**). Taking a closer look at $CD11b^+/Ly6G^-$ monocytes and macrophages as well as their subpopulations divided by their expression of Ly6C into $Ly6C^{low}$, $Ly6C^{intermediate}$ ($Ly6C^{int}$) and $Ly6C^{high}$, an overall reduction in their number was observed (**Fig. 23 E-H**). These findings suggest a hampered recruitment of monocytes and macrophages into the heart due to CD40 signaling inhibition, confirming the functionality of TRAF-STOP.

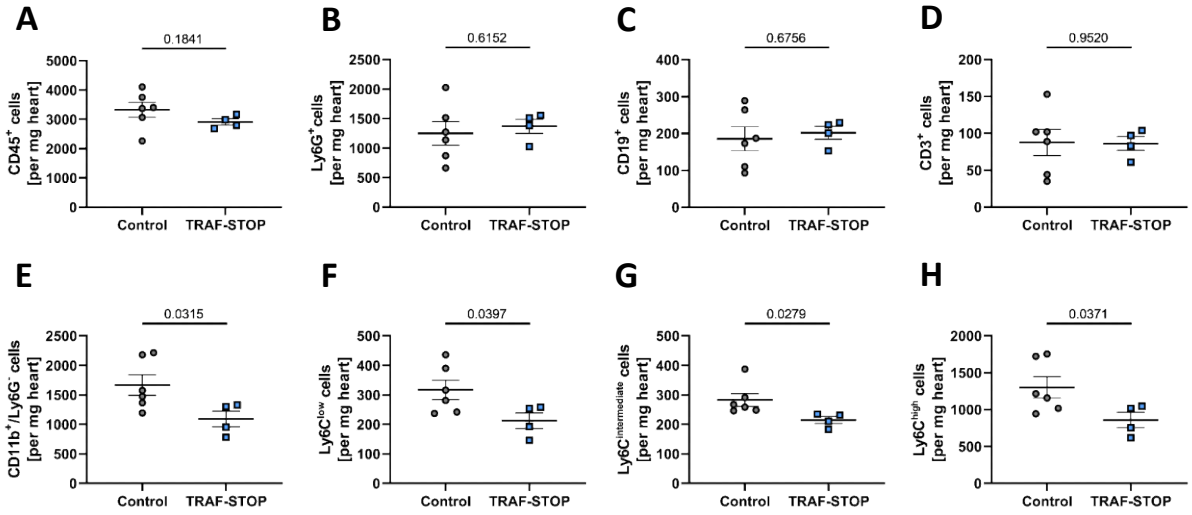

Figure 23: Preconditional TRAF-STOP treatment reduces amount of cardiac monocytes and macrophages 24 h post AMI. Mice were either treated with TRAF-STOP or vehicle control starting 7 days before IR surgery. 24 h after IR surgery mice were subjected to flow cytometry. CD40 inhibition via TRAF-STOP did not change quantity of cardiac **(A)** $CD45^+$ leukocytes, **(B)** $Ly6G^+$ neutrophils, **(C)** $CD19^+$ B cells and **(D)** $CD3^+$ T cells. However, TRAF-STOP treatment reduced the amount of cardiac **(E)** $CD11b^+/Ly6G^-$ monocytes and macrophages and of their subpopulations divided into **(F)** $Ly6C^{low}$, **(G)** $Ly6C^{int}$ and **(H)** $Ly6C^{high}$. N = 6 (control), 4 (TRAF-STOP). Data are presented as mean ± SEM. Statistical analyses were performed using unpaired t-test with Welch's correction.

Although no changes in cardiac function were observed upon TRAF-STOP treatment, it was checked via structural analysis, whether less monocyte and macrophage recruitment could affect infarct size after preconditional TRAF-STOP using TTC method. Therefore, explanted hearts underwent a series of stainings, making detection of infarct area (INF), area at risk (AAR) and healthy tissue possible (**Fig. 24 A**). The percentage of INF per LV as well as the AAR per LV were not altered between control and TRAF-STOP treated mice (**Fig. 24 B-C**). Consequently, no statistically significant differences for INF per AAR (**Fig. 24 D**) comparing control and TRAF-STOP treated mice could be observed, indicating no modification of infarct sizes due to preconditional CD40 inhibition.

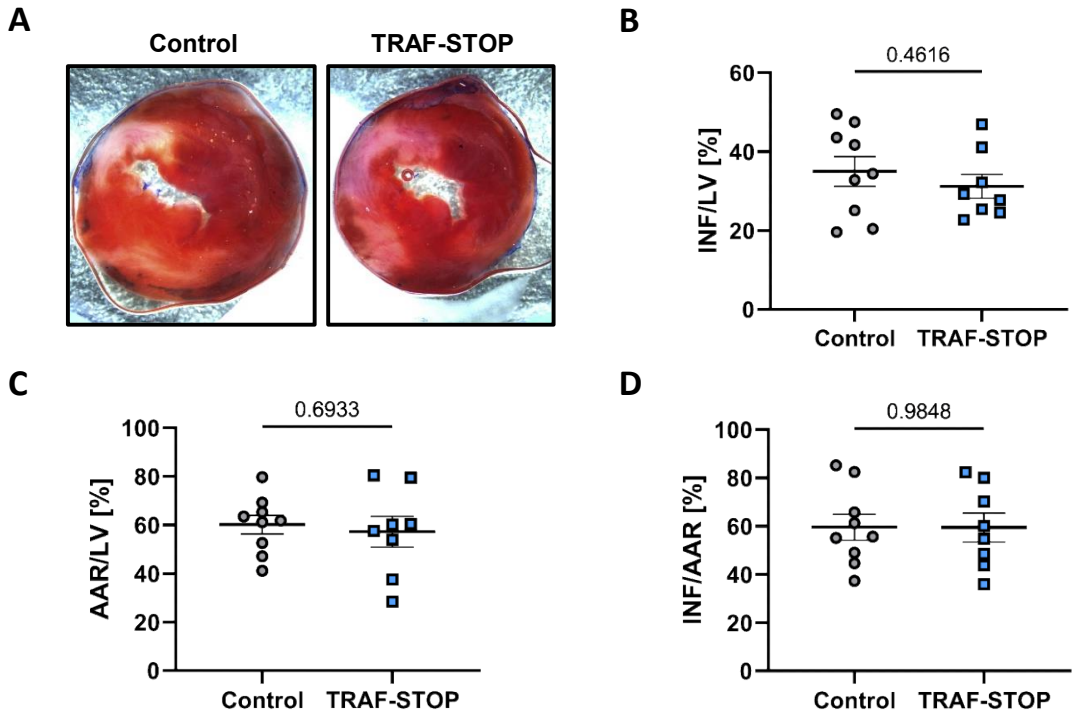

Figure 24: Infarct size is not altered by preconditional TRAF-STOP treatment at day 1 after AMI. Preconditionally-treated mice either receiving TRAF-STOP or vehicle control underwent IR surgery and 24 h later infarct size was determined by TTC staining. **(A)** Representative images of heart sections after Evans Blue and TTC staining. **(B)** Percentage of infarct size (INF) per left ventricle (LV). **(C)** Percentage of AAR per LV. **(D)** Percentage of INF per AAR. N = 9 (control), 8 (TRAF-STOP). Data are presented as mean ± SEM. Statistical analysis was performed using unpaired t-test.

4.4.2 Effects of continuous TRAF-STOP treatment in the late phase 28 days after AMI

The fact that preconditional TRAF-STOP treatment already altered immune cell distribution, specifically that of monocytes and macrophages 24 h post AMI, but did not affect cardiac function and infarct size, can possibly be explained by the time point chosen for analysis. It is conceivable that later end points after AMI induction are more eligible to reveal changes in functional, immunological and structural outcome, since they include healing and maturation processes. Accordingly, the treatment protocol was adapted so that mice, preconditional-treated with TRAF-STOP and after receiving AMI induction, were continuously injected with TRAF-STOP (3x per week) or control vehicle until the end point of 28 days. During the complete experimental period of TRAF-STOP treatment, cardiac function of mice was monitored via echocardiography once a week, at day 1 (**Fig. 22**), 7, 14, 21 and 28 after AMI, to check for changes over time. For all these time points no statistically significant alterations in cardiac parameters could be identified. As day 28 was the end point, at which also the immune cell distribution was analyzed, only representative data for cardiac function of this particular time point is shown (**Fig. 25**).

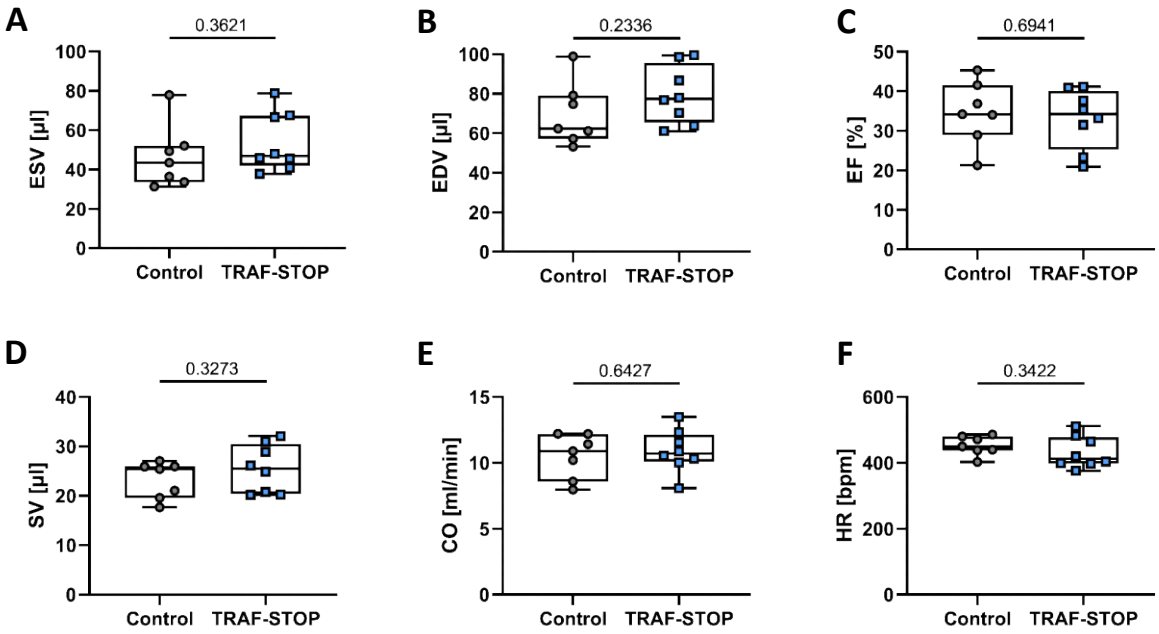

Figure 25: Continuous TRAF-STOP treatment until late healing phase does not affect cardiac function at day 28 post AMI. Prior to and after IR surgery, mice were continuously treated with either TRAF-STOP or vehicle control until 28 day after AMI. Following 28 days of reperfusion mice were subjected to echocardiography to analyze LV function by assessing following parameters: **(A)** End-systolic volume (ESV), **(B)** End-diastolic volume, **(C)** ejection fraction (EF), **(D)** stroke volume (SV), **(E)** cardiac output, **(F)** heart rate (HR). N = 7 (control), 8 (TRAF-STOP). Data are presented as box and whiskers plot with minimum and maximum. Statistical analyses were performed using unpaired t-test.

Next, the immune cell distribution was investigated, to see whether the reduction of monocytes and macrophage numbers found at the early time point of 24 h after AMI persisted or if other diversification could be observed. As before, the number of immune cells per heart was measured using flow cytometry. Analyses of $CD45^+$ leukocyte numbers affirmed that there are overall less immune cells 28 days after AMI (**Fig. 26 A**) compared to the numbers at day 1 (**Fig. 23 A**). However, long-term CD40 inhibition did not alter the numbers of all investigated immune cell populations, including $CD11b^+/Ly6G^-$ monocytes and macrophages as well as their Ly6C-differentiated subpopulations (**Fig. 26 B-H**). On account of these immunological findings at day 28, the acute effect of TRAF-STOP treatment to diminish the numbers of monocytes and macrophages 24h after AMI is negated over time.

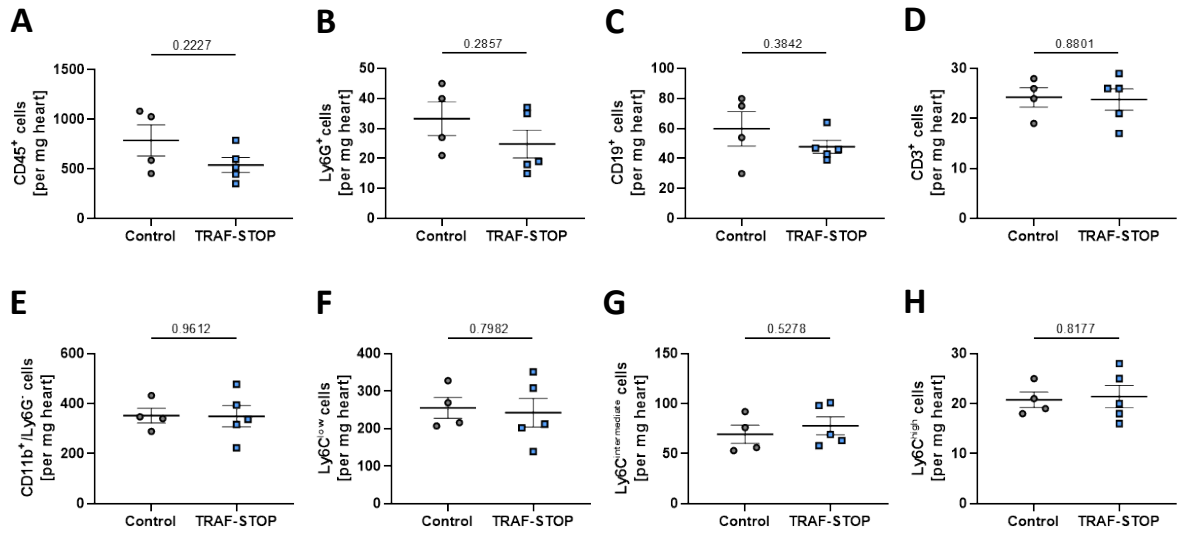

Figure 26: Continuous TRAF-STOP treatment until late healing phase does not alter cardiac immune cell numbers at day 28 post AMI. Prior to and after IR surgery, mice were continuously treated with either TRAF-STOP or vehicle control until 28 day after AMI. CD40 inhibition via TRAF-STOP did not change quantity of cardiac immune cells including **(A)** $CD45^+$ leukocytes, **(B)** $Ly6G^+$ neutrophils, **(C)** $CD19^+$ B cells, **(D)** $CD3^+$ T cells, **(E)** $CD11b^+/Ly6G^-$ monocytes/macrophages and their subpopulations divided into **(F)** $Ly6C^{low}$, **(G)** $Ly6C^{int}$ and **(H)** $Ly6C^{high}$. N = 4 (control), 5 (TRAF-STOP). Data are presented as mean ± SEM. Statistical analyses were performed using unpaired t-test with Welch's correction.

4.5 Inhibition of CD40 signaling by TRAF-STOP starting 5 days after AMI

The previous findings indicate that CD40 inhibition prior to AMI has no beneficial effect on infarct size and LV cardiac function. However, a reduction in monocyte numbers 24 h after AMI was determined, verifying inhibition of CD40 signaling on monocytes and macrophages due to TRAF-STOP treatment is functioning. Even after long-term TRAF-STOP treatment, covering all healing phases, there were no changes detectable. Taking this into account, a preconditional CD40 inhibition seems to be not the appropriate method as therapeutic approach for a better outcome after AMI. Knowing that CD40 expression during the first days in the acute phase after AMI is upregulated on gene and protein levels led to the hypothesis that CD40 signaling until day 5 post AMI is required during initial immune response and should not be inhibited. Whereas prolonged high levels of CD40 could be responsible for chronic inflammation deteriorating outcome after AMI. Therefore, a new TRAF-STOP treatment protocol was established, in that inhibition of CD40 was started at day 5 post AMI (**Fig. 9 B**). Mice were injected for 3 days per week until end points 14 and 28 days after IR surgery. End time points at day 14 and 28 were chosen to investigate, whether CD40 inhibition covering the subacute healing phase alone and for the later time point also the maturation phase alter cardiac function, quantity of immune cells and scar formation. First, LV cardiac function was evaluated via echocardiography at day 14 after AMI, unveiling a significantly increased EF, SV

and CO in mice treated with TRAF-STOP (**Fig. 27 C-E**) compared to control-treated animals. Meanwhile, ESV, EDV and HR stayed unchanged (**Fig. 27 A, B, F**). Significant elevation of EF, SV and CO indicates a beneficial effect of CD40 inhibition starting day 5 after AMI on the LV heart function already at day 14.

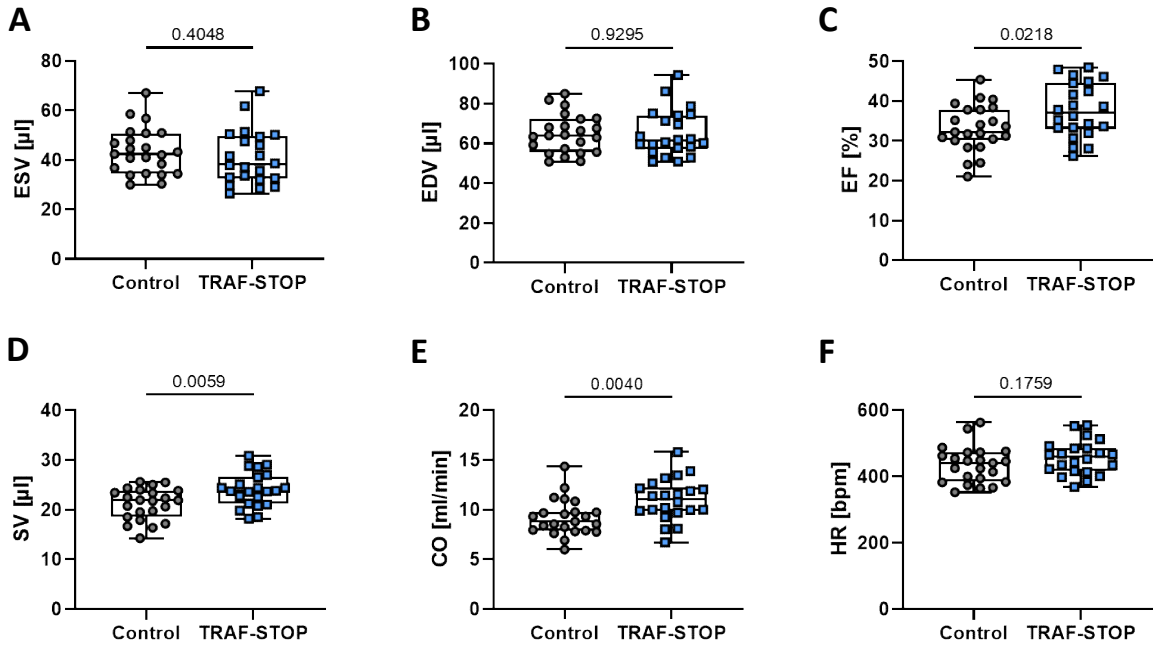

Figure 27: CD40 inhibition starting day 5 post AMI improves LV function at day 14. From day 5 until day 14 post AMI mice were injected with TRAF-STOP or vehicle control 3 times a week. Finally, mice underwent echocardiography to obtain following parameters: **(A)** End-systolic volume (ESV), **(B)** End-diastolic volume, **(C)** ejection fraction (EF), **(D)** stroke volume (SV), **(E)** cardiac output, **(F)** heart rate (HR). EF, SV and CO were significantly elevated displaying a beneficial influence of TRAF-STOP treatment on LV function. N = 23 (control), 22 (TRAF-STOP). Data are presented as box and whiskers plot with minimum and maximum. Statistical analyses were performed using unpaired t-test.

To test the persistence of this beneficial effect of TRAF-STOP treatment at day 14, mice at day 28 post AMI also underwent echocardiography. At the end point of 28 days no differences between control- and TRAF-STOP-treated mice could be observed in reference to ESV, EDV and HR (**Fig. 28 A, B, F**). Simultaneously, only a nearly significant trend for EF was recorded, while SV and CO were significantly increased (**Fig. 28 C-E**). Taking the elevation of SV and CO after CD40 inhibition into account validates that the improvement in heart function is preserved over time.

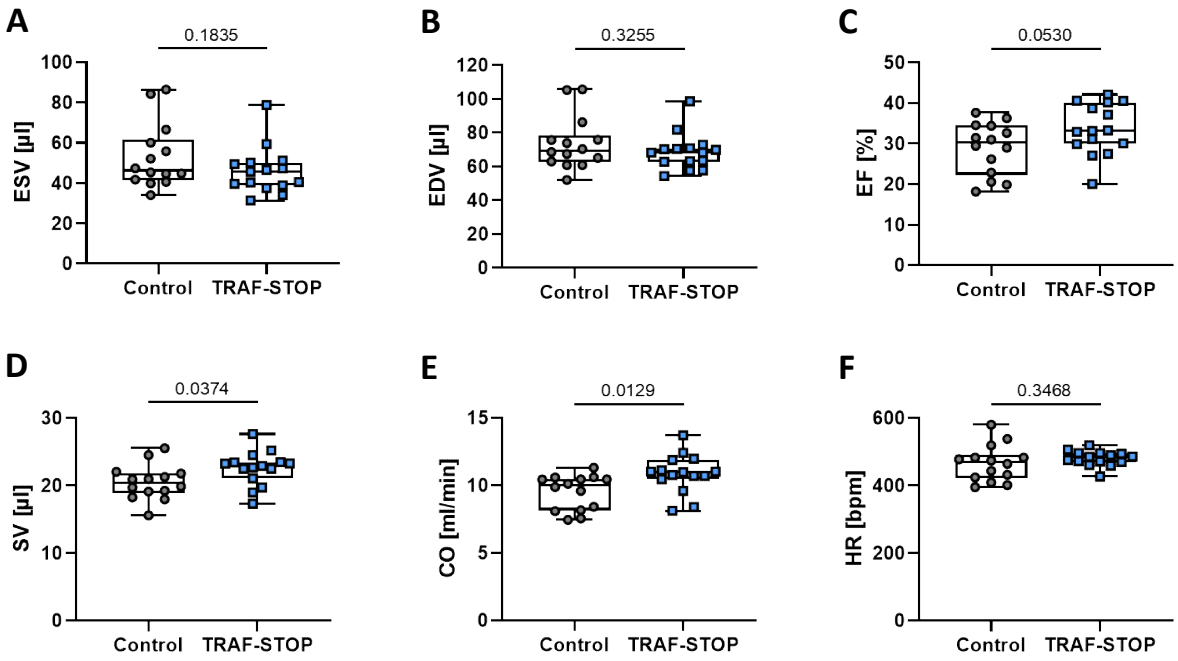

Figure 28: LV function is improved at day 28 after CD40 inhibition starting day 5 post AMI. From day 5 until day 28 post AMI mice were injected with TRAF-STOP or vehicle control 3 times a week. Finally, mice underwent echocardiography to obtain following parameters: **(A)** End-systolic volume (ESV), **(B)** End-diastolic volume, **(C)** ejection fraction (EF), **(D)** stroke volume (SV), **(E)** cardiac output, **(F)** heart rate (HR). SV and CO were significantly increased displaying a beneficial influence of TRAF-STOP treatment on LV function. N = 14 (control), 15 (TRAF-STOP). Data are presented as box and whiskers plot with minimum and maximum. Statistical analyses were performed using unpaired t-test.

Following the analyses of cardiac function, the immune cell distribution at day 14 after AMI was measured by covering the same populations via flow cytometry as previously shown. However, in the subacute phase lymphocytes were more prominent, so an additional antibody panel was used to also include further subpopulations of T cells. The overall numbers of $CD45^+$ leukocytes per mg heart of TRAF-STOP-treated mice remained at a similar level as of the control group (**Fig. 29 A**). Even after an in-depth characterization of leukocytes into $Ly6G^+$ neutrophils, $CD19^+$ B cells, $CD3^+$ T cells $CD11b^+/Ly6G^-$ monocytes and macrophages, no changes in these populations could be discovered (**Fig. 29 B-D, I**). This was also true for subpopulations of T cells, including $CD4^+$ Th cells, $CD4^+/FoxP3^+$ T_{reg} cells, $CD8^+$ cytotoxic T cells and the ratio of T helper to cytotoxic T cells (**Fig. 29 E-H**). Finally, the number of cells from monocyte and macrophage subpopulations remained constant (**Fig. 29 J-L**). In summary, cardiac immune cell composition at day 14 after AMI was not modified upon CD40 inhibition starting from day 5 post AMI.

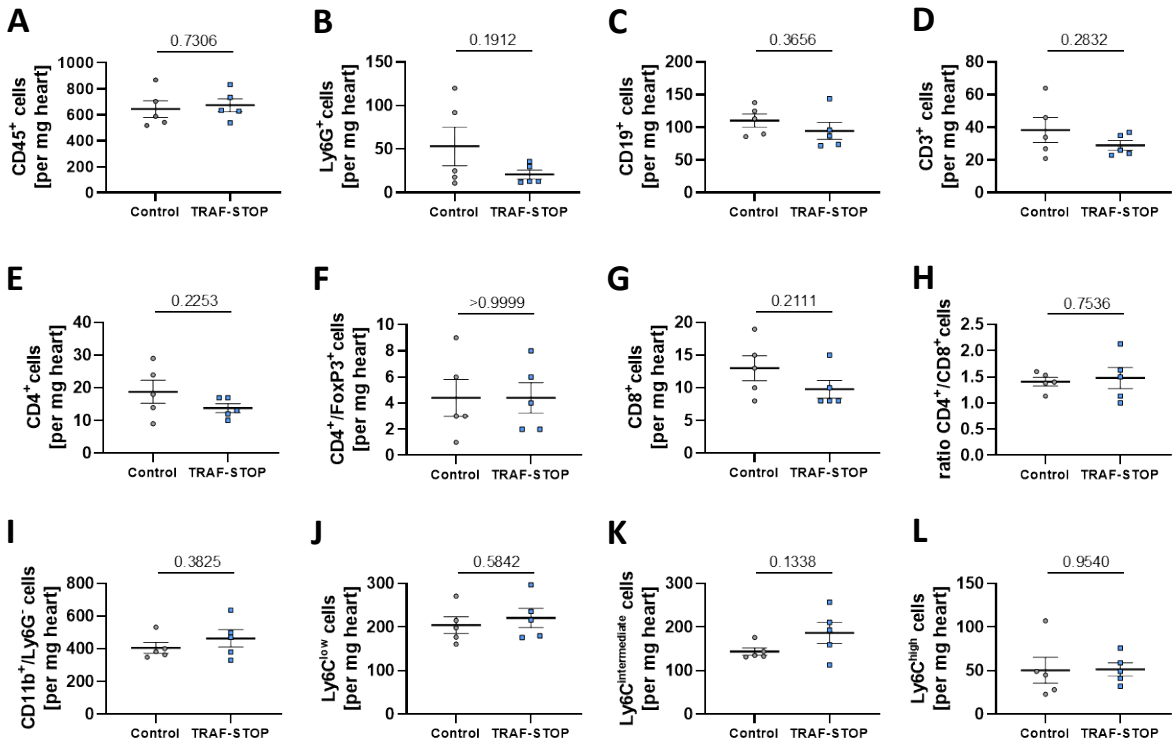

Figure 29: TRAF-STOP treatment during the subacute healing phase does not alter cardiac immune cell numbers at day 14 post AMI. Starting 5 days after IR surgery mice were injected with TRAF-STOP or vehicle control 3 times per week until day 14 post AMI. CD40 inhibition via TRAF-STOP did not change quantity of cardiac immune cells including **(A)** $CD45^+$ leukocytes, **(B)** $Ly6G^+$ neutrophils, **(C)** $CD19^+$ B cells, **(D)** $CD3^+$ T cells, **(E)** $CD4^+$ T helper cells, **(F)** $CD4^+/FoxP3^+$ regulatory T cells, **(G)** $CD8^+$ cytotoxic T cells, **(H)** ratio of $CD4^+$ to $CD8^+$ T cells, **(I)** $CD11b^+/Ly6G^-$ monocytes/macrophages and their subpopulations divided into **(J)** $Ly6C^{low}$, **(K)** $Ly6C^{int}$ and **(L)** $Ly6C^{high}$. N = 4 (control), 5 (TRAF-STOP). Data are presented as mean ± SEM. Statistical analyses were performed using unpaired t-test.

Even though immune cell distribution was not altered at day 14 post AMI, quantitative flow cytometry analyses of immune cells was performed to disclose if this still persists at day 28. All of the superordinate immune cell populations consisting of leukocytes, neutrophils, B cells, T cells and monocytes/macrophages remained unchanged in total numbers after TRAF-STOP administration (**Fig. 30 A-D, I**). Furthermore, the distribution of T cell subpopulations as well as the ratio of T helper to cytotoxic T cells was not affected (**Fig. 30 E-H**). Nevertheless, the analyses of monocyte and macrophage subpopulations revealed a statistically significant decrease of anti-inflammatory $Ly6C^{low}$ cells, whereas the other populations of $Ly6C^{int}$ and $Ly6C^{high}$ featured no alteration (**Fig. 30 J-L**). In total, this was the only change observed in immune cell distribution at day 14 and 28 after AMI upon TRAF-STOP treatment beginning at day 5 post AMI compared to controls.

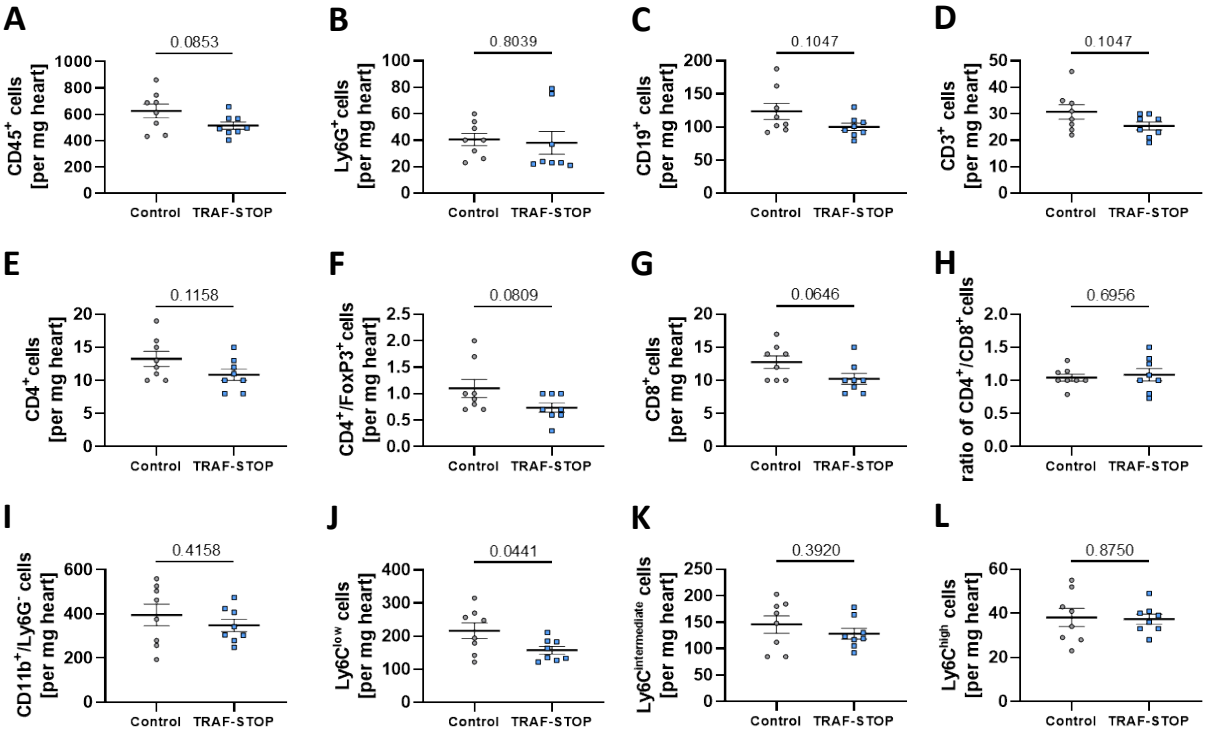

Figure 30: TRAF-STOP treatment starting in the subacute healing phase decreases number of anti-inflammatory Ly6C^{low} monocytes/macrophages at day 28 post AMI. Starting 5 days after IR surgery mice were continuously injected with TRAF-STOP or vehicle control for 3 days per week until day 28 post AMI. Quantity of following cardiac immune cell populations was not altered: **(A)** CD45$^+$ leukocytes, **(B)** Ly6G$^+$ neutrophils, **(C)** CD19$^+$ B cells, **(D)** CD3$^+$ T cells, **(E)** CD4$^+$ T helper cells, **(F)** CD4$^+$/FoxP3$^+$ regulatory T cells, **(G)** CD8$^+$ cytotoxic T cells, **(H)** ratio of CD4$^+$ to CD8$^+$ T cells, **(I)** CD11b$^+$/Ly6G$^-$ monocytes/macrophages. CD40 inhibition diminished amount of **(J)** Ly6C^{low}, while **(K)** Ly6C^{int} and **(L)** Ly6C^{high} remained unchanged. N = 8 (control), 8 (TRAF-STOP). Data are presented as mean ± SEM. Statistical analyses were performed using unpaired t-test.

Improvement in cardiac function frequently goes hand in hand with favorable changes in cardiac remodelling. In fact, excessive fibrosis leading to enhanced scar formation can impede proper cardiac function. To see whether inhibition with TRAF-STOP led to alterations in the LV morphology at day 14 post AMI, scar size was measured via histological staining of WGA and phalloidin. Combined staining using WGA, marking the fibrotic fibers, and phalloidin, that stains actin and therefore viable cardiomyocytes, allowed evaluation of the scar size per LV (**Fig. 31 A**). To measure the scar size over the entire infarct area, the hearts were sectioned over distinct distances beginning from the apex. Comparison between control and TRAF-STOP-treated mice, revealed a decreased scar size over all sections (**Fig. 31 B**). This was supported by a significant decline in the total mean scar size of the LV (**Fig. 31 C**). This structural modification of a smaller scar size after CD40 inhibition starting in the subacute phase is a possible explanation for the improved cardiac function at day 14 post AMI.

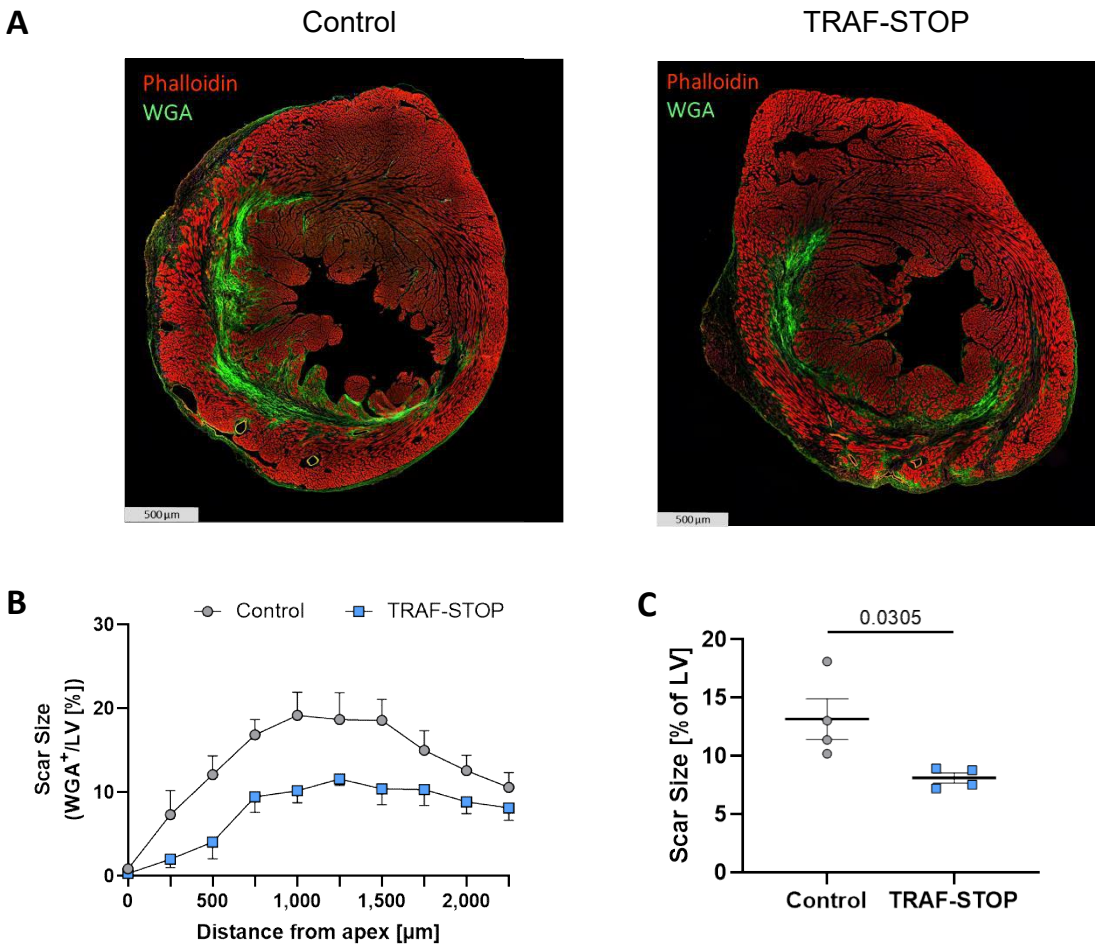

Figure 31: Reduction of scar size at day 14 due to CD40 inhibition starting from day 5 post AMI. **(A)** Representative heart sections stained with phalloidin (red) and WGA (green) at day 14 after TRAF-STOP treatment starting day 5 post AMI. **(B)** Scar size was determined by WGA signal per LV over different sections from apex to basis of the heart revealing a smaller scar size in TRAF-STOP-treated mice. **(C)** Comparison of the total scar size per LV displays a significant decrease of scar size due to CD40 inhibition. N = 4. Data are presented as mean ± SEM. Statistical analyses were performed using unpaired t-test.

Since, the heart function at day 28 post AMI was still improved, the question arose whether the structural changes regarding the scar size found at day 14 also persisted until day 28. Again, scar sizes were determined using histological stainings via WGA and phalloidin (**Fig. 32 A**). Irrespective of the treatment, the overall scar size increased in comparison with that observed at day 14, most likely due to maturation over time. However, the decrease in scar size in all assessed sections persisted and much stronger differences between control and TRAF-STOP-treated mice could be noticed (**Fig. 32 B**). Comparison of the total scar size of the LV supported these findings, unveiling a statistically significant reduction of scar size following inhibition of CD40 signaling starting from day 5 post AMI (**Fig. 32 C**). Again, the smaller scar size induced by TRAF-STOP treatment seems to be the most probable reason for the improved LV cardiac function at day 28 after AMI.

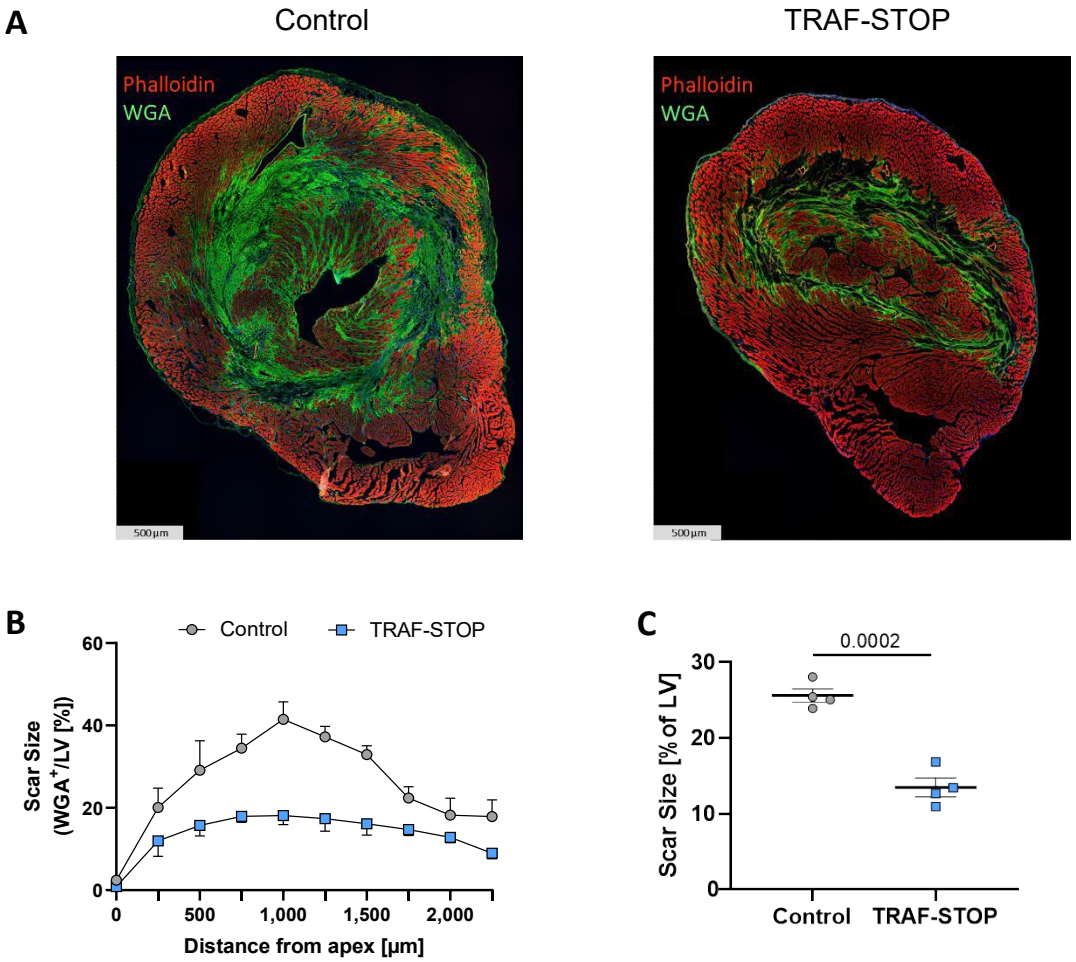

Figure 32: Reduction of scar size at day 28 following CD40 inhibition starting at day 5 post AMI. **(A)** Representative heart sections stained with phalloidin (red) and WGA (green) at day 14 after TRAF-STOP treatment starting day 5 post AMI. **(B)** Scar size was determined by WGA signal per LV over different sections from apex to basis of the heart revealing a smaller scar sizes in TRAF-STOP treated mice. **(C)** Comparison of the total scar size per LV displays a significant decrease of scar size due to CD40 inhibition. N = 4. Data are presented as mean ± SEM. Statistical analyses were performed using unpaired t-test.

In summary, treatment with TRAF-STOP starting at day 5 post AMI only led to minor changes in immune cell composition by reducing Ly6C^{low} monocytes and macrophages at day 28. Nevertheless, an improved LV heart function and smaller scar size at day 14 and day 28 were discovered, making CD40 inhibition after AMI a promising approach to influence cardiac repair and outcome in a favorable way.

4.6 Effect of CD40 activation via an agonistic antibody after AMI

Considering that inhibition of CD40 seems to be critically dependent on the time point of treatment initiation, and inflammatory processes driven by CD40/CD40L signaling appear to be vital in the acute phase after AMI and should not be halted, the next step was to investigate how additional activation of CD40 in the acute phase may affect cardiac outcome. Therefore, an agonistic CD40 antibody (αCD40) was used to mimic high levels of CD40L. To investigate, whether CD40 activation leads to changes in immune cell composition, mice received either αCD40 or an IgG2a isotype control at day 7 and day 1 before the usual time point of IR surgery, but AMI was not induced. According to the experimental setup, hearts were removed 24 h later (**Fig. 10 A**). Flow cytometric analyses displayed significant alterations of cardiac immune cell numbers, which were only induced by mimicking high levels of CD40L. The most prominent finding was the significant reduction of $CD19^+$ B cells numbers (**Fig. 33 C**). Although, the total number of $CD3^+$ T cells was not altered, the subpopulation of $CD4^+$ Th cells showed a decrease after αCD40 treatment, resulting in a changed $CD4^+/CD8^+$ ratio (**Fig. 33 E-H**). The αCD40 treatment resulted in lowered numbers of $Ly6C^{low}$ and $Ly6C^{int}$ populations, while $Ly6C^{high}$ cells remained constant (**Fig. 33 J-L**). These remarkable shifts of immune cell patterns in the heart upon treatment with αCD40 may predispose the heart for less-favorable outcomes following injury such as AMI, as investigated in the following experiments.

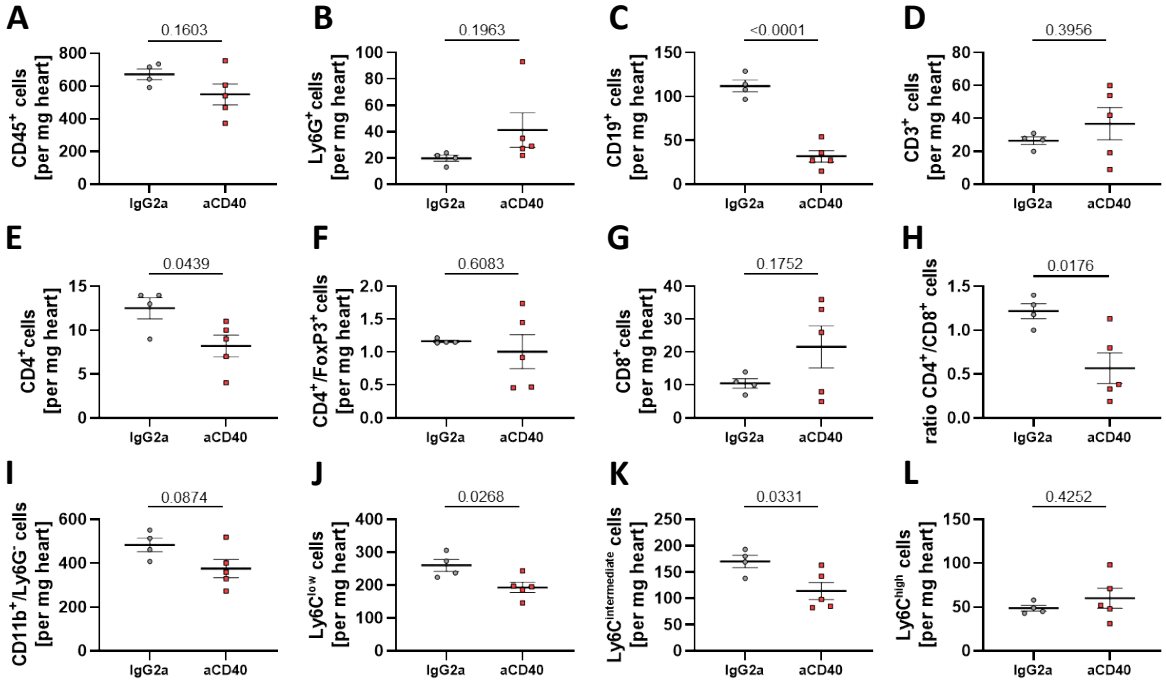

Figure 33: Basal αCD40 treatment alters cardiac immune cell populations. Mice received either αCD40 or IgG2a at day 7 and 1 before actual IR surgery. 24 h later hearts were removed and analyzed by flow cytometry. CD40 activation led to a decrease of **(C)** $CD19^+$ B cells, **(E)** $CD4^+$ T helper cells, **(H)** ratio of $CD4^+$ to $CD8^+$ T cells, **(J)** $Ly6C^{low}$, and **(K)** $Ly6C^{int}$ monocytes/macrophages while all other populations did not vary: **(A)** $CD45^+$ leukocytes, **(B)** $Ly6G^+$ neutrophils, **(D)** $CD3^+$ T cells, **(F)** $CD4^+/FoxP3^+$ regulatory T cells, **(G)** $CD8^+$ cytotoxic T cells, **(I)** $CD11b^+/Ly6G^-$, and **(L)** $Ly6C^{high}$ monocytes/macrophages. N = 4 (IgG2a), 5 (αCD40). Data are presented as mean ± SEM. Statistical analyses were performed using unpaired t-test.

Mice were treated once with either αCD40 or an IgG2a isotype control directly after IR surgery and sacrificed at end points day 1 and day 7 following AMI. The early time point of 24h after IR should reveal whether a single dose of CD40-activating antibody already affects immune cell composition, cardiac function and infarct size. During organ harvesting it was noticed that spleens were larger in mice injected with αCD40. To validate the visible impression spleens were excised and weighed. Comparison of spleen weights between αCD40- and control-treated mice confirmed that spleens were heavier, thus confirming a splenomegaly after CD40 activation (**Fig. 34 A**). Additionally, ratio of spleen weight towards body weight (SW/BW) of mice was calculated, to exclude that merely a higher body weight is the reason of heavier spleens. A significant increase of SW/BW proves that the splenomegaly cannot be explained by heavier mice and is a side effect of αCD40 treatment (**Fig. 34 B**). Given this influence of αCD40 on spleens, the heart weight was checked, yet no alterations of weight and ratio of heart weight towards body weight (HW/BW) were found (**Fig. 34 C-D**).

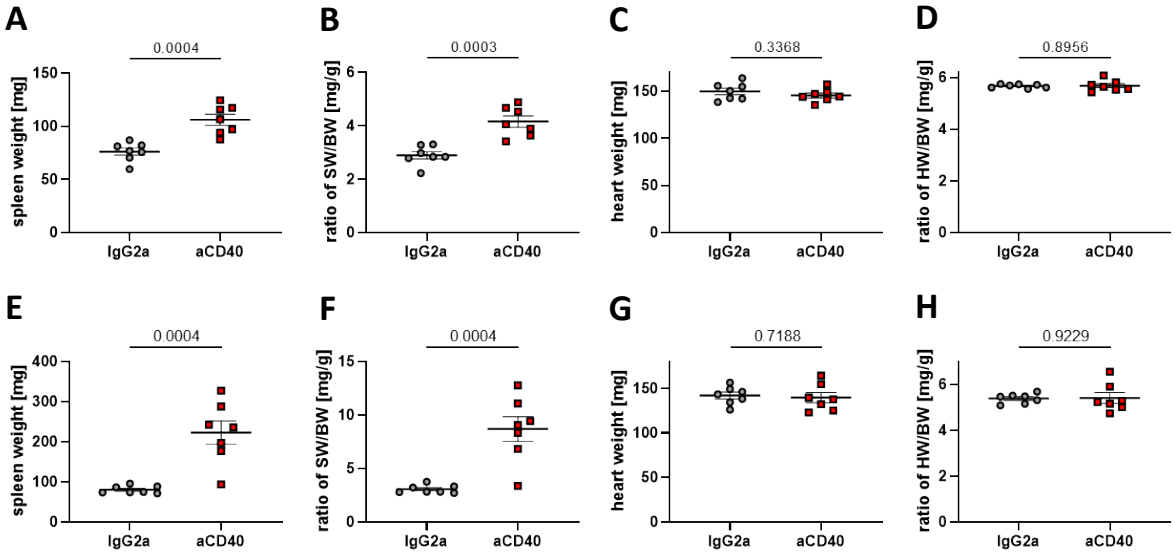

Figure 34: CD40 activation causes splenomegaly at day 1 and 7 post AMI. 24 h **(A-D)** and 7 days **(E-H)** after mice received either one dose of αCD40 or IgG2a post AMI, spleens and hearts were explanted and weighed before further procession. **(A, E)** Spleens weight; **(B, F)** ratio of spleen to body weight; **(C, G)** heart weights and **(D, H)** ratio of heart to body weight. N = 7. Data are presented as mean ± SEM. Statistical analyses were performed using unpaired t-test **(A-D)** and Mann-Whitney test **(E-H)**.

To check whether the splenomegaly is still present at day 7 after AMI and αCD40 treatment, spleen weights were measured, revealing a twofold increase in average weight. In comparison to the findings at day 1 (**Fig. 34 A**) these spleens were even heavier when CD40 was activated (**Fig. 34 E**). Beyond that, elevation of SW towards BW ratio confirmed that αCD40 treatment is the reason for the splenomegaly (**Fig. 34 F**). Visually all other organs including the hearts appeared to be macroscopically unaffected after CD40 activation, supported by no differences in heart weight regarding αCD40- and IgG2a-treated mice (**Fig. 34 G-H**).

In the course of flow cytometry analyses of cardiac immune cells 24 h after AMI and αCD40 administration a decrease of anti-inflammatory Ly6C^{low} monocytes and macrophages was found (**Fig. 35 J**). The overall numbers of monocytes and macrophages as well as their subpopulations remained constant (**Fig. 35 I, K, L**). Moreover, there were no changes visible in numbers of leukocytes, neutrophils, B cells, T cells and T cell subpopulations (**Fig. 35 A-H**). Thus, the decline of Ly6C^{low} cells is a specific finding at 24 h after αCD40 treatment.

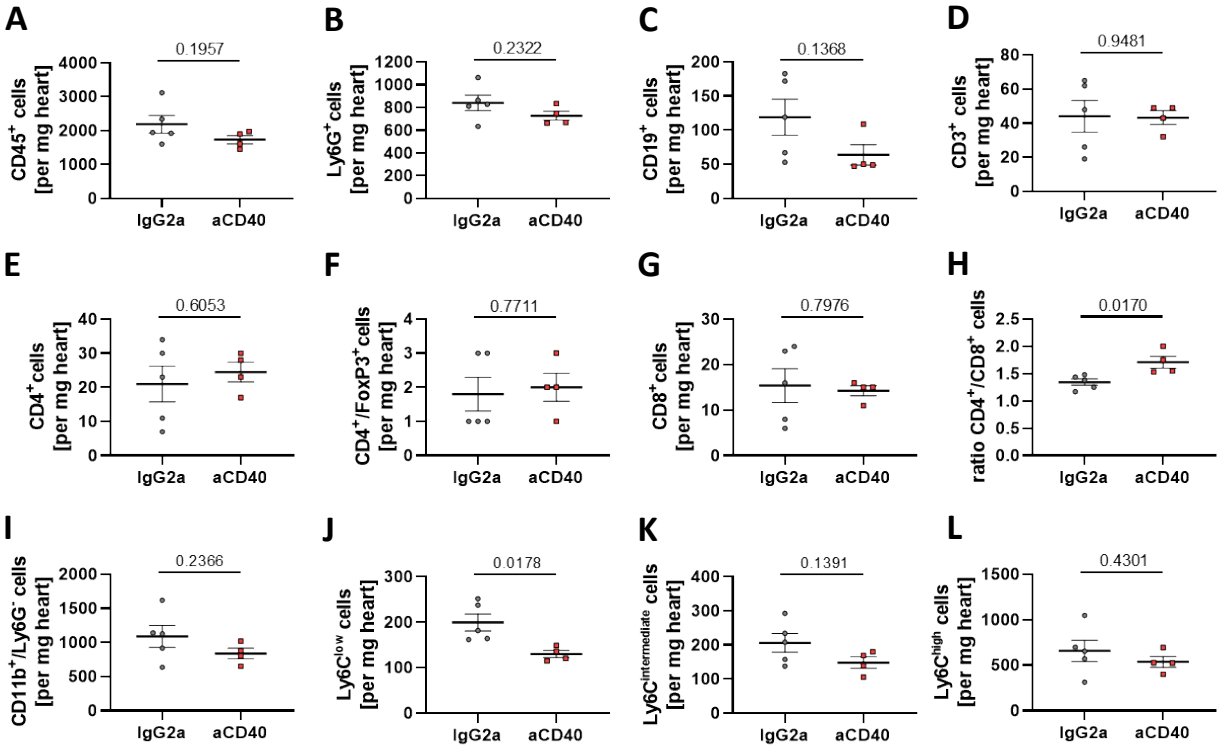

Figure 35: Quantity of cardiac anti-inflammatory Ly6C^{low} monocytes and macrophages after CD40 activation is diminished at day 1 post AMI. Directly after IR surgery mice received one dose of either αCD40 or IgG2a. 24 h after IR hearts were digested and numbers of cardiac immune cells were measured by flow cytometry. CD40 activation led to a decrease of **(J)** Ly6C^{low} monocytes/macrophages while all other populations did not vary: **(A)** CD45$^+$ leukocytes, **(B)** Ly6G$^+$ neutrophils, **(C)** CD19$^+$ B cells, **(D)** CD3$^+$ T cells, **(E)** CD4$^+$ T helper cells, **(F)** CD4$^+$/FoxP3$^+$ regulatory T cells, **(G)** CD8$^+$ cytotoxic T cells, **(H)** ratio of CD4$^+$ to CD8$^+$ T cells, **(I)** CD11b$^+$/Ly6G$^-$, **(K)** Ly6C^{int} and **(L)** Ly6C^{high} monocytes/macrophages. N = 5 (IgG2a), 4 (αCD40). Data are presented as mean ± SEM. Statistical analyses were performed using unpaired t-test.

Next, the end point of 7 days after AMI and application of one dose of αCD40 was investigated. When monitoring cardiac immune cells, numbers of CD45$^+$ leukocytes, Ly6G$^+$ neutrophils and CD11b$^+$/Ly6G$^-$ monocytes and macrophages, including subpopulations showed no significant variation, while lymphocytes displayed large alterations (**Fig. 36**). CD40 activation significantly reduced the amount of CD19$^+$ B cells within the myocardium and by tendency increased quantity of CD3$^+$ T cells. Interestingly, both major T cell subpopulations appeared to have a contrary development of cell numbers. CD4$^+$ helper T cell count seemed to be tendentially decreased whereas CD8$^+$ cytotoxic T cells were significantly raised, resulting in a massive

change of their ratio. In addition, a decline of regulatory CD4⁺/FoxP3⁺ T cells was noticed (**Fig. 36 F**). In summary, the immune response at day 7 after AMI and CD40 activation is mainly altered in reference to lymphocyte numbers, whereas the situation at day 1 after AMI only shows a specific reduction of anti-inflammatory monocytes and macrophages that is abrogated over time and can no longer be found at day 7.

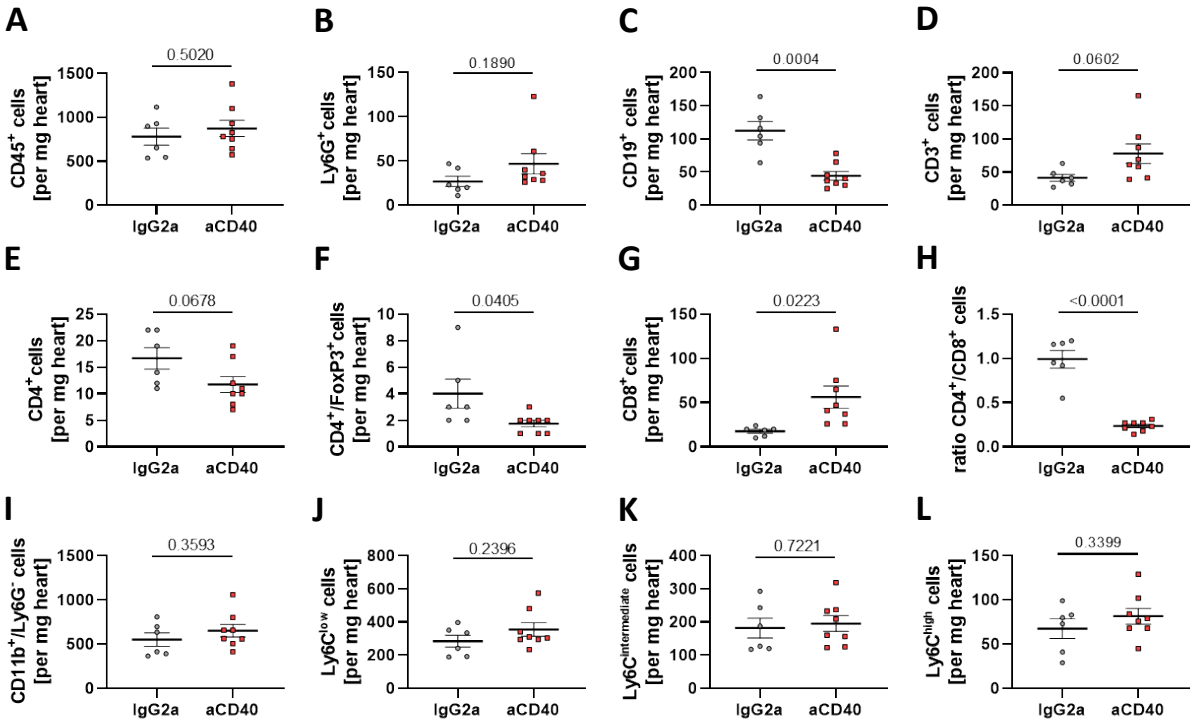

Figure 36: αCD40 treatment alters quantity and composition of lymphocyte immune cells within the heart at day 7 following AMI. Mice were injected with either αCD40 or IgG2a directly after IR and sacrificed for flow cytometry analyses of hearts at day 7. CD40 activation changed lymphocyte numbers in detail: **(C)** CD19⁺ B cells, **(F)** CD4⁺/FoxP3⁺ regulatory T cells and **(H)** ratio of CD4⁺ to CD8⁺ T cells were decreased; while **(G)** CD8⁺ cytotoxic T cells were increased. In other immune cell populations including **(A)** CD45⁺ leukocytes, **(B)** Ly6G⁺ neutrophils, **(D)** CD3⁺ T cells, **(E)** CD4⁺ T helper cells, **(I)** CD11b⁺/Ly6G⁻, **(J)** Ly6C^{low} **(K)** Ly6C^{int} and **(L)** Ly6C^{high} monocytes/macrophages numbers were stable. N = 6 (IgG2a), 8 (αCD40). Data are presented as mean ± SEM. Statistical analyses were performed using unpaired t-test.

Activation of CD40 reduces anti-inflammatory monocytes and macrophages 24 h after AMI, possibly driving acute inflammation after AMI into a more pro-inflammatory situation, which could influence cardiac outcome. Echocardiographic measurements of the LV function 24 h after IR surgery revealed a severe impairment of cardiac function, covered by declined EF, SV and CO (**Fig. 37 C-E**). Since an impairment of LV function is commonly linked to structural modification in the myocardium the infarct size of hearts was assessed by TTC staining. Indeed, infarct size of αCD40 treated mice was significantly increased 24 h following AMI (**Fig. 37 G, H**). Taken together, all these findings indicate that even a single dose of αCD40,

activating CD40 signaling, has a rapid deteriorating effect on the functional and structural outcome in the acute phase 24 h after AMI.

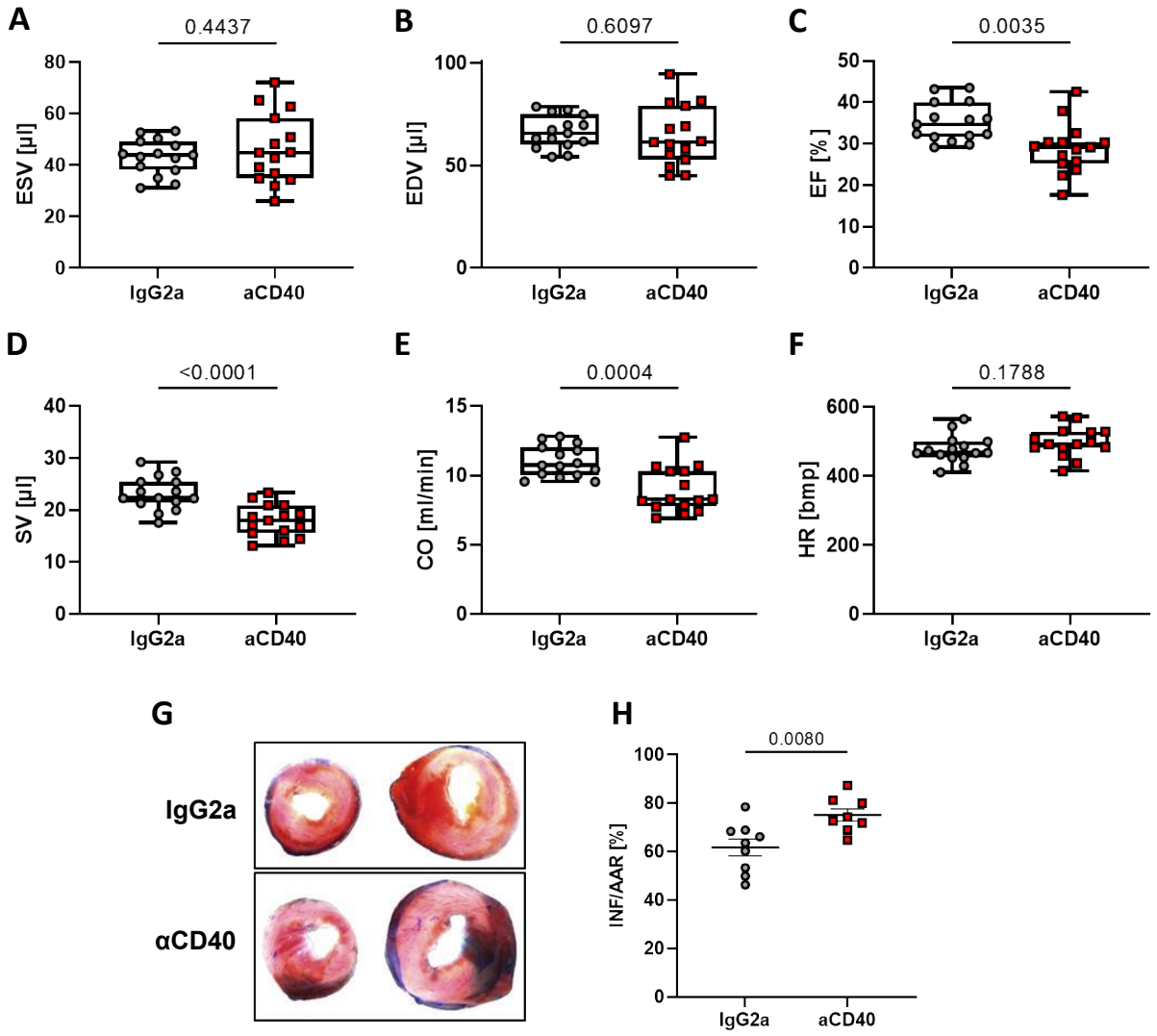

Figure 37: CD40 activation significantly impairs LV function and increases infarct size 24 h following AMI. Instantly after AMI induction mice were injected with either αCD40 or IgG2a. Finally, mice underwent echocardiography to obtain following parameters: **(A)** End-systolic volume (ESV), **(B)** End-diastolic volume, **(C)** ejection fraction (EF), **(D)** stroke volume (SV), **(E)** cardiac output, **(F)** heart rate (HR). EF, SV and CO were significantly decreased displaying an impairing influence of CD40 activation. N = 15 (IgG2a), 15 (αCD40). αCD40 treatment also increased infarct size, stated by **(G)** representative images of heart sections after Evans Blue and TTC staining and **(H)** percentage of infarct size (INF) per area at risk (AAR). N = 9 (IgG2a), 8 (αCD40). Data are presented as mean ± SEM. Statistical analysis was performed using unpaired t-test.

Taking into account that even after a short time of activating CD40 signaling via αCD40 treatment cardiac outcome was deteriorated, the next step was to observe whether these effects also persisted over time. Analyses of cardiac function via echocardiography at day 7 following AMI still exhibited a decline of EF, SV and CO as before at day 1 (**Fig. 38 C-E**). Therefore, the LV impairment began at day 1 and persisted until day 7, making short-term treatment with αCD40 a quite strong factor when it comes to severe cardiac function. Overall

CD40 activation during the acute healing phase negatively affected cardiac outcome and infarct size after AMI, supporting the hypothesis that inhibition of CD40 represents a suitable target to improve healing processes following AMI.

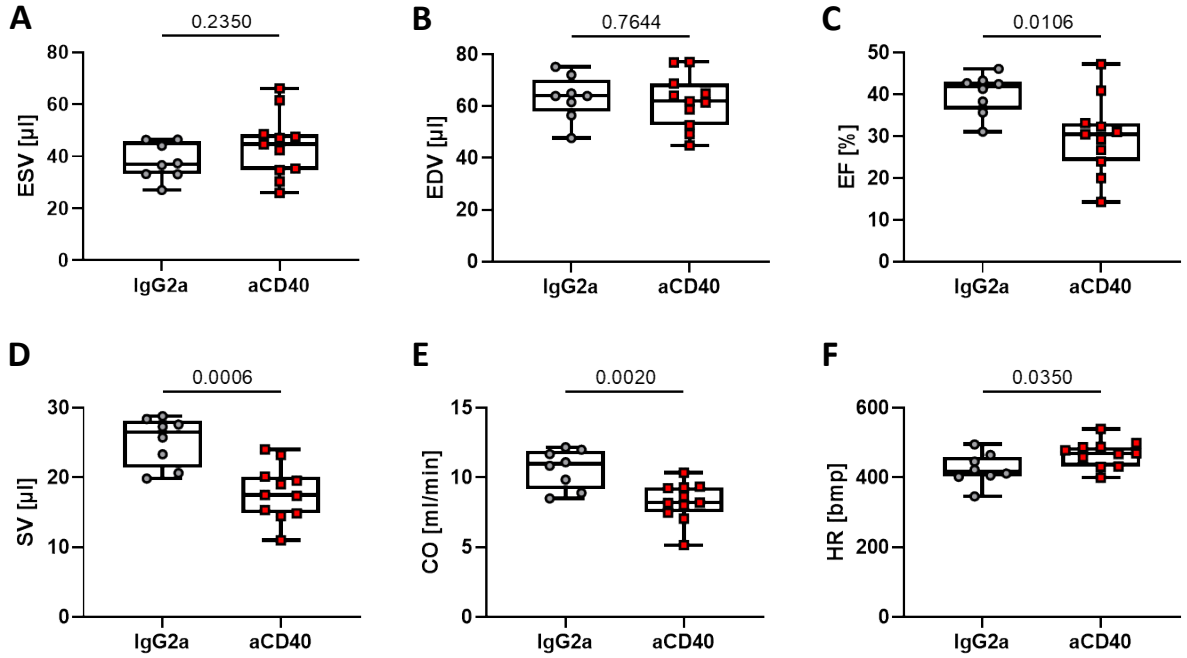

Figure 38: CD40 activation significantly impairs LV function at day 7 following AMI. Instantly after AMI induction mice were injected with either a single dose of αCD40 or IgG2a. Finally, mice underwent echocardiography to obtain following parameters: **(A)** End-systolic volume (ESV), **(B)** End-diastolic volume, **(C)** ejection fraction (EF), **(D)** stroke volume (SV), **(E)** cardiac output, **(F)** heart rate (HR). EF, SV and CO were significantly decreased displaying an impairing influence of CD40 activation, while HR was increased. N = 8 (control), 15 (αCD40). Data are presented as mean ± SEM. Statistical analyses were performed using unpaired t-test.

4.7 Role of CD40L expressing cells in the acute phase after AMI

Inhibition of CD40 signaling via TRAF-STOP had beneficial effects on the outcome after AMI, while the correct time point of treatment was critical. In contrast, activation of CD40 via mimicking high levels of CD40L during the acute phase after AMI resulted in a decrease of heart function and larger infarct sizes. This led to the hypothesis, that reduced CD40L expression could have a similar beneficial effect on outcome following AMI as observed under TRAF-STOP treatment. Given that CD40L is most frequently expressed on T cell and platelets, cell type-specific deficient mice for CD40L focusing on these two cell types were used. Both cell type-specific deficient lines were generated by our group making use of the Cre-loxP recombination technology targeting the *Cd40lg* genes in either T cells (*Cd40lg*$^{fl/fl}$*Cd4-Cre*) or platelets (*Cd40lg*$^{fl/fl}$*Pf4-Cre*), leading to a continuous loss of CD40L expression. Only in mice possessing the gene for Cre recombinase (Cre^{+}) the cell type-restricted deletion of CD40L is present, while mice without it (Cre^{-}) are not affected. Regarding *Cd4* it should be noted, that in the end not only the CD4^{+} helper T cells are affected by the genetical modification of CD40L, but rather the entire T cell population, because all T cells go through a double positive differentiation stage for CD4 and CD8 during their maturation in the thymus.[130] Since genetic modification could possibly influence the steady state of immune cell composition in hearts or circulation, mice were first examined without IR setting to establish a baseline for potential variation. After assessing baseline parameters for immune cell numbers, mice underwent IR surgery and cardiac function, infarct size and also immune cell distribution were determined.

4.7.1 T cell-specific loss of CD40L

For measurements of baseline immune cell numbers of T cell-specific loss of CD40L, hearts and blood from *Cd40lg*$^{fl/fl}$*Cd4-Cre*$^{-}$ and *Cd40lg*$^{fl/fl}$*Cd4-Cre*$^{+}$ mice were removed and composition of immune cells analyzed. For that purpose blood of mice was taken via heart puncture and measured by two different methods to consolidate potential results. On the one hand, by flow cytometric protocol and on the other hand by the use of a blood cell counter. Taking a closer look at circulating immune cell numbers unveiled that the cell type-specific depletion of CD40L in T cells already diversified distribution of immune cells. Flow cytometry revealed a significant increase of CD45^{+} leukocyte numbers per microliter blood in *Cd40lg*$^{fl/fl}$*Cd4-Cre*$^{+}$ mice mostly derived from elevated CD19^{+} B cell and CD3^{+} T cell counts (**Fig. 39 A, C, D**). Moreover, the number of Ly6C^{low} monocytes and macrophages was exalted (**Fig. 39 F**). These results were confirmed after evaluating the total numbers of circulating leukocytes divided into lymphocytes, monocytes and neutrophils by the blood cell counter although this method cannot differentiate the different subpopulations (**Fig. 39 I-M**). In summary, both methods state an elevation in numbers of leukocytes, lymphocytes and monocytes upon T cell-specific deficiency of CD40L.

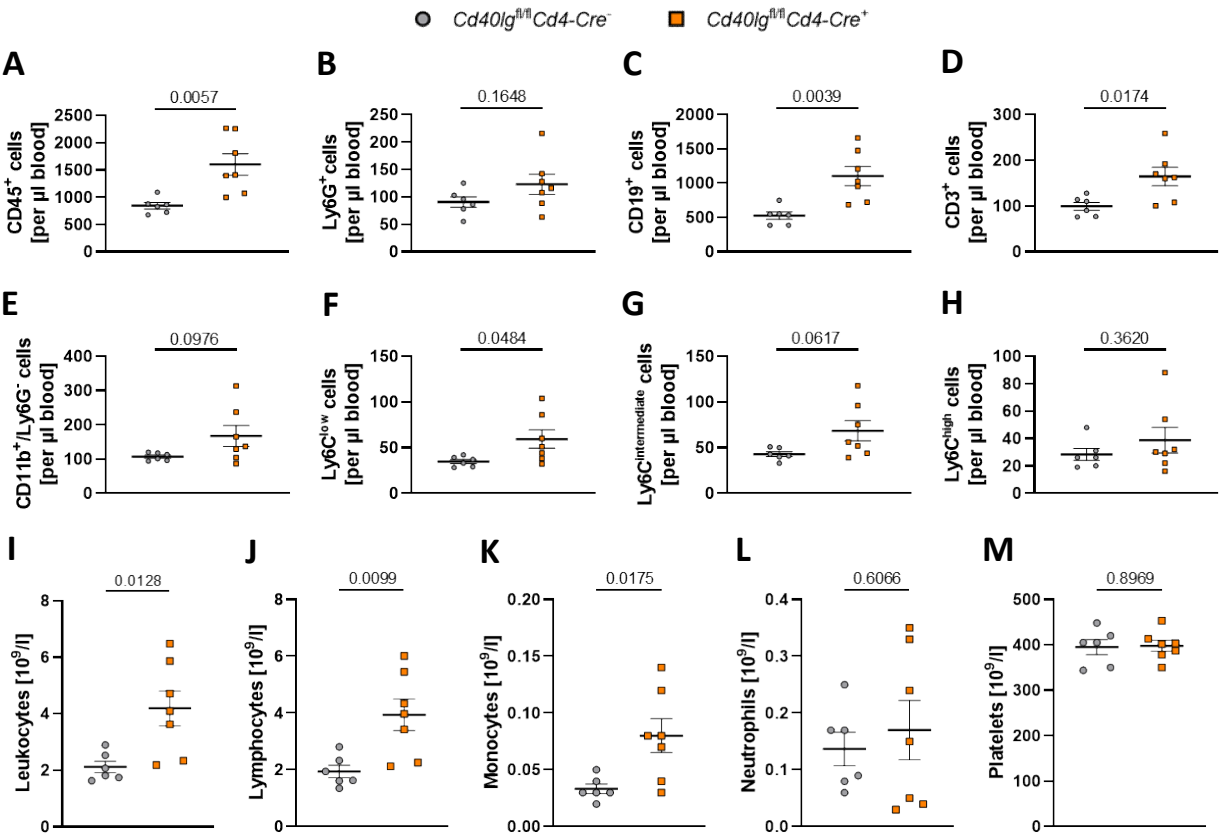

Figure 39: Increased numbers of circulating leukocytes, lymphocytes and monocytes in *Cd40lg$^{fl/fl}$Cd4-Cre^{+}* mice. Blood from the *Cd40lg$^{fl/fl}$Cd4-Cre^{-}* or *Cd40lg$^{fl/fl}$Cd4-Cre^{+}* mice was measured via flow cytometry **(A-H)** and blood cell counter **(I-M)**. Following immune cell populations were acquired per µl of blood: **(A)** CD45^{+} leukocytes, **(B)** Ly6G^{+} neutrophils, **(C)** CD19^{+} B cells, **(D)** CD3^{+} T cells, **(E)** CD11b^{+}/Ly6G^{-}, **(F)** Ly6C^{low} **(G)** Ly6C^{int} and **(H)** Ly6C^{high} monocytes/macrophages. Loss of CD40L on T cells (Cre^{+}) led to elevated numbers of leukocytes, B cells, T cells and anti-inflammatory monocytes/macrophages. Analyses via blood cell counter validated that circulating **(I)** leukocytes **(J)** lymphocytes and **(K)** monocytes increased in numbers in Cre^{+} mice. **(L)** neutrophils and **(M)** platelets remained stable. N = 6 (Cre^{-}), 7 (Cre^{+}). Data are presented as mean ± SEM. Statistical analyses were performed using unpaired t-test.

Circulating leukocytes, lymphocytes and monocytes are already increased in *Cd40lg$^{fl/fl}$Cd4-Cre^{+}* mice due to a loss of CD40L expression on T cells under baseline conditions. Accordingly, the immune cell distribution in blood was also measured 24 h after mice underwent IR surgery. Increased numbers of CD45^{+} leukocytes, CD19^{+} B cells and CD3^{+} T cells could no longer be detected via flow cytometry 24 h after AMI (**Fig. 40 A, C, D**). Furthermore, the monocyte subpopulation of Ly6C^{low} cells was no longer elevated, instead the population of Ly6C^{int} monocytes and macrophages was increased (**Fig. 40 F, G**). Strikingly, the total number of circulating monocytes calculated by use of a blood cell counter was not modified, probably because Ly6C^{int} cells are only a small proportion of the entire monocyte population (**Fig. 40 K**). Similar to flow cytometry analyses, numbers of leukocytes and lymphocytes between *Cd40lg$^{fl/fl}$Cd4-Cre^{-}* and *Cd40lg$^{fl/fl}$Cd4-Cre^{+}* mice remained constant (**Fig. 40 I, J**). This also applies to quantity of platelets (**Fig. 40 M**). A remarkable finding of the measurements by

blood cell meter was the fact that neutrophils were significantly raised, although no deviations for Ly6G$^+$ neutrophils were noticed by flow cytometric studies (**Fig. 40 L**).

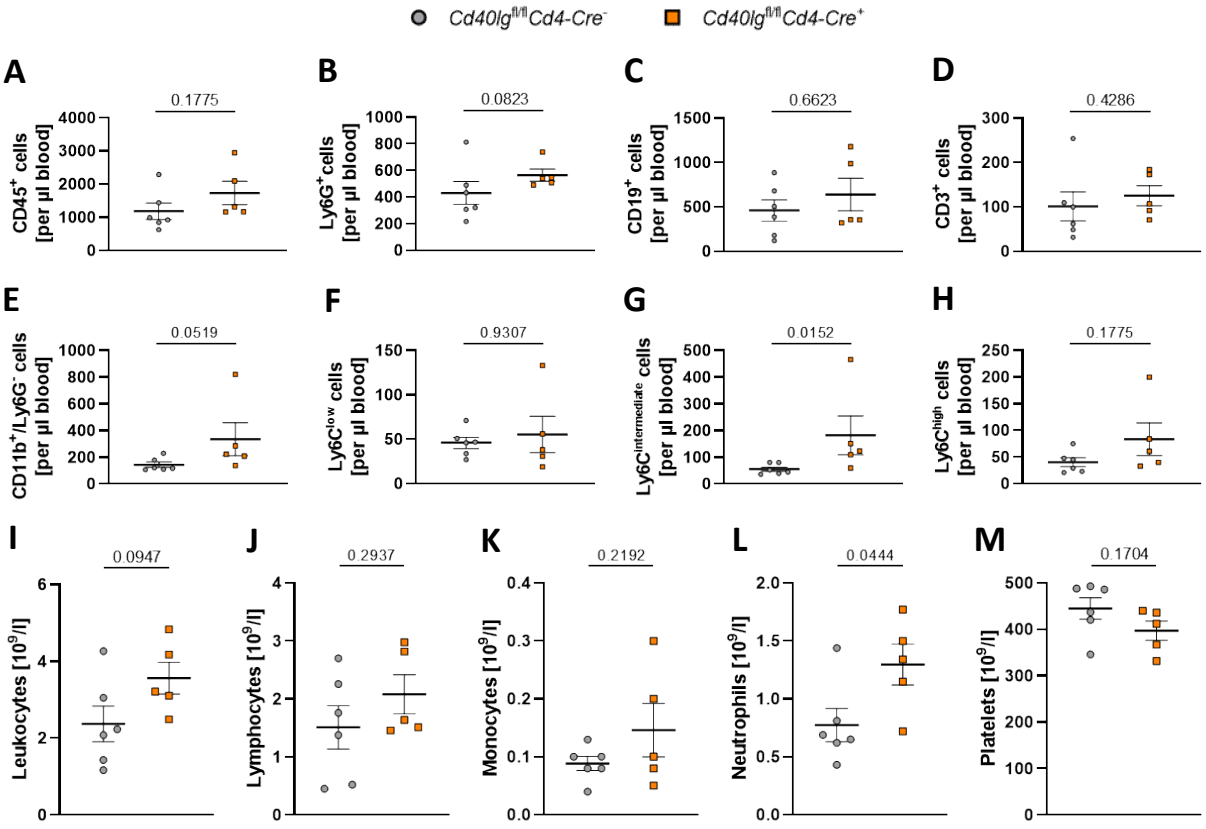

Figure 40: Higher numbers of circulating Ly6C^{int} monocytes and neutrophils in *Cd40lg$^{fl/fl}$Cd4-Cre$^+$* mice 24 h after AMI. Blood from the same *Cd40lg$^{fl/fl}$Cd4-Cre$^-$* or *Cd40lg$^{fl/fl}$Cd4-Cre$^+$* mice was measured via flow cytometry **(A-H)** and blood cell counter **(I-M)**. Following immune cell populations were acquired per µl of blood: **(A)** CD45$^+$ leukocytes, **(B)** Ly6G$^+$ neutrophils, **(C)** CD19$^+$ B cells, **(D)** CD3$^+$ T cells, **(E)** CD11b$^+$/Ly6G$^-$, **(F)** Ly6C^{low} **(G)** Ly6C^{int} and **(H)** Ly6C^{high} monocytes/macrophages. *Cd40lg$^{fl/fl}$Cd4-Cre$^+$* mice have higher numbers of Ly6C^{int} monocytes and macrophages. Blood cell counter measurements included circulating **(I)** leukocytes **(J)** lymphocytes **(K)** monocytes, **(L)** neutrophils and **(M)** platelets. Loss of CD40L on T cells led to elevation of neutrophils. N = 6 (Cre$^-$), 5 (Cre$^+$). Data are presented as mean ± SEM. Statistical analyses were performed using Mann Whitney test **(A-H)** and unpaired t-test **(I-M)**.

Consequently, numbers of cardiac immune cells were calculated, to display whether the loss of CD40L expression on T cells also influences distribution of immune cells only due to this cell type-specific deficiency of CD40L. Interestingly, changes were not only found for populations and subpopulations of T cells, since these are most likely affected in this gene-deficient model, but also for monocytes and macrophages (**Fig. 41**). In particular, the number of Ly6C^{int} monocytes and macrophages was increased in *Cd40lg$^{fl/fl}$Cd4-Cre$^+$* mice, causing a raised number of all CD11b$^+$/Ly6G$^-$ monocytes and macrophage counts (**Fig. 41 I, K**). The number of neutrophils and B cells was not affected by loss of CD40L on T cells (**Fig. 41 B, C**). Concerning T cell populations an overall decrease in cells per milligram heart was spotted, mainly caused by a decline of CD4$^+$ helper T cells (**Fig. 41 D, E**). Furthermore, the count of

CD4$^+$/FoxP3$^+$ T_{reg} cells was also reduced (**Fig. 41 F**). Despite all these changes in immune cell composition the overall number of CD45$^+$ leukocytes was not affected (**Fig. 41 A**).

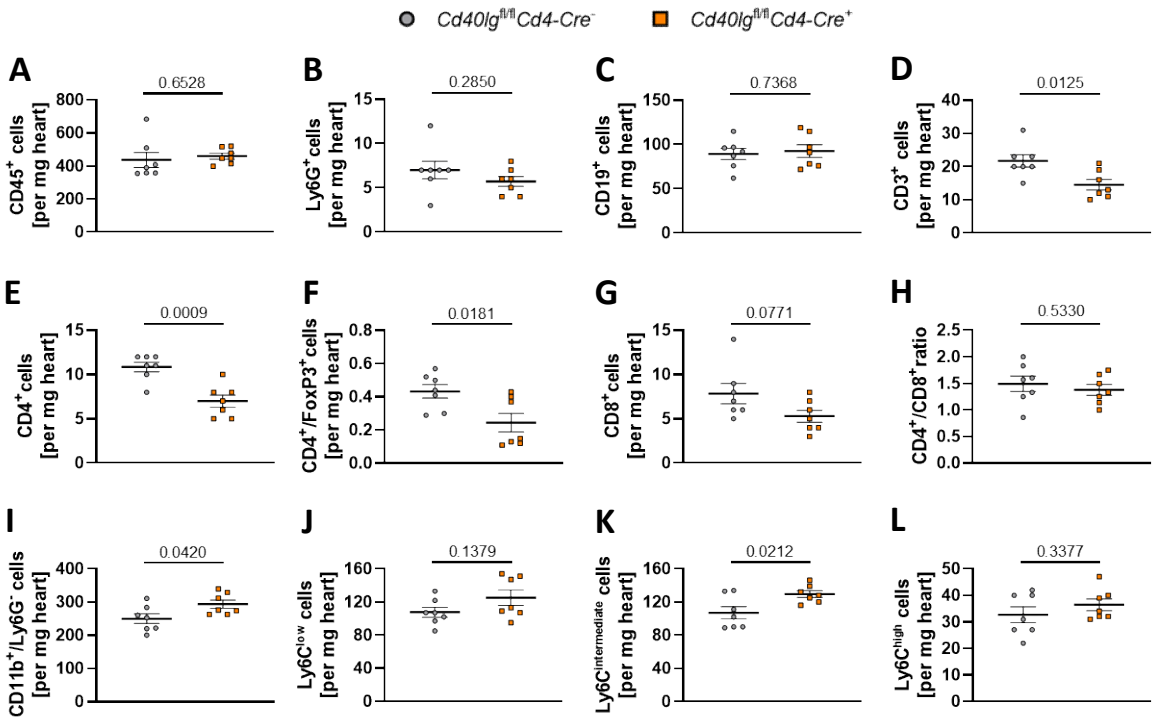

Figure 41: T cell-specific loss of CD40L leads to altered cardiac immune cell composition. Hearts of *Cd40lg*$^{fl/fl}$*Cd4-Cre*$^-$ or *Cd40lg*$^{fl/fl}$*Cd4-Cre*$^+$ mice were enzymatically digested and immune cell numbers counted via flow cytometry. Following immune cell populations were acquired: **(A)** CD45$^+$ leukocytes, **(B)** Ly6G$^+$ neutrophils, **(C)** CD19$^+$ B cells, **(D)** CD3$^+$ T cells, **(E)** CD4$^+$ T helper cells, **(F)** CD4$^+$/FoxP3$^+$ regulatory T cells, **(G)** CD8$^+$ cytotoxic T cells, **(H)** ratio of CD4$^+$ to CD8$^+$ T cells, **(I)** CD11b$^+$/Ly6G$^-$, **(J)** Ly6C^{low} **(K)** Ly6C^{int} and **(L)** Ly6C^{high} monocytes/macrophages. The loss of CD40L on T cells (Cre$^+$) led to a reduced quantity of overall T cells, as well as helper and regulatory T cells. In addition, Cre$^+$ mice had elevated numbers of monocytes and macrophages specifically of Ly6C^{int} subpopulation. N = 7 (Cre$^-$), 7 (Cre$^+$). Data are presented as mean ± SEM. Statistical analyses were performed using unpaired t-test.

Keeping in mind, that loss of CD40L on T cells led to variation in different immune cell populations and subpopulations, *Cd40lg*$^{fl/fl}$*Cd4-Cre*$^-$ or *Cd40lg*$^{fl/fl}$*Cd4-Cre*$^+$ mice underwent IR surgery and counts of cardiac immune cells were determined 24 h after AMI. One day after AMI, these changes are no longer present in *Cd40lg*$^{fl/fl}$*Cd4-Cre*$^+$ mice, suggesting that induction of AMI and the migration of immune cells into the myocardium offset alterations **(Fig. 42**). Instead, a significant enhancement of CD19$^+$ B cell numbers in *Cd40lg*$^{fl/fl}$*Cd4-Cre*$^+$ mice was observed, making it the only difference of immune cell distribution between mice with or without CD40L expression on T cells 24 h after AMI (**Fig. 42 C**).

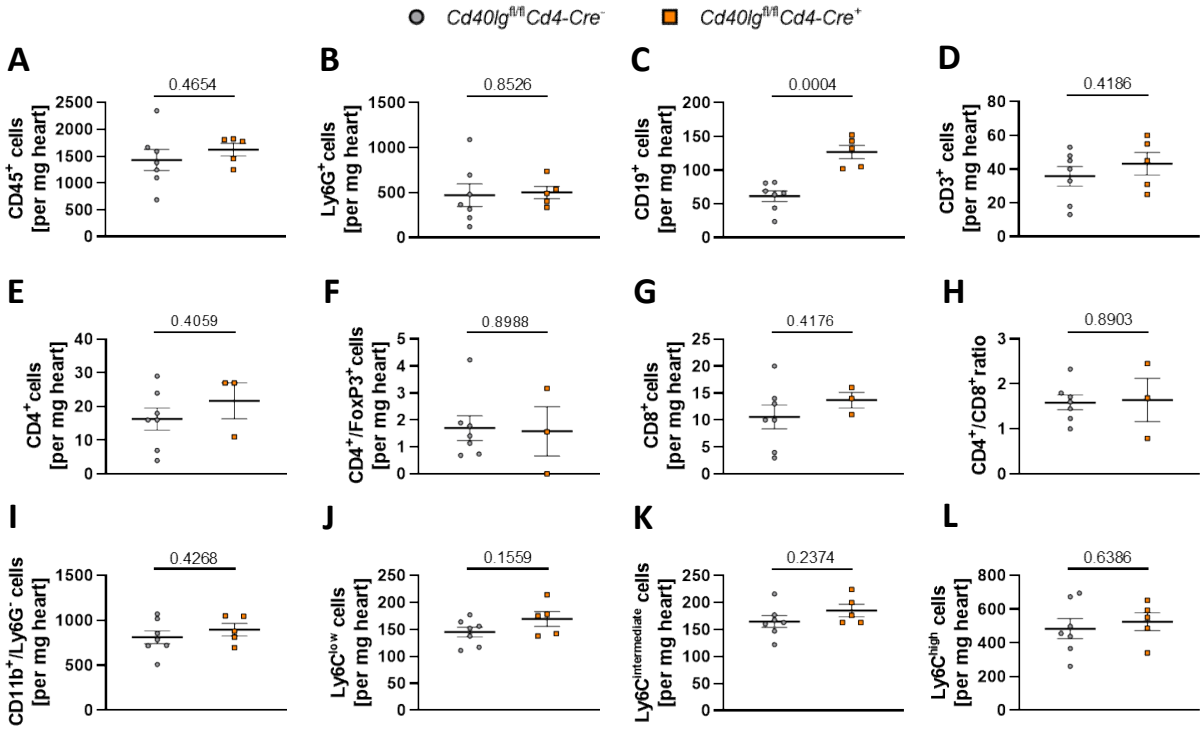

Figure 42: Number of cardiac B cells in *Cd40lg*$^{fl/fl}$*Cd4-Cre*$^{+}$ mice is increased 24 h after AMI. Hearts of *Cd40lg*$^{fl/fl}$*Cd4-Cre*$^{-}$ or *Cd40lg*$^{fl/fl}$*Cd4-Cre*$^{+}$ mice were enzymatically digested at day 1 after IR surgery and immune cell numbers counted via flow cytometry. Following immune cell populations were acquired: **(A)** CD45^{+} leukocytes, **(B)** Ly6G^{+} neutrophils, **(C)** CD19^{+} B cells, **(D)** CD3^{+} T cells, **(E)** CD4^{+} T helper cells, **(F)** CD4^{+}/FoxP3^{+} regulatory T cells, **(G)** CD8^{+} cytotoxic T cells, **(H)** ratio of CD4^{+} to CD8^{+} T cells, **(I)** CD11b^{+}/Ly6G^{-}, **(J)** Ly6C^{low} **(K)** Ly6C^{int} and **(L)** Ly6C^{high} monocytes/macrophages. B cells numbers were significantly increased in mice with loss of CD40L expression on T cells (Cre^{+}). N = 7 (Cre^{-}), 5 [3]; because of technical issues two mice could not be measured for subpopulations of T cells (E-H)] (Cre^{+}). Data are presented as mean ± SEM. Statistical analyses were performed using unpaired t-test.

Given the mentioned alterations in cardiac and circulating immune cell composition at day 1 post AMI, their influence on outcome after AMI was investigated by determining LV function and infarct size. Measurement of echocardiographic parameters from *Cd40lg*$^{fl/fl}$*Cd4-Cre*$^{-}$ and *Cd40lg*$^{fl/fl}$*Cd4-Cre*$^{+}$ mice exposed heightened EDV, EF, SV and CO for the Cre^{+} mice, while HR and ESV remained unchanged, marking a beneficial effect of T cell-specific CD40L loss on cardiac function (**Fig. 43 A-F**). Since an improved cardiac function often associates with changes in myocardial tissue structure, infarct size was assessed via staining for healthy tissue, AAR and INF of the left ventricle. The positive effect on LV function in *Cd40lg*$^{fl/fl}$*Cd4-Cre*$^{+}$ mice could be explained by smaller infarct size, in terms of INF per AAR (**Fig. 43 G-H**). In summary, the loss of CD40L modulates cardiac B cell numbers and thereby has an advantageous effect onto infarct size and cardiac function at day 1 after AMI. Nevertheless, the modifications in cardiac and circulating immune cells under baseline settings need to be taken into account and require further investigation.

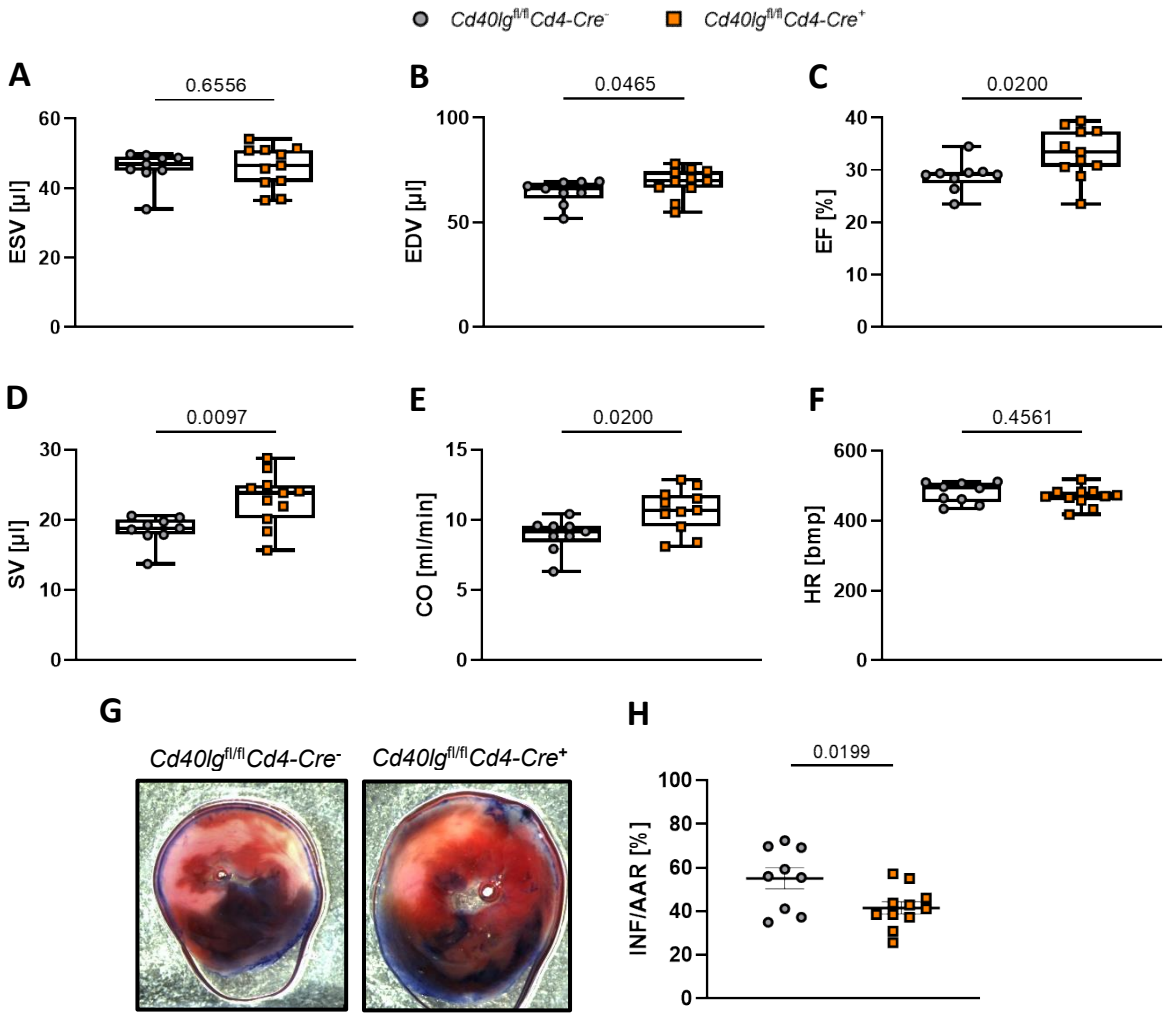

Figure 43: Loss of CD40L on T cells has beneficial effect on cardiac function and reduces infarct size 24 h post AMI. At day 1 after AMI mice with either *Cd40lg*$^{fl/fl}$*Cd4-Cre*$^{-}$ or *Cd40lg*$^{fl/fl}$*Cd4-Cre*$^{+}$ genotype underwent echocardiography. **(A)** End-systolic volume (ESV), **(B)** End-diastolic volume, **(C)** ejection fraction (EF), **(D)** stroke volume (SV), **(E)** cardiac output, **(F)** heart rate (HR). EDV, EF, SV and CO were significantly increased in mice with loss of CD40L on T cells representing a beneficial effect on LV cardiac function. N = 9 (Cre^{-}), 11 (Cre^{+}). Statistical analyses were performed using Mann-Whitney test. Evaluation of infarct sizes revealed a decline for Cre^{+}, stated by **(G)** representative images of heart sections after Evans Blue and TTC staining and **(H)** percentage of infarct size (INF) per area at risk (AAR). N = 9 (Cre^{-}), 5 (Cre^{+}). Statistical analyses were performed using unpaired t-test.

4.7.2 Platelet-specific loss of CD40L

Besides T cells, platelets are the other major cell population known for their high expression of CD40L. To see how a loss of CD40L on platelets affects cardiac outcome along with immune response, a cell type-specific deficient mouse line *Cd40lg*$^{fl/fl}$*Pf4-Cre* was generated and used. As previously described for cell type-specific deletion of CD40L on T cells, baseline measurements of immune cell distribution were performed to check for alterations in cardiac and circulating immune cell numbers occurring due to genetic modification. First, analyses of circulating immune cells were accomplished via flow cytometry and blood counter. Flow cytometry measurements revealed stable numbers of immune cells per microliter blood (**Fig. 44 A-H**). These findings were supported by the observed results through blood cell counter evaluation for leukocytes, lymphocytes, monocytes and neutrophils (**Fig. 44 I-L**). Of note, this method also analyzed the number of platelets, the cell population most likely affected by the genetic modification. However, platelet numbers displayed no changes (**Fig. 44 M**).

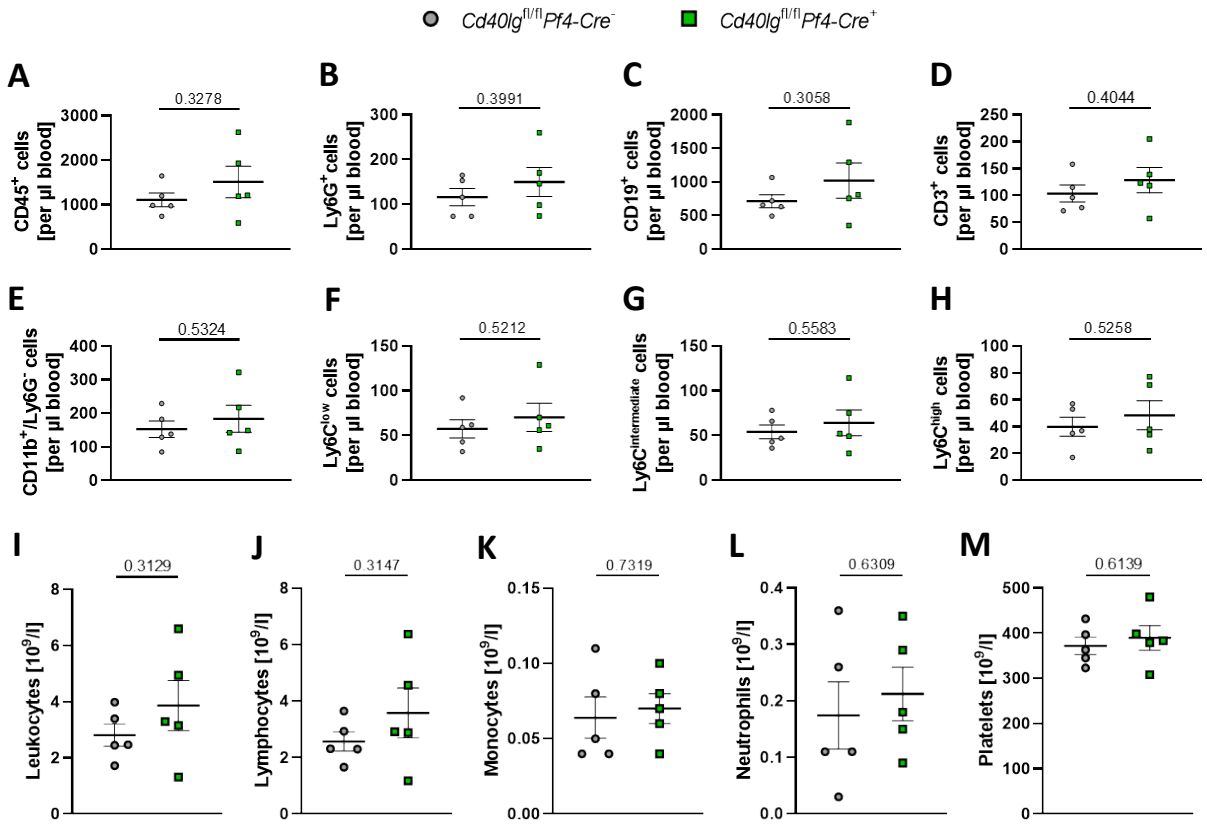

Figure 44: Quantities of circulating immune cell numbers are not altered by platelet specific loss of CD40L. Blood from the same *Cd40lg*$^{fl/fl}$*Pf4-Cre*$^{-}$ or *Cd40lg*$^{fl/fl}$*Pf4-Cre*$^{+}$ mice was measured via flow cytometry **(A-H)** and blood cell counter **(I-M)**. Following immune cell populations were acquired per µl of blood: **(A)** CD45^{+} leukocytes, **(B)** Ly6G^{+} neutrophils, **(C)** CD19^{+} B cells, **(D)** CD3^{+} T cells, **(E)** CD11b^{+}/Ly6G^{-}, **(F)** Ly6C^{low} **(G)** Ly6C^{int} and **(H)** Ly6C^{high} monocytes/macrophages. Blood cell counter measurements included circulating **(I)** leukocytes **(J)** lymphocytes **(K)** monocytes, **(L)** neutrophils and **(M)** platelets. Loss of CD40L on platelets did not affect numbers of circulating immune cells. N = 5 (Cre^{-}), 5 (Cre^{+}). Data are presented as mean ± SEM. Statistical analyses were performed using unpaired t-test.

After assessing the effect of the platelet-specific CD40L loss on circulating immune cells, composition of immune cells inside the myocardium was examined. Evaluation of cardiac tissue uncovered no statistically significant changes in quantity of immune cell populations and even their subpopulations comparing mice with and without a loss of CD40L on platelets (**Fig. 45**). Only the number of CD45$^+$ leukocytes was raised by tendency (**Fig. 45 A**).

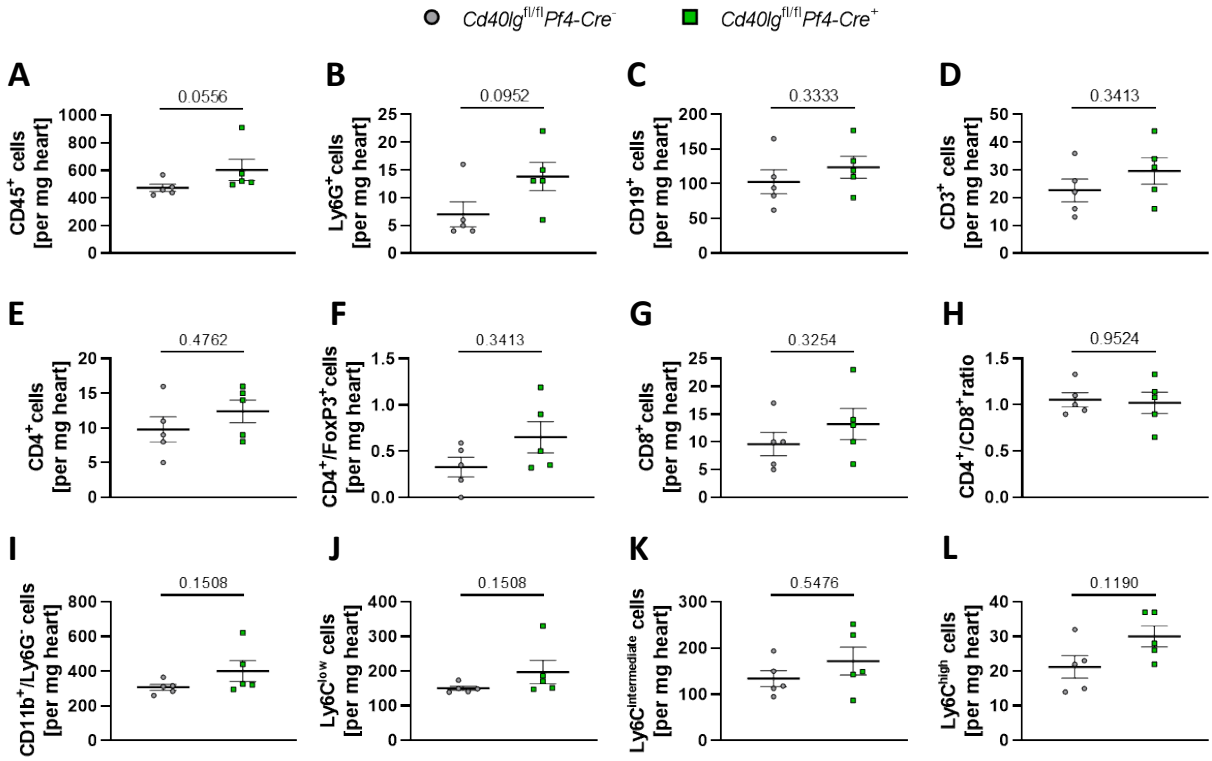

Figure 45: Cardiac immune cell numbers remain stable among loss of CD40L on platelets. Hearts of *Cd40lg*$^{fl/fl}$*Pf4-Cre*$^-$ or *Cd40lg*$^{fl/fl}$*Pf4-Cre*$^+$ mice were enzymatically digested and immune cell numbers counted via flow cytometry. Following immune cell populations were acquired: **(A)** CD45$^+$ leukocytes, **(B)** Ly6G$^+$ neutrophils, **(C)** CD19$^+$ B cells, **(D)** CD3$^+$ T cells, **(E)** CD4$^+$ T helper cells, **(F)** CD4$^+$/FoxP3$^+$ regulatory T cells, **(G)** CD8$^+$ cytotoxic T cells, **(H)** ratio of CD4$^+$ to CD8$^+$ T cells, **(I)** CD11b$^+$/Ly6G$^-$, **(J)** Ly6C^{low} **(K)** Ly6C^{int} and **(L)** Ly6C^{high} monocytes/macrophages. Loss of CD40L on platelets did not alter quantity of cardiac immune cells. N = 5 (Cre$^-$), 5 (Cre$^+$). Data are presented as mean ± SEM. Statistical analyses were performed using Mann Whitney t-test.

Comparison of baseline immune cell numbers in hearts and blood of *Cd40lg*$^{fl/fl}$*Pf4-Cre*$^-$ and *Cd40lg*$^{fl/fl}$*Pf4-Cre*$^+$ mice demonstrated that the genetic modification of CD40L on platelets did not change distribution of immune cells and platelets. Next, mice with or without a loss of CD40L on platelets underwent IR surgery and hearts were removed after 24 h following AMI. Again, immune cell numbers inside cardiac tissue were assessed via flow cytometry, unveiling equal numbers in all populations between *Cd40lg*$^{fl/fl}$*Pf4-Cre*$^-$ and *Cd40lg*$^{fl/fl}$*Pf4-Cre*$^+$ mice (**Fig. 46**). Hence, lack of CD40L on platelets had no effect on the distribution and migration of immune cells into the heart.

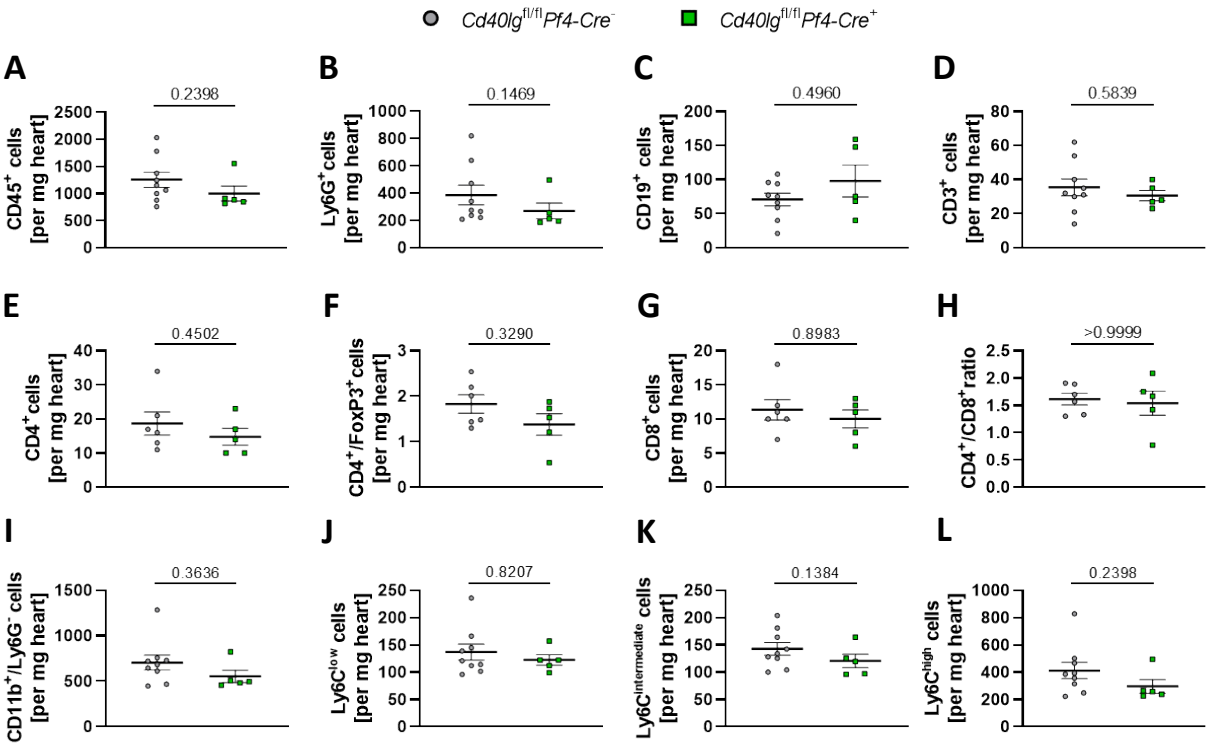

Figure 46: Loss of CD40L on platelets does not change cardiac immune cell numbers 24 h following AMI. Hearts of *Cd40lg*$^{fl/fl}$*Pf4-Cre*$^{-}$ or *Cd40lg*$^{fl/fl}$*Pf4-Cre*$^{+}$ mice were enzymatically digested at day 1 after IR and immune cell numbers counted via flow cytometry. Following immune cell populations were acquired: **(A)** CD45^{+} leukocytes, **(B)** Ly6G^{+} neutrophils, **(C)** CD19^{+} B cells, **(D)** CD3^{+} T cells, **(E)** CD4^{+} T helper cells, **(F)** CD4^{+}/FoxP3^{+} regulatory T cells, **(G)** CD8^{+} cytotoxic T cells, **(H)** ratio of CD4^{+} to CD8^{+} T cells, **(I)** CD11b^{+}/Ly6G^{-}, **(J)** Ly6C^{low} **(K)** Ly6C^{int} and **(L)** Ly6C^{high} monocytes/macrophages. N = 5 (Cre^{-}), 6-9 (Cre^{+}). Data are presented as mean ± SEM. Statistical analyses were performed using Mann Whitney t-test.

As cardiac immune cell patterns were not altered upon loss of CD40L on platelets, the next aspect to investigate was the LV heart function. Measurements via echocardiography revealed no differences between the *Cd40lg*$^{fl/fl}$*Pf4-Cre*$^{-}$ or *Cd40lg*$^{fl/fl}$*Pf4-Cre*$^{+}$ mice, since all assessed parameters, including EF, SV and CO remained unchanged (**Fig. 47 A-F**). Finally, to assess structural remodelling, infarct size was determined via TTC staining demonstrating no alterations in infarct accumulation when CD40L was missing on platelets (**Fig. 47 G-H**). In summary, the loss of CD40L on platelets has no significant effect on circulating and cardiac immune cell composition with or without AMI induction, and did not affect the outcome after AMI, as LV heart function and infarct size between the *Cd40lg*$^{fl/fl}$*Pf4-Cre*$^{-}$ or *Cd40lg*$^{fl/fl}$*Pf4-Cre*$^{+}$ mice were not different.

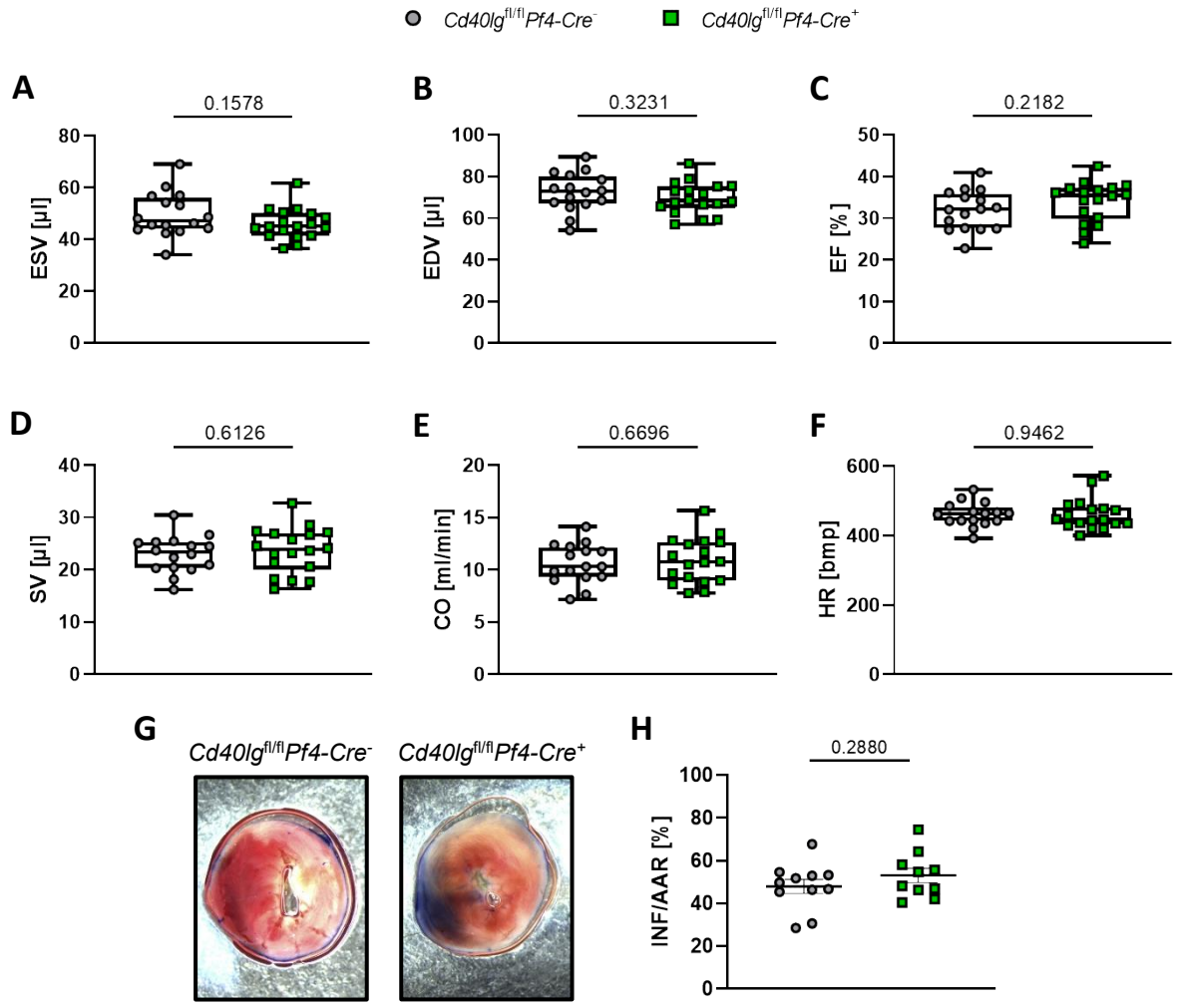

Figure 47: Loss of CD40L on platelets does not affect LV heart function and infarct size 24 h post AMI. At day 1 after AMI mice with either *Cd40lg*$^{fl/fl}$*Pf4-Cre*$^{-}$ or *Cd40lg*$^{fl/fl}$*Pf4-Cre*$^{+}$ genotype underwent echocardiography. **(A)** End-systolic volume (ESV), **(B)** End-diastolic volume, **(C)** ejection fraction (EF), **(D)** stroke volume (SV), **(E)** cardiac output, **(F)** heart rate (HR) remained constant. N = 16 (Cre^{-}), 18 (Cre^{+}). Evaluation of scar sizes showed no differences due to loss of CD40L on platelets stated by **(G)** representative images of heart sections after Evans Blue and TTC staining and **(H)** percentage of infarct size (INF) per area at risk (AAR). N = 11 (Cre^{-}), 10 (Cre^{+}). Statistical analyses were performed using unpaired t-test.

5 Discussion

Inflammation following AMI is necessary to trigger an immune response via pro- and anti-inflammatory processes initiating repair and healing mechanisms of the affected myocardial region. Even though a broad variety of these processes during and after AMI like the LV remodelling have already been studied, there are still characteristics, like immune cell migration and involved signaling pathways, that need further and more detailed investigation offering a better understanding that potentially results in future therapies for AMI and its consequences. While studies showed that the co-stimulatory molecules CD40 and CD40L play a crucial role during the immune response in other CVDs (e.g. in atherosclerosis) less is known about their effect during the inflammation post AMI. This thesis investigates the role of CD40 and CD40L on the immunological cell composition and how this affects the cardiac function after AMI. First validation of methods including flow cytometry and echocardiography were performed to prove their functionality and reproducibility of general immune cell infiltration and activation following AMI. Next, expression of CD40 in the acute phase post AMI was assessed on gene and protein levels, clarifying whether CD40 signaling is important during inflammation after AMI and modulation of the signaling could be a promising approach to beneficially influence cardiovascular remodelling and outcome. Analyses of the CD40 signaling were carried off via three different experimental modulation setups of the CD40/CD40L signaling pathway including inhibition, activation and cell type-specific deletion. As a consequence, the discussion of the abovementioned results will be structured into four main parts, beginning with the method validation and CD40 expression, followed by the three modes of CD40 modulation. Additionally, limitations of methods and mouse model will be discussed as well as an overall summary of the findings of this thesis will be provided. Finally, an outlook is given to project future steps in overcoming the burden of AMI based on the findings of this thesis.

5.1 Acute inflammation and expression of CD40 post AMI

Ischemia and the following reperfusion prompt immunological mechanisms that are characterized by a distinct time dependent recruitment, function and reduction of leukocytes in the myocardium including pro and anti-inflammatory (sub)populations of different immune cells. The immune response after AMI can be divided into three separate phases: inflammation, proliferation and maturation, each playing a distinct role regarding healing and repair of the myocardium.[44, 45] Directly after the initial AMI during the acute phase a rapid and massive migration of leukocytes mostly consisting of neutrophils and macrophages takes place reaching its total peak over the whole time period around day 1 after the infarction. This accumulation is consistent with the increased amount of viable $CD45^+$ cells in the heart one day after AMI compared to sham and baseline analyses. More in depth analyses featuring

subpopulations of leukocytes unveiled that all major subsets of immune cells were elevated, while the total increase was mainly caused by heightened numbers of neutrophils and macrophages. At this point the inflammatory phase begins during which the infiltration of immune cells into the myocardium continues, sustaining a high number of leukocytes inside the heart.[44, 45] This is illustrated by the total number of leukocytes on day 3, which remained at a relatively high level. Nevertheless, from day 1 on the leukocyte number of IR-operated mice decreases steadily and finally returns to basal level at day 28. This decline is the consequence of a shift from an inflammatory to a repair and healing phase, whereby inflammation is reduced.[131] The observed temporal dynamics and phasic infiltration into the myocardium of immune cell numbers, both innate and adaptive, in the first weeks after IR surgery match previous findings of other groups.[67, 132] The increase of cardiac leukocytes of mice with infarction compared to the sham group, at least for day 1 and 3, reveals that IR surgery is potent to induce infarction and inflammation comparable to the immune response after human AMI.[133] Furthermore, the flow cytometric analysis is validated to be functional, given the case of reproducing the time dependent immune cell profile following infarction, which is consistent with previously described cell numbers and kinetics after AMI.[67, 134, 135] Thus, it is feasible to identify changes of cardiac immune cell patterns in our IR model upon CD40 signaling modification.

Cardiac function is one of the most important parameters in the context of diagnosis, monitoring the patients pathway and management of therapy after AMI by keeping track of how severely the infarct impairs the systolic and diastolic function of the heart.[136] In this study, the experimental setup includes echocardiographic measurements before and after infarction to provide information about the LV function. Mice that underwent IR operation demonstrate a lowered EF and SV in comparison to sham mice, confirming results of previous studies.[135, 137] This also affirms that AMI is successfully induced and allows to exclude mice without an appropriate infarct. Consequently, monitoring the mice via echocardiography at distinct time points after AMI will allow to see whether there are changes in the cardiac function, resulting from the different CD40 signaling modulations and how the LV function will develop over time.

The CD40/CD40L dyad is an important regulator of the immune response during several diseases and pathological processes, especially those evolving autoimmunity or chronic inflammation.[138, 139] In the context of CVD, the role of the CD40/CD40L system has mostly been studied in atherosclerosis, where CD40 signaling pathways contribute to inflammation, leukocyte recruitment and plaque formation, resembling an auspicious therapeutical target.[140, 141] Comparatively, AMI is followed by a distinct temporal infiltration of leukocytes into the myocardium, which is linked to pro- and anti-inflammatory processes that are generally associated with signaling of co-stimulatory molecules, including CD40 and CD40L.[45] Thus far, studies could demonstrate that AMI patients exhibit increased serum levels of sCD40L, which

correlate with cardiovascular outcome.[103, 108] High levels of sCD40L were also found in patients suffering from acute or chronic heart failure, prevalent ischemic stroke and myocardial infarction.[105, 142] In the latter two, elevated plasma CD40 concentrations were additionally observed.[142] In contrast to this, other studies could not find any correlations between plasma sCD40L levels in CVD, indicating that more investigation is needed to elucidate the biomarker potential of CD40 and CD40L.[143, 144] One possible way is to understand the precise mechanisms of CD40 and CD40L during the immune response and remodelling post AMI, as their function remains vastly elusive by now.

It is known that CD40 is expressed on a broad variety of immune cells and non-hematopoietic cells.[81-83] However, the expression pattern of CD40 after AMI is still unclear. To overcome this, CD40 gene expression levels in the infarct and remote area at day 1 and 3 after AMI were measured. CD40 mRNA was particularly and significantly upregulated in the infarcted region for both time points in comparison to the remote area, suggesting CD40 is somehow required in the acute phase post AMI. As analysis of the overall gene expression of CD40 was limited, a more detailed evaluation via single cell RNA sequencing could identify the specific cell clusters expressing CD40. Furthermore, a comparison between day 1 and 5 after AMI allowed for screening of shifts in expression levels or clusters. Strikingly, immune cells were the most abundant cells expressing high levels of CD40, especially B cells, DCs and macrophages at day 1, displaying a shift towards another cluster of $CCR2^-$ and $CCR2^+$ macrophages at day 5. The high CD40 expression levels of macrophages are of particular interest, as macrophages play a crucial role during the inflammation and resolution phase after AMI.[60, 145] Similar studies from Jin et al. and Zhuang et al. bolster the findings of immune cell populations and their dynamic changes in the early phase after myocardial infarction emphasizing the macrophages and their subpopulations, but lacking information about CD40 expression.[146, 147] Considering that cells were sorted for $CD45^+$ leukocytes before sequencing, other cell types including fibroblasts and endothelial cells, that were still detected as minor contaminations, only showed a low CD40 expression and were therefore part of another study. In this thesis, the focus was directed towards the aforementioned immune cell populations.

Changes in the gene expression provide a first indication of the relevance of CD40 on immune cells during the first days post AMI. However, gene expression does not necessarily have to reflect the actual protein expression patterns. As a direct consequence the protein expression of surface-bound CD40 at day 1, 3 and 5 after AMI was analyzed via flow cytometry for the most remarkable immune cell populations. Viable $CD45^+$ leukocytes of mice that underwent IR surgery displayed a 60-70 % higher CD40 MFI at day 3 and 5 compared to day 1. Surprisingly, the CD40 MFI of the sham group featured a similar increase matching the altitude of the AMI group at day 3, with the exception that the MFI at day 5 had returned to the level of day 1. A possible explanation to this could be the procedure of the sham operation, where the thorax is

opened and a thread put underneath the LAD, which triggers leukocytes to express CD40 upon inflammation, but to a much lesser extent.

To assess the level of CD40 expression on individual cells, revealing their contribution to the overall CD40 expression on leukocytes, the MFI for CD40 on $CD11b^+/Ly6G^-$ monocytes and macrophages and $CD19^+$ B cells was measured. Focus was specially laid on these two cell populations, because of their high CD40 gene expression and due to the fact, that these cells are known to exhibit high levels of CD40 protein expression, making them potential targets for modification of CD40 signaling.[81, 82] While the CD40 MFI of $CD19^+$ B cells mostly remained unchanged, a significant increase in CD40 surface expression at day 3 and 5 could be observed. This CD40 expression pattern of $CD11b^+/Ly6G^-$ macrophages is very similar compared to the one of $CD45^+$ leukocytes, which leads to the assumption that this subpopulation is predominantly responsible for the observed dynamics of CD40 expression in the overall leukocyte population. The increase of CD40 expression on monocytes and macrophages during the first days after AMI hints at a more pro-inflammatory profile of these cells, since mice with CD40-deficient macrophages displayed less inflammation in atherosclerosis, probably caused by a shift towards an anti-inflammatory profile.[122] As this shift seems to rely on CD40 signaling the upregulated CD40 expression on macrophages, both on gene and protein level, during the first days of inflammation after AMI suggests a potential for intervention, since high levels of (s)CD40 are also associated with deteriorated outcome in myocardial infarction.[142]

5.2 Inhibition of CD40 signaling via administration of TRAF-STOP in AMI

CD40 signaling via TRAF6 is of great interest in the immune response, as it is involved in pro-inflammatory processes and its modulation can shift the direction of response towards a more anti-inflammatory profile.[123] Furthermore, studies have indicated that blocking of CD40/TRAF6 signaling, especially in macrophages, under atherosclerotic conditions promotes beneficial effects by reducing atherosclerosis.[125] To achieve this, Seijkens et al. used a small molecule inhibitor called TRAF-STOP blocking the intracellular signaling.[124, 125] We hypothesized that this molecule could also be promising in context of AMI, since CD40 expression on monocytes and macrophages displays dynamic upregulation and contributes to a more pro-inflammatory immune response that deteriorates myocardial healing.[148] Inhibition of CD40-TRAF6 signaling could be potent to reduce inflammation by shifting the pro-inflammatory profile towards an anti-inflammatory profile and altering cardiac immune cell distribution that finally results in cardioprotection along with an improved overall cardiac healing and outcome.

The initial approach of CD40 signaling inhibition was to use an *ex-vivo* model, in which the explanted hearts of wild type C57BL/6J mice were administered to a Langendorff apparatus and treated with blood containing TRAF-STOP during ischemia to investigate potential efficacy of cardioprotective therapy onto the LV cardiac function after reperfusion. No alterations of investigated parameters upon TRAF-STOP treatment could be observed, pointing out that the TRAF-STOP application was not potent to change LV cardiac function in this *ex-vivo* model. Whether this result really relies on the TRAF-STOP must be handled with caution, since there are many restrictions and limitations in the Langendorff model. First of all inducing the 40 min ischemia is done via total obstruction of coronary flow, causing global ischemia, where the affected areas will most likely differ between each sample, complicating the comparison of LVDP functional analyses within the experiments. To avoid this it would be recommendable to additionally measure the infarct size via TTC staining and drawing a correlation between both parameters. Moreover, the loading of blood with or without TRAF-STOP during the ischemia occasionally resulted in coagulation of coronary arteries, although the blood was heparinized, blocking or at least diminishing coronary flow during reperfusion. Obvious disruption or strong reduction of coronary flow in the first minutes of reperfusion led to termination of the running experiment. However, smaller obstructions can occur and not been noticed, may giving false results. There are many more parameters that can compromise measurements via Langendorff apparatus, making it a fairly challenging method.[149] At last, the most probable issue, that there is no effect of TRAF-STOP detectable, is the very short duration of treatment, observance, and ultimately the *ex-vivo* model itself. This model only focuses on the heart separating it from any systemic influences and other physiological impacts *in-vivo*, including vasculature and viscera[150]. Since infiltration of immune cells is vital for the resolution of inflammation, the Langendorff *ex-vivo* model seems to be not the appropriate experimental setup to analyze the potential effect of pharmacological CD40/TRAF6 signaling inhibition via TRAF-STOP treatment.

Considering this, the next step was to block CD40 signaling in an *in-vivo* experimental setup, enabling a more detailed and comprehensive analyses of cardiac and immunological parameters. In the first approach, mice were treated with TRAF-STOP for one week before the IR surgery, to achieve a preconditional inhibition of CD40/TRAF6 signaling to the time point of myocardial infarction and acute immune response. Since AMI is accompanied by loss of cardiomyocytes due to ischemic injury and cardiac remodelling, the pump function of the heart is impaired.[50, 151] Rapid restoration of cardiac function is one key factor when it comes to prevention of chronic heart failure as long-lasting course of AMI.[22] So far, the preconditional CD40 inhibition could not improve LV cardiac function one day post AMI, as no changes between control and TRAF-STOP treated mice were identified. In close association with this, the infarct size along with the AAR remained also unchanged after TRAF-STOP administration.

One reason for this could be the relatively early stage post AMI, leaving not enough time for the immune response, which is mainly driven by neutrophils in the first hours, to reduce inflammation and prevent death of cardiomyocytes.[52, 152] Moreover, neutrophils indeed express CD40[83], but not at high levels as previously described, making the blocking of CD40 signaling somewhat obsolete. Besides neutrophils, monocytes and macrophages are involved in the acute immune response expressing high amounts of CD40, thus presenting an optimal target for CD40 signaling inhibition. Analyses of infiltrating immune cells provided detailed insights and revealed a significant reduction of $CD11b^+$ $Ly6G^-$ monocytes and macrophages and all their Ly6C-differentiated subpopulations upon TRAF-STOP treatment, while leukocyte, neutrophil, B and T cell numbers were not altered. This implicates that blocking CD40 signaling prior to AMI is functional, as it reduces the number of infiltrating monocytes and macrophages into the myocardium, recapitulating similar findings in the development of atherosclerosis.[125] However, solely less monocytes and macrophages are not potent enough to redirect the immunological processes following AMI, as infarct size and with it the cardiac function remain unmodified. A possible explanation for this is the time required for adjustments via immunological changes after AMI.

Given that the reparative process after AMI proceeds over a longer period of time, which includes different required phases of healing[45], the experimental setup was expanded by continuing the TRAF-STOP administration three times per week post IR surgery until the end point of 28 days. Despite the prolonged duration allowing healing post AMI, weekly monitoring of LV cardiac function unveiled no alterations between control and TRAF-STOP-treated mice, as well as the represented analyses at day 28. Therefore, inhibition of CD40/TRAF6 signaling showed no beneficial effect to restore LV function. Comparable structural analysis via TTC at day 28 was not possible, since this method is limited to the early time points after infarction[153, 154], concentrating on infarct size rather than scar size, which are a result of cardiac remodeling and scar formation. An alternative method to measure scar size in histological heart slices was established by Christin Elster and later performed by Ashley-Jane Duplessis in the course of their respective master's thesis. In context of day 28 after preconditional and continuous TRAF-STOP treatment, the latter could state that scar size, evaluated by staining fibrotic tissue, revealed no significant differences between control- and TRAF-STOP-treated mice, supporting the previous results of echocardiography. Quantification of cardiac immune cells at day 28 was able to prove the general reduction in cell numbers due to resolution of inflammation for both groups after AMI. Meanwhile all assessed cell populations displayed no alterations due to continuous blockage of CD40 signaling, including $CD11b^+$ $Ly6G^-$ monocytes and macrophages along with their subpopulations. At day 28 post AMI the inflammatory and reparative processes are largely completed and an immunological homeostasis is established[45, 46], which most likely explains that there are no more alterations in cell numbers

present. Based on the fact, that global and thus constant CD40 inhibition can lead to severe immunosuppression, preconditional CD40 inhibition could already initiate an adverse immune cell repertoire prior to AMI preventing beneficial effects on LV remodeling and cardiac function.[39, 93] This might explain that no differences between the control- and TRAF-STOP-treated mice were observed, suggesting that identification of the exact time point of CD40 inhibition before, during or after AMI is essential. Nevertheless, taking the neutral findings of day 1 and 28 for preconditional TRAF-STOP treatment into account and considering that CD40 expression was highly upregulated at day 3 and 5 after AMI led to the hypothesis that CD40/TRAF6 signaling is essential during the initial phase and conceivably should not be blocked. Setting the focus on a later time point for CD40 inhibition.

Over the last years, various studies pointed out that the early inflammatory phase is essential for the progression of an appropriate healing by initiating all relevant processes like removal of dead cardiomyocytes, rendering an inhibition of this early inflammatory signal a potential burden for the ensuing cardiac repair.[155, 156] The concept that CD40 signaling until day 5 post AMI is necessary during early immune response together with the knowledge of CD40 gene and protein expression patterns prompted us to apply resulted in an adjusted TRAF-STOP therapy strategy, starting continuous CD40 inhibition at day 5 after AMI. This should ensure that both the healing phase alone and in combination with the maturation phase are taken into account. Echocardiographic analyses revealed a significantly improved LV cardiac function at day 14 after AMI that continued over day 21 and still persisted until day 28, almost restoring the basal cardiac function. Thereupon the question arose whether changes of the immunological cell distribution of the heart triggered this beneficial outcome, because modifications of distinct immune cell populations (e.g neutrophils[60], monocytes and macrophages[157] or lymphocytes[68, 158]) are a promising strategy to improve cardiac outcome after AMI.

Obviously, monocytes and macrophages were of specific interest as they become more positive for CD40 until day 5 after AMI and are the most prominent cell population in which TRAF-STOP treatment was implemented. Flow cytometry measurements at day 14 for control- and TRAF-STOP-treated mice offered no significant numerical alterations for all immune cell populations observed including monocytes and macrophages. A possible explanation for this is the fact that day 14 after AMI marks the end of the proliferative phase, when the immune response is already downregulated and myofibroblasts define the scar formation via a dense collagen-based extracellular matrix.[45, 67] This means that potential alterations in the immune cell composition triggered by TRAF-STOP could be reversed by this time, making quantification of immune cells at earlier time points after treatment necessary. In contrast to the neutral findings at day 14 quantification of immune cells at day 28 post AMI displayed at least a significant decrease of $CD11b^{+}Ly6G^{-}Ly6C^{low}$ monocytes and macrophages upon

CD40/TRAF6 inhibition, without changing the overall numbers of monocytes and macrophages. The immune cell populations of leukocytes, neutrophils, B and T cells featured no alterations. In the first place, a reduction of anti-inflammatory monocytes and macrophages appears counterintuitive given that various studies confirmed cardioprotection due to less pro-inflammatory monocytes shifting the immune response to a more reparative designation in experimental mouse models and in humans.[64, 159, 160] On the other hand, day 28 is an even later time point to monitor infiltrated immune cells in the myocardium, since downregulation of inflammation already occurred and scar maturation is ongoing.[45, 161] Whereas the immunosuppressive effect of prolonged CD40 inhibition must also be taken into account. A more detailed analysis including more subpopulations of monocytes and macrophages regarding earlier time points could be helpful to obtain a deeper insight. In particular, further investigation of anti-inflammatory Ly6C^{low} and pro- inflammatory Ly6C^{high} macrophages is required, as their biphasic accumulation and effector processes are a key factor in cardiac healing and a reduction of Ly6C^{high} monocytes and macrophages improves cardiac outcome and remodelling.[64, 132, 162] Furthermore, DCs play a crucial role as they enhance recruitment of monocytes and macrophages, resulting in cardioprotection, improving cardiac function and prevention of adverse cardiac remodeling.[55, 65] In their function as APCs, DCs shape the adaptive immunity, by activation of Th and T_{reg} cells, which then initiate the anti-inflammatory phase contributing to better cardiac healing.[58, 69]

Even though the remarkable beneficial effect on LV cardiac function via CD40 inhibition post AMI cannot be clarified via immune cell infiltration by now, structural analyses focusing on scar size and fibrosis were performed. Scar size was evaluated by histological WGA and phalloidin staining of heart slices covering the whole infarct area, identifying the proportion of fibrotic tissue. These analyses were performed by Chiara Wernet. For day 14 and 28 the cardiac scar size across all sections of TRAF-STOP- treated mice was lower compared to the control group, affirmed by significant differences when assessing the area under the curve. Strikingly, the contrast in actual scar size is smaller at day 14 and becomes even more evident at day 28, because the scar size of control-treated mice nearly doubles over this time, while scar size of TRAF-STOP-treated mice remains almost the same. This indicates that CD40 inhibition post AMI triggers distinct processes, which in the end are sufficient to reduce scar formation, possibly by reducing fibrosis. However, the actual mechanisms driving this effect of CD40 inhibition remain unclear, since there are many viable reasons how inflammation and healing could contribute, as progression of these phases determines fibroblast activation, initiated via a synergic communication with cardiomyocytes, endothelial and immune cells.[163] Following activation fibroblasts differentiate into extracellular matrix producing myofibroblasts, forming a fibrotic scar in the affected region.[164] The timeline of fibrosis is crucial considering it is required for genuine healing and granting the structural integrity of the ventricle, whereas prolongation

results in chronic consequences to heart function and survival.[165] Inhibition of CD40 at day 5 post AMI seems to modify fibrosis, either directly, since fibroblasts also express CD40 to a certain extent at least in humans[166], or indirect via altering activation through changes of immune or endothelial cells expressing CD40. In a model of heart failure similar results considering the reduction of adverse cardiac remodeling, improvement of cardiac function and decrease of fibrosis upon TRAF-STOP treatment were found, supporting the results of CD40 inhibition in CVD.[127]

Taken all the findings of CD40 inhibition via TRAF-STOP together, it appears that the exact time point and duration of CD40 blockage is highly relevant for the outcome post AMI. Preconditional administration could not affect recovery of LV function, as well as infarct and scar size although changes of pro- and anti-inflammatory monocytes and macrophages were observed in the acute phase. Leaving the early inflammatory phase untouched and starting CD40 inhibition at day 5 post AMI, a time point with highly upregulated CD40, resulted in a significant improved LV cardiac function already beginning at day 14, that was apparently achieved due to less fibrosis, causing smaller scar sizes. Even though the cardiac immune cell distributions remained mostly unchanged, TRAF-STOP treatment modified the repair after AMI, raising the question of the exact underlying mechanisms. Further investigation to determine the perfect time point and the duration of CD40 inhibition is needed, as well as a more detailed analysis on the contribution of immune cells and other cell types to fibrosis. Nevertheless, the results demonstrated so far signify a beneficial role of CD40 inhibition for cardiac outcome after AMI, making TRAF-STOP a promising therapeutical mediator for future handling of AMI patients.

5.3 Activation of CD40 signaling via an agonistic antibody in AMI

Patients suffering from CVD, particularly including acute or chronic heart failure, ischemic stroke and myocardial infarction, display high levels of sCD40L.[105, 142] Furthermore, there is an ongoing debate about the efficiency of elevated sCD40L levels as marker for an increased risk of cardiovascular events and AMI, with studies that support an association of sCD40L[103, 109] and others that fail to reproduce such an association.[167, 168] Raised levels of sCD40L are also present in diseases that are affiliated risk factors of CVD, most prominently in diabetes.[169, 170] Since it is well known, that AMI patients with the comorbid diabetes mellitus inhabit an increased mortality risk and suffer from a severe impaired cardiac outcome[171, 172], understanding the underlying mechanisms is of great interest to develop prospective therapy. According to these findings, increased levels of CD40L seem to play a crucial role during the immune response and reparative phase after AMI, raising the hypothesis, that simulation of elevated sCD40L levels can replicate increased inflammation and impaired function that occur

in AMI in combination with diabetes, under normo-glycemic conditions. Additionally, the activation of CD40 signaling is kind of the opposite of the previous inhibition via TRAF-STOP making it a suitable modulation to gain more insights into CD40 signaling.

Activation of CD40 signaling was realized via administration of an agonistic CD40 antibody with clone FGK45 (αCD40) that mimics elevated levels of sCD40L. Stimulation of CD40 via different αCD40 antibodies was used in inflammatory diseases like lupus and rheumatoid arthritis[173, 174], and by now intensely in cancer therapy, because it enhances the immune response and recruits different immune cells to the tumor site.[175] Mice were treated either with αCD40 or a corresponding IgG antibody control for two times over 7 days without any IR surgery. Analyses of cardiac immune cells via flow cytometry revealed significant changes in the numbers of different populations. Interestingly, the activation of CD40 signaling led unitary to reductions within these cell populations. The decrease in $CD19^+$ B cell numbers was the most remarkable, as αCD40-treated mice featured an 80 % reduction in cell numbers compared to control mice. Besides this, $CD4^+$ Th cells, $Ly6C^{low}$ and $Ly6C^{int}$ monocytes and macrophages, as well as the CD4/CD8 ratio were lowered. All in all, these results are somewhat surprising, bearing in mind that agonistic CD40 antibodies are used to enhance the immune response in cancer therapy[175], while here the amount of infiltrating immune cells is downregulated. In this case, the most conceivable explanation is the circumstance that the mice were healthy and exhibited no other substantial progressing immune response, which could interfere with CD40 activation. Nevertheless, these results should not be ignored when evaluating immune cell distribution in the following experiments.

During the organ harvesting for quantification of cardiac immune cells at day 1 and 7 upon AMI, along with a single treatment of αCD40 directly after IR surgery, a splenomegaly was recognized. At both time points, spleens were visually larger in αCD40-treated mice and a comparison of spleen weights confirmed this impression. In contrast, no alterations of heart weights were detected. The exposed splenomegaly was rather severe as the increase was already noticeable after one day and weights at day 7 were at least doubled. Normalization to body weight confirmed the increased weight of spleens and thus the splenomegaly. A similar phenomenon has only been observed in αCD40-treated mice without AMI induction, but to a much lesser extent. However, a study in the context of hemophagocytic syndrome and treatment with the same αCD40 antibody, encountered a splenomegaly thirty hours after a single dose injection, caused by expansion of the white pulp due to B cell activation and proliferation.[176] Activation of splenic B cells could explain that less B cells infiltrate the heart after αCD40 treatment without AMI. Furthermore, mice developed typical clinical and biochemical features of a hemophagocytic syndrome, including acute ischemic liver disease and elevation of inflammatory cytokines.[176] These severe side effects altering the

inflammatory response and leading to leukopenia in peripheral blood need to be considered when further analyzing the infiltration of cardiac immune cells.

Flow cytometry analysis at day 1 post AMI and single dose treatment of αCD40 revealed a very specific reduction of anti-inflammatory Ly6C^{low} monocytes and macrophages, while other populations remained unchanged, providing first evidence that the immune response is shifted towards a more pro-inflammatory phenotype. Induction of AMI also neglected the decrease of immune cell populations that were present without IR surgery. At day 7 post AMI treatment with αCD40 modified quantity and composition of lymphocytes within the heart. Again, B cells were significantly reduced, which is consistent with the documented splenomegaly. A tendency of increased CD3$^+$ T cells is underlined by significant differences in the respective subpopulations. CD4$^+$ Th cells show a tendency of reduction, while CD8$^+$ cytotoxic T cells were significantly elevated. This led to a consequential reduction in the ratio of CD4$^+$ Th towards CD8$^+$ cytotoxic T cells. Finally, a decrease in the number of CD4$^+$FoxP3$^+$ T_{reg} cells was observed. Sckisel et al. described comparable alterations of CD4$^+$ and CD8$^+$ T cells following immunostimulatory therapy for lymphoid and peripheral organs, not covering the heart.[177] Therefore, the splenomegaly is a potential explanation for the changes in T cell numbers infiltrating the heart, since the massive change in B cell recruitment within the spleen, possibly interferes with T cell homeostasis and migration. In AMI, the T cell-mediated immune function is critical for wound healing and activation but also silencing of other immune cells.[66] CD4$^+$ Th cells are essential to promote cardiac repair[178], while CD8$^+$ cytotoxic T cells contribute to adverse cardiac remodelling via release of granzyme B.[179] T_{reg} cells control the proliferation of CD4$^+$ and CD8$^+$ T cells exhibiting immunosuppressive function and it has been demonstrated that infiltration of T_{reg} cells into the heart leads to cardioprotection.[158, 180] Relying on these facts, the observed changes in proportion of CD4$^+$ towards CD8$^+$ T cells, caused by significantly increased CD8$^+$ cytotoxic T cells, combined with the reduction of CD4$^+$FoxP3$^+$ T_{reg} cells, offers a first indication on the expected impairing effect of CD40 activation on cardiac outcome.

In line with this, echocardiographic analyses revealed a drastic impairment of LV function, evidenced by significant reduction of EF, SV and CO starting one day after AMI and persisting until day 7 post AMI. Histological examination supported the findings insofar as activation of CD40 resulted in increased infarct sizes compared to the control group at day 1. Larger infarct size and impaired LV cardiac function are the consequences of the increased inflammation marked by the splenomegaly aligned with reduced anti-inflammatory monocytes and macrophages at day 1. The most likely underlying mechanisms are the shift towards a more pro-inflammatory macrophage response, causing adverse cardiac healing, and the overall increased inflammation throughout multiple organs, altering the explicit cardiac immune response.[132, 159] However, the modified proportions of B and T cells could also explain that

compromised LV function is sustained until day 7, via induction of adverse cardiac remodelling and wound healing. Within the T cell compartment the loss of $CD4^+$ Th cells and increase of cytotoxic $CD8^+$ cells, in conjunction with a decreased number of $CD4^+FoxP3^+$ T_{reg} cells may altogether have a negative impact on cardiac outcome post AMI.[178-180] This T cell-mediated modulation of cardiac repair seems to counter the positive effect of a B cell depletion after AMI, which was proclaimed by Zouggari et al., where pro-inflammatory $Ly6C^{high}$ monocytes and macrophages are reduced, improving the cardiac function.[68] The potential countering effect upon CD40 activation is indicated as $Ly6C^{high}$ monocytes and macrophages remained stable, even though B cell numbers were drastically decreased.

Activation of CD40 signaling in normo-glycemic mice via simulating high levels of sCD40L, led to a more severe outcome after AMI, impairing LV function, increasing infarct size and modulating the composition of immune cells. These findings corroborate the deteriorated outcome of patients after AMI, that additionally suffer from diabetes, where sCD40L levels are elevated.[169, 170] On top of that, it emphasizes that exaggerated CD40 signaling adversely influences the development of cardiac healing, pointing out that inhibition of CD40 signaling is a promising strategy to overcome this burden. However, the definite mechanisms behind these results, including inflammation and release of cytokines, as well as the long-term outcome and impact on mechanisms such as fibrosis, remain unclear. Since activation of CD40 signaling was only mimicked via αCD40 treatment, an experimental diabetic mouse model should be used to gain more insight into cardiac repair after AMI under diabetic conditions. Especially, following the result of Steven et al., stating that CD40L controls obesity-associated vascular inflammation, oxidative stress, and endothelial dysfunction in high fat diet-treated and db/db mice.[181] All these aspects have to be the target of future research to better understand the pathways behind CD40L-mediated immune response.

5.4 Effect of cell type-specific CD40L deficiency in AMI

So far, this study showed that inhibition of CD40-TRAF6 signaling is beneficial for cardiac outcome after AMI, while elevated levels of sCD40L lead to the opposite effect. Considering that high levels of sCD40L were artificially simulated, the next part of research, was to investigate the cell types that commonly express CD40L during the immune response after AMI, as they represent a possible target to reduce CD40L and thus also CD40 signaling. Given that CD40L is mostly expressed on T cells and platelets[87, 88], corresponding CD40L cell type-specific deficient mice were generated using the Cre/loxP system[128], to allow an indirect inhibition of CD40 signaling due to loss of CD40L. We hypothesized that deleting CD40L from most prevalent expressing cells (i.e., T cells and platelets) could reduce the activation of CD40 signaling, thereby decreasing inflammation and improving prognosis of the heart after AMI.

This approach will also yield insight, which CD40L-expressing cell type is primarily involved in CD40 signaling during the acute phase after AMI.

First of all, considering the fact that the cell type specific depletion of CD40L on T cells could shape the basal distribution of immune cells, peripheral blood and cardiac immune cells were quantified under non-ischemic conditions. Flow cytometric analysis of circulating immune cells unveiled multiple differences comparing *Cd40lg*$^{fl/fl}$*Cd4-Cre*$^{-}$ and *Cd40lg*$^{fl/fl}$*Cd4-Cre*$^{+}$ mice. Total numbers of leukocytes were significantly increased together with subpopulations of anti-inflammatory monocytes and macrophages, B cells and T cells. In line with this blood cell counter measurements displayed raised leukocyte, lymphocyte and monocyte numbers, while neutrophils and platelets remained stable. Corresponding analysis of peripheral blood was performed in a study of Lacy et al., in that mice were crossed to *Apoe*$^{-/-}$ mice to study atherosclerosis. The authors noted the same increase of leukocytes and lymphocytes, whereby no changes on monocytes and macrophages were observed.[120] Evaluation of cardiac immune cells exposed deviant changes for various populations. Significant reduction of T cells and associated subpopulations, amongst them Th and T_{reg} cells, was somehow expected, as the loss of CD40L on T cells will likely feature a direct influence on their function. Surprisingly, monocytes and macrophage populations were also altered, displaying an increase of Ly6C^{int} cells. Simultaneous T cell reduction in the heart and increased T cell numbers in the peripheral blood suspect that T cell-specific CD40L deficiency halts the infiltration of T cells into the healthy myocardium, decreasing the number of CD4^{+} Th and CD4^{+}FoxP3^{+} T_{reg} cells. Consequently, CD40L expression seems to be vital for T cell activation and migration into the myocardium. However, the concurrent elevation in circulating and cardiac monocyte and macrophage numbers after loss of CD40L on T cells could further indicate that T cell activation by APCs is no longer sufficient enough, as the co-stimulatory signal of CD40L is needed, whereby accumulation of monocytes and macrophages happens.[77] The amendment of immunological composition all alone due to CD40L deficiency must be taken into account, considering inflammation and immune response when mice undergo AMI.

For peripheral blood of *Cd40lg*$^{fl/fl}$*Cd4-Cre*$^{+}$ mice one day post AMI the number of Ly6C^{int} monocytes and macrophages in flow cytometry measurements was significantly increased, whereas blood count analysis showed more neutrophils. The previous alterations found under non-ischemic basal conditions were all overturned, suggesting a decrease of leukocytes, lymphocytes and monocytes due to cardiac inflammation, as the overall cell numbers in control mice stayed nearly the same. Except for Ly6G^{+} neutrophils, the numbers between AMI compared to baseline were elevated for both groups, marking the rapid response of neutrophils after AMI.[52, 67] Intriguingly, calculation via blood counter identified a significant elevation of neutrophils for *Cd40lg*$^{fl/fl}$*Cd4-Cre*$^{+}$ mice, that was not detected in flow cytometry. These

observations could be a first hint that less neutrophils migrate into the heart and are restrained in the blood. A closer look at the cardiac immune cell distribution refutes this expectation, as no differences for neutrophils can be examined. Instead, B cells were exclusively changed and featured higher numbers after T cell specific loss of CD40L.

Relevance of these alterations in cardiac and circulating immune response on cardiac outcome was demonstrated via functional and structural analyses. LV cardiac function, covering EF, SV and CO, was significantly improved in mice with CD40L deficient T cells. This was accompanied by smaller infarct sizes of *Cd40lg*$^{fl/fl}$*Cd4-Cre*$^{+}$ mice one day post AMI. The rapid recovery of cardiac function together with the structural changes in the infarct area imply drastic changes of inflammatory processes during the first 24h. As neutrophils and macrophages are the most abundant cell types during this phase, shaping the immune response and cardiac remodelling via apoptosis and chemokine signaling, differences in this populations would be awaited.[52, 53] However, as immunological analyses proved, there were no alterations in frequency of these two cell types within the myocardium. In contrast, raised numbers of B cells were present one day after AMI. This is somewhat surprising as B cells are actually known to peak around day 7 after AMI and depletion of B cells accounts as a promising strategy to improve cardiac outcome.[67, 68] Here the beneficial effect may occur as a consequence of B cell and neutrophil interaction, since neutrophils were increased in peripheral blood, inducing an antibody-mediated response, while the specific role of this response regarding the heart still requires further study.[182, 183] In a corresponding study from Lacy et al. on the effect of CD40L deficiency on T cell in atherosclerosis, reduced lesion size and plaque inflammation due to a restrained Th1 response and reduced IFN-γ levels were reported.[120] Perhaps this mechanism also occurs in AMI and leads to improved cardiac function and smaller infarct sizes recognized in this study. However, the precise mechanisms of T cell-specific deficiency of CD40L in AMI remain unclear, requiring future research of this topic.

Platelets are another cell population known for their CD40L expression after activation and thereby triggering inflammatory reactions.[184] CD40L on activated platelets can induce multiple immune responses, among them B cell isotype switching and maturation of DCs.[185, 186] Direct interaction of platelets expressing CD40L is limited, because binding of surface CD40 on other cells results in cleavage of CD40L and release in its soluble form.[186, 187] Since high levels of (s)CD40L are associated with impaired cardiac outcome and induction of inflammatory processes in atherosclerosis, a reduction of CD40L is a potential target to overcome this burden.[103, 121] In this study a platelet-specific deficient mouse for CD40L (*Cd40lg*$^{fl/fl}$*Pf4-Cre*$^{+}$) was used to investigate the role of the CD40/CD40L dyad in the acute phase following AMI. To exclude any changes in immune cell composition due to the loss of CD40L on platelets, flow cytometry and blood count baseline measurements of peripheral blood and hearts were

performed. In both methods, the quantities of circulating immune cell numbers were not altered by platelet-specific loss of CD40L. Even the number of platelets stayed the same. For cardiac immune cells a tendency of increased $CD45^+$ leukocytes was noticed in *Cd40lg*$^{fl/fl}$*Pf4-Cre*$^+$ mice, otherwise there were no differences caused by CD40L platelet deficiency. Again, these results are consistent with the observations of Lacy et al. in a comparable, yet hyperlipidemic mouse model (*Apoe*$^{-/-}$).[120]

Next, cardiac immune cell numbers of mice with and without a platelet specific defiance for CD40L at day 1 after AMI were assessed. Total amounts of all cell populations remained unchanged. Along with the findings in cell proportions no alterations regarding LV function and infarct size were observed. All in all, these findings were a bit surprising, since CD40/CD40L signaling is a key factor in platelet-mediated inflammation that is also relevant after AMI.[188, 189] The time point of analyses could be a major factor that needs to be considered, as inflammation is an ongoing process and the exact moment where platelets are involved is not fully known by now. Hence, a prolonged experimental setup could provide more information about long-term influence of the platelet-specific loss of CD40L on cardiac outcome. Overall, the down regulation of CD40 signaling via cell type-specific CD40L deficiency revealed that T cells and not platelets are mainly involved in the acute phase of inflammation after AMI, contributing to a beneficial cardiac outcome, which makes further concentration on T cell-mediated cardiac injury and repair in the context of CD40/CD40L signaling inevitable.

5.5 Conclusion and future perspectives

Worldwide the high and increasing impact of CVD and in particular AMI on morbidity and mortality points out the relevance to understand the underlying processes and mechanisms of cardiac pathogenesis to establish adequate prevention or therapy of patients. For this purpose, the main goal of this thesis was focused onto the investigation of co-stimulatory molecules CD40 and CD40L and uncovering their role during inflammation and repair after AMI. Via different modulation strategies of CD40 signaling, new insights into the relevance of the CD40/CD40L dyad and their cell-type specific interactions were gained. Specific blocking of CD40-TRAF6 signaling in monocytes and macrophages five days after AMI resulted in a significantly improved cardiac outcome by altering fibrotic scar formation indicating a promising therapeutical approach. These findings were supported, when exaggerated activation of CD40 signaling by simulation of high sCD40L levels led to severe immunological changes, causing deterioration of cardiac function and enlarged infarct sizes. Further analyses of the CD40L cell types that predominately mediate CD40 signaling under acute inflammatory conditions, revealed the important impact of T cell-specific CD40L, as deficiency rapidly improved cardiac outcome. Together all these findings highlight the importance of CD40/CD40L signaling and

interaction following AMI, shifting the focus towards a time dependent and either direct or indirect inhibition of CD40 signaling as potential therapy.

Nevertheless, additional research using TRAF-STOP as inhibitor is required, to beneficially influence long-term prognosis, define the perfect time point and duration of treatment and to provide further information about the underlying mechanisms. Since the CD40/CD40L dyad is involved in many other immunological processes potential aspects of immunosuppressive complications must also be taken into account when it comes to a future perspective as pharmacological treatment of AMI patients. In this respect, the results of this study expand the knowledge of CD40/CD40L signaling following AMI providing new insights in immunological, functional and structural characteristics. At the same time, this thesis presents for the first time a strategy for the development of a promising CD40-directed therapy to overcome the burden of AMI.

6 References

1. World Health Organization. *Cardiovascular diseases (CVDs)*. [20.03.2023]; Available from: https://www.who.int/news-room/fact-sheets/detail/cardiovascular-diseases-(cvds).
2. Tsao, C.W., et al., *Heart Disease and Stroke Statistics-2023 Update: A Report From the American Heart Association.* Circulation, 2023. **147**(8): p. e93-e621, doi: https://doi.org/10.1161/CIR.0000000000001123.
3. Roth, G.A., et al., *Global, regional, and national age-sex-specific mortality for 282 causes of death in 195 countries and territories, 1980–2017: a systematic analysis for the Global Burden of Disease Study 2017.* The Lancet, 2018. **392**(10159): p. 1736-1788, doi: https://doi.org/10.1016/S0140-6736(18)32203-7.
4. Roth, G.A., et al., *Global Burden of Cardiovascular Diseases and Risk Factors, 1990–2019: Update From the GBD 2019 Study.* Journal of the American College of Cardiology, 2020. **76**(25): p. 2982-3021, doi: https://doi.org/10.1016/j.jacc.2020.11.010.
5. Sonawane, A.R., E. Aikawa, and M. Aikawa, *Connections for Matters of the Heart: Network Medicine in Cardiovascular Diseases.* Frontiers in Cardiovascular Medicine, 2022. **9**, doi: https://doi.org/10.3389/fcvm.2022.873582.
6. Bhatnagar, A., *Environmental Determinants of Cardiovascular Disease.* Circulation Research, 2017. **121**(2): p. 162-180, doi: https://doi.org/10.1161/CIRCRESAHA.117.306458.
7. Mozaffarian, D., P.W.F. Wilson, and W.B. Kannel, *Beyond Established and Novel Risk Factors.* Circulation, 2008. **117**(23): p. 3031-3038, doi: https://doi.org/10.1161/CIRCULATIONAHA.107.738732.
8. Bays, H.E., et al., *Ten things to know about ten cardiovascular disease risk factors.* American Journal of Preventive Cardiology, 2021. **5**: p. 100149, doi: https://doi.org/10.1016/j.ajpc.2021.100149.
9. Kaminsky, L.A., et al., *The importance of healthy lifestyle behaviors in the prevention of cardiovascular disease.* Progress in Cardiovascular Diseases, 2022. **70**: p. 8-15, doi: https://doi.org/10.1016/j.pcad.2021.12.001.
10. Turer, C.B., T.M. Brady, and S.D.d. Ferranti, *Obesity, Hypertension, and Dyslipidemia in Childhood Are Key Modifiable Antecedents of Adult Cardiovascular Disease.* Circulation, 2018. **137**(12): p. 1256-1259, doi: https://doi.org/10.1161/CIRCULATIONAHA.118.032531.
11. Daviglus, M.L., D.M. Lloyd-Jones, and A. Pirzada, *Preventing Cardiovascular Disease in the 21st Century.* American Journal of Cardiovascular Drugs, 2006. **6**(2): p. 87-101, doi: https://doi.org/10.2165/00129784-200606020-00003.
12. Francula-Zaninovic, S. and A.I. Nola, *Management of Measurable Variable Cardiovascular Disease' Risk Factors.* Current Cardiology Reviews, 2018. **14**(3): p. 153-163, doi: http://dx.doi.org/10.2174/1573403X14666180222102312.
13. Arora, G. and V. Bittner, *Chest Pain Characteristics and Gender in the Early Diagnosis of Acute Myocardial Infarction.* Current Cardiology Reports, 2015. **17**(2): p. 5, doi: https://doi.org/10.1007/s11886-014-0557-5.
14. Ferry, A.V., et al., *Presenting Symptoms in Men and Women Diagnosed With Myocardial Infarction Using Sex-Specific Criteria.* Journal of the American Heart Association, 2019. **8**(17): p. e012307, doi: https://doi.org/10.1161/JAHA.119.012307.
15. Stengaard, C., et al., *Prehospital diagnosis of patients with acute myocardial infarction.* Diagnosis, 2016. **3**(4): p. 155-166, doi: https://doi.org/10.1515/dx-2016-0021.
16. Vafaie, M., *State-of-the-art diagnosis of myocardial infarction.* Diagnosis, 2016. **3**(4): p. 137-142, doi: https://doi.org/10.1515/dx-2016-0024.
17. Park, K.C., et al., *Cardiac troponins: from myocardial infarction to chronic disease.* Cardiovascular Research, 2017. **113**(14): p. 1708-1718, doi: https://doi.org/10.1093/cvr/cvx183.

18. Brush, J.E., S. Kaul, and H.M. Krumholz, *Troponin Testing for Clinicians.* Journal of the American College of Cardiology, 2016. **68**(21): p. 2365-2375, doi: https://doi.org/10.1016/j.jacc.2016.08.066.
19. Thygesen, K., et al., *Third universal definition of myocardial infarction.* European Heart Journal, 2012. **33**(20): p. 2551-2567, doi: https://doi.org/10.1093/eurheartj/ehs184.
20. O'Gara, P.T., et al., *2013 ACCF/AHA Guideline for the Management of ST-Elevation Myocardial Infarction: A Report of the American College of Cardiology Foundation/American Heart Association Task Force on Practice Guidelines.* Journal of the American College of Cardiology, 2013. **61**(4): p. e78-e140, doi: https://doi.org/10.1016/j.jacc.2012.11.019.
21. Reed, G.W., J.E. Rossi, and C.P. Cannon, *Acute myocardial infarction.* The Lancet, 2017. **389**(10065): p. 197-210, doi: https://doi.org/10.1016/S0140-6736(16)30677-8.
22. Minicucci, M.F., et al., *Heart Failure After Myocardial Infarction: Clinical Implications and Treatment.* Clinical Cardiology, 2011. **34**(7): p. 410-414, doi: https://doi.org/10.1002/clc.20922.
23. Thygesen, K., et al., *Fourth Universal Definition of Myocardial Infarction (2018).* Circulation, 2018. **138**(20): p. e618-e651, doi: https://doi.org/10.1161/CIR.0000000000000617.
24. Lu, L., et al., *Myocardial Infarction: Symptoms and Treatments.* Cell Biochemistry and Biophysics, 2015. **72**(3): p. 865-867, doi: https://doi.org/10.1007/s12013-015-0553-4.
25. Abdelghany, M., et al., *Kounis syndrome: A review article on epidemiology, diagnostic findings, management and complications of allergic acute coronary syndrome.* International Journal of Cardiology, 2017. **232**: p. 1-4, doi: https://doi.org/10.1016/j.ijcard.2017.01.124.
26. Davies, M.J., *Acute coronary thrombosis—the role of plaque disruption and its initiation and prevention.* European Heart Journal, 1995. **16**(suppl_L): p. 3-7, doi: https://doi.org/10.1093/eurheartj/16.suppl_L.3.
27. Palasubramaniam, J., X. Wang, and K. Peter, *Myocardial Infarction—From Atherosclerosis to Thrombosis.* Arteriosclerosis, Thrombosis, and Vascular Biology, 2019. **39**(8): p. e176-e185, doi: https://doi.org/10.1161/ATVBAHA.119.312578.
28. Hasche, E.T., et al., *Relation Between Ischemia Time, Infarct Size, and Left Ventricular Function in Humans.* Circulation, 1995. **92**(4): p. 710-719, doi: https://doi.org/10.1161/01.CIR.92.4.710.
29. Simoons, M.L., et al., *Early thrombolysis in acute myocardial infarction: Limitation of infarct size and improved survival.* Journal of the American College of Cardiology, 1986. **7**(4): p. 717-728, doi: https://doi.org/10.1016/S0735-1097(86)80329-1.
30. Damluji, A.A., et al., *Mechanical Complications of Acute Myocardial Infarction: A Scientific Statement From the American Heart Association.* Circulation, 2021. **144**(2): p. e16-e35, doi: https://doi.org/10.1161/CIR.0000000000000985.
31. Simonis, G., R.H. Strasser, and B. Ebner, *Reperfusion injury in acute myocardial infarction.* Critical Care, 2012. **16**(2): p. A22, doi: https://doi.org/10.1186/cc11280.
32. Nielsen, P.H., et al., *Primary Angioplasty Versus Fibrinolysis in Acute Myocardial Infarction.* Circulation, 2010. **121**(13): p. 1484-1491, doi: https://doi.org/10.1161/CIRCULATIONAHA.109.873224.
33. D'Souza, S.P., et al., *Routine early coronary angioplasty versus ischaemia-guided angioplasty after thrombolysis in acute ST-elevation myocardial infarction: a meta-analysis.* European Heart Journal, 2011. **32**(8): p. 972-982, doi: https://doi.org/10.1093/eurheartj/ehq398.
34. Yellon, D.M. and D.J. Hausenloy, *Myocardial Reperfusion Injury.* New England Journal of Medicine, 2007. **357**(11): p. 1121-1135, doi: https://doi.org/10.1056/NEJMra071667.
35. Hausenloy, D.J. and D.M. Yellon, *Myocardial ischemia-reperfusion injury: a neglected therapeutic target.* The Journal of Clinical Investigation, 2013. **123**(1): p. 92-100, doi: https://doi.org/10.1172/JCI62874.
36. Kalogeris, T., et al., *Ischemia/Reperfusion*, in *Comprehensive Physiology*. 2016. p. 113-170, doi: https://doi.org/10.1002/cphy.c160006.

37. Ibáñez, B., et al., *Evolving Therapies for Myocardial Ischemia/Reperfusion Injury.* Journal of the American College of Cardiology, 2015. **65**(14): p. 1454-1471, doi: https://doi.org/10.1016/j.jacc.2015.02.032.
38. Bhatt, A.S., A.P. Ambrosy, and E.J. Velazquez, *Adverse Remodeling and Reverse Remodeling After Myocardial Infarction.* Current Cardiology Reports, 2017. **19**(8): p. 71, doi: https://doi.org/10.1007/s11886-017-0876-4.
39. Ong, S.-B., et al., *Inflammation following acute myocardial infarction: Multiple players, dynamic roles, and novel therapeutic opportunities.* Pharmacology & Therapeutics, 2018. **186**: p. 73-87, doi: https://doi.org/10.1016/j.pharmthera.2018.01.001.
40. Lavine, K.J., et al., *Distinct macrophage lineages contribute to disparate patterns of cardiac recovery and remodeling in the neonatal and adult heart.* Proceedings of the National Academy of Sciences, 2014. **111**(45): p. 16029-16034, doi: https://doi.org/10.1073/pnas.1406508111.
41. Dittrich, A. and H. Lauridsen, *Myocardial infarction and the immune response - Scarring or regeneration? A comparative look at mammals and popular regenerating animal models.* Journal of Immunology and Regenerative Medicine, 2019. **4**: p. 100016, doi: https://doi.org/10.1016/j.regen.2019.100016.
42. Gentek, R. and G. Hoeffel, *The Innate Immune Response in Myocardial Infarction, Repair, and Regeneration*, in *The Immunology of Cardiovascular Homeostasis and Pathology*, S. Sattler and T. Kennedy-Lydon, Editors. 2017, Springer International Publishing: Cham. p. 251-272, doi: https://doi.org/10.1007/978-3-319-57613-8_12.
43. Frangogiannis, N.G., *The immune system and cardiac repair.* Pharmacological Research, 2008. **58**(2): p. 88-111, doi: https://doi.org/10.1016/j.phrs.2008.06.007.
44. Frangogiannis, N.G., *The Immune System and the Remodeling Infarcted Heart: Cell Biological Insights and Therapeutic Opportunities.* Journal of Cardiovascular Pharmacology, 2014. **63**(3), doi: https://doi.org/10.1097/FJC.0000000000000003.
45. Forte, E., M.B. Furtado, and N. Rosenthal, *The interstitium in cardiac repair: role of the immune–stromal cell interplay.* Nature Reviews Cardiology, 2018. **15**(10): p. 601-616, doi: https://doi.org/10.1038/s41569-018-0077-x.
46. Prabhu, S.D. and N.G. Frangogiannis, *The Biological Basis for Cardiac Repair After Myocardial Infarction: From Inflammation to Fibrosis.* Circ Res, 2016. **119**(1): p. 91-112, doi: https://doi.org/10.1161/circresaha.116.303577.
47. Timmers, L., et al., *The innate immune response in reperfused myocardium.* Cardiovascular Research, 2012. **94**(2): p. 276-283, doi: https://doi.org/10.1093/cvr/cvs018.
48. van Hout, G.P.J., et al., *Targeting danger-associated molecular patterns after myocardial infarction.* Expert Opinion on Therapeutic Targets, 2016. **20**(2): p. 223-239, doi: https://doi.org/10.1517/14728222.2016.1088005.
49. Timmers, L., et al., *Toll-Like Receptor 4 Mediates Maladaptive Left Ventricular Remodeling and Impairs Cardiac Function After Myocardial Infarction.* Circulation Research, 2008. **102**(2): p. 257-264, doi: https://doi.org/10.1161/CIRCRESAHA.107.158220.
50. Frangogiannis, N.G., *The inflammatory response in myocardial injury, repair, and remodelling.* Nat Rev Cardiol, 2014. **11**(5): p. 255-65, doi: https://doi.org/10.1038/nrcardio.2014.28.
51. Rossen, R.D., et al., *Cardiolipin-protein complexes and initiation of complement activation after coronary artery occlusion.* Circulation Research, 1994. **75**(3): p. 546-555, doi: https://doi.org/10.1161/01.RES.75.3.546.
52. Ma, Y., A. Yabluchanskiy, and M.L. Lindsey, *Neutrophil roles in left ventricular remodeling following myocardial infarction.* Fibrogenesis & Tissue Repair, 2013. **6**(1): p. 11, doi: https://doi.org/10.1186/1755-1536-6-11.
53. Frodermann, V. and M. Nahrendorf, *Neutrophil–macrophage cross-talk in acute myocardial infarction.* European Heart Journal, 2017. **38**(3): p. 198-200, doi: https://doi.org/10.1093/eurheartj/ehw085.

54. Ravichandran, Kodi S., *Beginnings of a Good Apoptotic Meal: The Find-Me and Eat-Me Signaling Pathways.* Immunity, 2011. **35**(4): p. 445-455, doi: https://doi.org/10.1016/j.immuni.2011.09.004.
55. Nagai, T., et al., *Decreased Myocardial Dendritic Cells is Associated With Impaired Reparative Fibrosis and Development of Cardiac Rupture After Myocardial Infarction in Humans.* Journal of the American Heart Association, 2014. **3**(3): p. e000839, doi: https://doi.org/10.1161/JAHA.114.000839.
56. Shortman, K. and S.H. Naik, *Steady-state and inflammatory dendritic-cell development.* Nature Reviews Immunology, 2007. **7**(1): p. 19-30, doi: https://doi.org/10.1038/nri1996.
57. Banchereau, J. and R.M. Steinman, *Dendritic cells and the control of immunity.* Nature, 1998. **392**(6673): p. 245-252, doi: https://doi.org/10.1038/32588.
58. Christ, A., et al., *Dendritic Cells in Cardiovascular Diseases.* Circulation, 2013. **128**(24): p. 2603-2613, doi: https://doi.org/10.1161/CIRCULATIONAHA.113.003364.
59. Bianchi, M.E., *DAMPs, PAMPs and alarmins: all we need to know about danger.* Journal of Leukocyte Biology, 2007. **81**(1): p. 1-5, doi: https://doi.org/10.1189/jlb.0306164.
60. Horckmans, M., et al., *Neutrophils orchestrate post-myocardial infarction healing by polarizing macrophages towards a reparative phenotype.* European Heart Journal, 2017. **38**(3): p. 187-197, doi: https://doi.org/10.1093/eurheartj/ehw002.
61. Dobaczewski, M., et al., *Smad3 Signaling Critically Regulates Fibroblast Phenotype and Function in Healing Myocardial Infarction.* Circulation Research, 2010. **107**(3): p. 418-428, doi: https://doi.org/10.1161/CIRCRESAHA.109.216101.
62. Venugopal, H., et al. *Properties and Functions of Fibroblasts and Myofibroblasts in Myocardial Infarction*. Cells, 2022. **11**, DOI: https://doi.org/10.3390/cells11091386.
63. Nahrendorf, M., M.J. Pittet, and F.K. Swirski, *Monocytes: Protagonists of Infarct Inflammation and Repair After Myocardial Infarction.* Circulation, 2010. **121**(22): p. 2437-2445, doi: https://doi.org/10.1161/CIRCULATIONAHA.109.916346.
64. Hilgendorf, I., et al., *Ly-6Chigh Monocytes Depend on Nr4a1 to Balance Both Inflammatory and Reparative Phases in the Infarcted Myocardium.* Circulation Research, 2014. **114**(10): p. 1611-1622, doi: https://doi.org/10.1161/CIRCRESAHA.114.303204.
65. Anzai, A., et al., *Regulatory Role of Dendritic Cells in Postinfarction Healing and Left Ventricular Remodeling.* Circulation, 2012. **125**(10): p. 1234-1245, doi: https://doi.org/10.1161/CIRCULATIONAHA.111.052126.
66. Hofmann, U. and S. Frantz, *Role of Lymphocytes in Myocardial Injury, Healing, and Remodeling After Myocardial Infarction.* Circulation Research, 2015. **116**(2): p. 354-367, doi: https://doi.org/10.1161/CIRCRESAHA.116.304072.
67. Yan, X., et al., *Temporal dynamics of cardiac immune cell accumulation following acute myocardial infarction.* Journal of Molecular and Cellular Cardiology, 2013. **62**: p. 24-35, doi: https://doi.org/10.1016/j.yjmcc.2013.04.023.
68. Zouggari, Y., et al., *B lymphocytes trigger monocyte mobilization and impair heart function after acute myocardial infarction.* Nature Medicine, 2013. **19**(10): p. 1273-1280, doi: https://doi.org/10.1038/nm.3284.
69. Kino, T., M. Khan, and S. Mohsin *The Regulatory Role of T Cell Responses in Cardiac Remodeling Following Myocardial Infarction*. International Journal of Molecular Sciences, 2020. **21**, DOI: https://doi.org/10.3390/ijms21145013.
70. Weirather, J., et al., *Foxp3+ CD4+ T Cells Improve Healing After Myocardial Infarction by Modulating Monocyte/Macrophage Differentiation.* Circulation Research, 2014. **115**(1): p. 55-67, doi: https://doi.org/10.1161/CIRCRESAHA.115.303895.
71. Frangogiannis, N.G., *The extracellular matrix in myocardial injury, repair, and remodeling.* The Journal of Clinical Investigation, 2017. **127**(5): p. 1600-1612, doi: https://doi.org/10.1172/JCI87491.
72. Weber, K.T., et al., *Myofibroblast-mediated mechanisms of pathological remodelling of the heart.* Nature Reviews Cardiology, 2013. **10**(1): p. 15-26, doi: https://doi.org/10.1038/nrcardio.2012.158.

73. Friedl, P. and J. Storim, *Diversity in immune-cell interactions: states and functions of the immunological synapse.* Trends in Cell Biology, 2004. **14**(10): p. 557-567, doi: https://doi.org/10.1016/j.tcb.2004.09.005.
74. Turvey, S.E. and D.H. Broide, *Innate immunity.* Journal of Allergy and Clinical Immunology, 2010. **125**(2): p. S24-S32, doi: https://doi.org/10.1016/j.jaci.2009.07.016.
75. Kambayashi, T. and T.M. Laufer, *Atypical MHC class II-expressing antigen-presenting cells: can anything replace a dendritic cell?* Nature Reviews Immunology, 2014. **14**(11): p. 719-730, doi: https://doi.org/10.1038/nri3754.
76. Hilligan, K.L. and F. Ronchese, *Antigen presentation by dendritic cells and their instruction of CD4+ T helper cell responses.* Cellular & Molecular Immunology, 2020. **17**(6): p. 587-599, doi: https://doi.org/10.1038/s41423-020-0465-0.
77. Schwartz, R.H., *T Cell Anergy.* Annual Review of Immunology, 2003. **21**(1): p. 305-334, doi: https://doi.org/10.1146/annurev.immunol.21.120601.141110.
78. Kapsenberg, M.L., *Dendritic-cell control of pathogen-driven T-cell polarization.* Nature Reviews Immunology, 2003. **3**(12): p. 984-993, doi: https://doi.org/10.1038/nri1246.
79. van Kooten, C. and J. Banchereau, *CD40-CD40 ligand.* Journal of Leukocyte Biology, 2000. **67**(1): p. 2-17, doi: https://doi.org/10.1002/jlb.67.1.2.
80. An, H.-J., et al., *Crystallographic and Mutational Analysis of the CD40-CD154 Complex and Its Implications for Receptor Activation*.* Journal of Biological Chemistry, 2011. **286**(13): p. 11226-11235, doi: https://doi.org/10.1074/jbc.M110.208215.
81. Banchereau, J., et al., *Functional CD40 Antigen on B Cells, Dendritic Cells and Fibroblasts*, in *Dendritic Cells in Fundamental and Clinical Immunology: Volume 2*, J. Banchereau and D. Schmitt, Editors. 1995, Springer US: Boston, MA. p. 79-83, doi: https://doi.org/10.1007/978-1-4615-1971-3_16.
82. Kooten, C.v. and J. Banchereau, *Functions of CD40 on B cells, dendritic cells and other cells.* Current Opinion in Immunology, 1997. **9**(3): p. 330-337, doi: https://doi.org/10.1016/S0952-7915(97)80078-7.
83. Vanichakarn, P., et al., *Neutrophil CD40 enhances platelet-mediated inflammation.* Thrombosis Research, 2008. **122**(3): p. 346-358, doi: https://doi.org/10.1016/j.thromres.2007.12.019.
84. Elgueta, R., et al., *Molecular mechanism and function of CD40/CD40L engagement in the immune system.* Immunological Reviews, 2009. **229**(1): p. 152-172, doi: https://doi.org/10.1111/j.1600-065X.2009.00782.x.
85. Karpusas, M., et al., *2 å crystal structure of an extracellular fragment of human CD40 ligand.* Structure, 1995. **3**(10): p. 1031-1039, doi: https://doi.org/10.1016/S0969-2126(01)00239-8.
86. Graf, D., et al., *A soluble form of TRAP (CD40 ligand) is rapidly released after T cell activation.* European Journal of Immunology, 1995. **25**(6): p. 1749-1754, doi: https://doi.org/10.1002/eji.1830250639.
87. Schönbeck, U., F. Mach, and P. Libby, *CD154 (CD40 ligand).* The International Journal of Biochemistry & Cell Biology, 2000. **32**(7): p. 687-693, doi: https://doi.org/10.1016/S1357-2725(00)00016-9.
88. Schönbeck, U. and P. Libby, *The CD40/CD154 receptor/ligand dyad.* Cellular and Molecular Life Sciences CMLS, 2001. **58**(1): p. 4-43, doi: https://doi.org/10.1007/PL00000776.
89. Dadgostar, H., et al., *Cooperation of multiple signaling pathways in CD40-regulated gene expression in B lymphocytes.* Proceedings of the National Academy of Sciences, 2002. **99**(3): p. 1497-1502, doi: https://doi.org/10.1073/pnas.032665099.
90. Foy, T.M., et al., *gp39-CD40 interactions are essential for germinal center formation and the development of B cell memory.* Journal of Experimental Medicine, 1994. **180**(1): p. 157-163, doi: https://doi.org/10.1084/jem.180.1.157.
91. Bishop, G.A. and B.S. Hostager, *Molecular mechanisms of CD40 signaling.* Archivum immunologiae et therapiae experimentalis, 2001. **49**(2): p. 129-137.
92. Bradley, J.R. and J.S. Pober, *Tumor necrosis factor receptor-associated factors (TRAFs).* Oncogene, 2001. **20**(44): p. 6482-6491, doi: https://doi.org/10.1038/sj.onc.1204788.

93. Strohm, L., et al., *Role of CD40(L)-TRAF signaling in inflammation and resolution—a double-edged sword.* Frontiers in Pharmacology, 2022. **13**, doi: https://doi.org/10.3389/fphar.2022.995061.
94. Bishop, G.A., et al., *TRAF Proteins in CD40 Signaling*, in *TNF Receptor Associated Factors (TRAFs)*, H. Wu, Editor. 2007, Springer New York: New York, NY. p. 131-151, doi: https://doi.org/10.1007/978-0-387-70630-6_11.
95. He, J.Q., et al., *TRAF3 and Its Biological Function*, in *TNF Receptor Associated Factors (TRAFs)*, H. Wu, Editor. 2007, Springer New York: New York, NY. p. 48-59, doi: https://doi.org/10.1007/978-0-387-70630-6_4.
96. Arron, J.R., et al., *Regulation of the Subcellular Localization of Tumor Necrosis Factor Receptor–associated Factor (TRAF)2 by TRAF1 Reveals Mechanisms of TRAF2 Signaling.* Journal of Experimental Medicine, 2002. **196**(7): p. 923-934, doi: https://doi.org/10.1084/jem.20020774.
97. Hostager, B.S., *Roles of TRAF6 in CD40 signaling.* Immunologic Research, 2007. **39**(1): p. 105-114, doi: https://doi.org/10.1007/s12026-007-0082-3.
98. Davies, C.C., et al., *TRAF6 Is Required for TRAF2-Dependent CD40 Signal Transduction in Nonhemopoietic Cells.* Molecular and Cellular Biology, 2005. **25**(22): p. 9806-9819, doi: https://doi.org/10.1128/MCB.25.22.9806-9819.2005.
99. Säemann, M.D., et al., *Prevention of CD40-Triggered Dendritic Cell Maturation and Induction of T-Cell Hyporeactivity by Targeting of Janus Kinase 3.* American Journal of Transplantation, 2003. **3**(11): p. 1341-1349, doi: https://doi.org/10.1046/j.1600-6143.2003.00225.x.
100. Westman, P.C., et al., *Inflammation as a Driver of Adverse Left Ventricular Remodeling After Acute Myocardial Infarction.* Journal of the American College of Cardiology, 2016. **67**(17): p. 2050-2060, doi: https://doi.org/10.1016/j.jacc.2016.01.073.
101. Tang, T., et al., *Molecular basis and therapeutic implications of CD40/CD40L immune checkpoint.* Pharmacology & Therapeutics, 2021. **219**: p. 107709, doi: https://doi.org/10.1016/j.pharmthera.2020.107709.
102. André, P., et al., *Platelet-Derived CD40L.* Circulation, 2002. **106**(8): p. 896-899, doi: https://doi.org/10.1161/01.CIR.0000028962.04520.01.
103. Heeschen, C., et al., *Soluble CD40 Ligand in Acute Coronary Syndromes.* New England Journal of Medicine, 2003. **348**(12): p. 1104-1111, doi: https://doi.org/10.1056/NEJMoa022600.
104. Huang, Y.-q., et al., *The relationship between soluble CD40 ligand level and atherosclerosis in white-coat hypertension.* Journal of Human Hypertension, 2018. **32**(1): p. 40-45, doi: https://doi.org/10.1038/s41371-017-0016-z.
105. Ueland, T., et al., *Soluble CD40 ligand in acute and chronic heart failure.* European Heart Journal, 2005. **26**(11): p. 1101-1107, doi: https://doi.org/10.1093/eurheartj/ehi132.
106. Lobbes, M.B.I., et al., *Is there more than C-reactive protein and fibrinogen?: The prognostic value of soluble CD40 ligand, interleukin-6 and oxidized low-density lipoprotein with respect to coronary and cerebral vascular disease.* Atherosclerosis, 2006. **187**(1): p. 18-25, doi: https://doi.org/10.1016/j.atherosclerosis.2005.11.005.
107. Varo, N., et al., *Elevated Plasma Levels of the Atherogenic Mediator Soluble CD40 Ligand in Diabetic Patients.* Circulation, 2003. **107**(21): p. 2664-2669, doi: https://doi.org/10.1161/01.CIR.0000074043.46437.44.
108. Pusuroglu, H., et al., *Predictive value of elevated soluble CD40 ligand in patients undergoing primary angioplasty for ST-segment elevation myocardial infarction.* Coronary Artery Disease, 2014. **25**(7), doi: https://doi.org/10.1097/MCA.0000000000000142.
109. Schönbeck, U., et al., *Soluble CD40L and Cardiovascular Risk in Women.* Circulation, 2001. **104**(19): p. 2266-2268, doi: https://doi.org/10.1161/hc4401.099447.
110. Kotowicz, K., et al., *Biological function of CD40 on human endothelial cells: costimulation with CD40 ligand and interleukin-4 selectively induces expression of vascular cell adhesion molecule-1 and P-selectin resulting in preferential adhesion of lymphocytes.* Immunology, 2000. **100**(4): p. 441-448, doi: https://doi.org/10.1046/j.1365-2567.2000.00061.x.

111. Gerdes, N., et al., *Platelet CD40 Exacerbates Atherosclerosis by Transcellular Activation of Endothelial Cells and Leukocytes.* Arteriosclerosis, Thrombosis, and Vascular Biology, 2016. **36**(3): p. 482-490, doi: https://doi.org/10.1161/ATVBAHA.115.307074.
112. Lutgens, E. and M.J.A.P. Daemen, *CD40-CD40L Interactions in Atherosclerosis.* Trends in Cardiovascular Medicine, 2002. **12**(1): p. 27-32, doi: https://doi.org/10.1016/S1050-1738(01)00142-6.
113. Libby, P., et al., *Regulation of the Thrombotic Potential of Atheroma.* Thromb Haemost, 1999. **82**(08): p. 736-741, doi: https://doi.org/10.1055/s-0037-1615905.
114. Lutgens, E., et al., *Requirement for CD154 in the progression of atherosclerosis.* Nature Medicine, 1999. **5**(11): p. 1313-1316, doi: https://doi.org/10.1038/15271.
115. Mach, F., et al., *Reduction of atherosclerosis in mice by inhibition of CD40 signalling.* Nature, 1998. **394**(6689): p. 200-203, doi: https://doi.org/10.1038/28204.
116. Lutgens, E., et al., *Both early and delayed anti-CD40L antibody treatment induces a stable plaque phenotype.* Proceedings of the National Academy of Sciences, 2000. **97**(13): p. 7464-7469, doi: https://doi.org/10.1073/pnas.97.13.7464.
117. Boumpas, D.T., et al., *A short course of BG9588 (anti–CD40 ligand antibody) improves serologic activity and decreases hematuria in patients with proliferative lupus glomerulonephritis.* Arthritis & Rheumatism, 2003. **48**(3): p. 719-727, doi: https://doi.org/10.1002/art.10856.
118. Robles-Carrillo, L., et al., *Anti-CD40L Immune Complexes Potently Activate Platelets In Vitro and Cause Thrombosis in FCGR2A Transgenic Mice.* The Journal of Immunology, 2010. **185**(3): p. 1577-1583, doi: https://doi.org/10.4049/jimmunol.0903888.
119. Engel, D., et al., *The immunobiology of CD154–CD40–TRAF interactions in atherosclerosis.* Seminars in Immunology, 2009. **21**(5): p. 308-312, doi: https://doi.org/10.1016/j.smim.2009.06.004.
120. Lacy, M., et al., *Cell-specific and divergent roles of the CD40L-CD40 axis in atherosclerotic vascular disease.* Nature Communications, 2021. **12**(1): p. 3754, doi: https://doi.org/10.1038/s41467-021-23909-z.
121. Lievens, D., et al., *Platelet CD40L mediates thrombotic and inflammatory processes in atherosclerosis.* Blood, 2010. **116**(20): p. 4317-4327, doi: https://doi.org/10.1182/blood-2010-01-261206.
122. Bosmans, L.A., et al., *Myeloid CD40 deficiency reduces atherosclerosis by impairing macrophages' transition into a pro-inflammatory state.* Cardiovascular Research, 2022: p. cvac084, doi: https://doi.org/10.1093/cvr/cvac084.
123. Lutgens, E., et al., *Deficient CD40-TRAF6 signaling in leukocytes prevents atherosclerosis by skewing the immune response toward an antiinflammatory profile.* Journal of Experimental Medicine, 2010. **207**(2): p. 391-404, doi: https://doi.org/10.1084/jem.20091293.
124. Zarzycka, B., et al., *Discovery of Small Molecule CD40–TRAF6 Inhibitors.* Journal of Chemical Information and Modeling, 2015. **55**(2): p. 294-307, doi: https://doi.org/10.1021/ci500631e.
125. Seijkens, T.T.P., et al., *Targeting CD40-Induced TRAF6 Signaling in Macrophages Reduces Atherosclerosis.* Journal of the American College of Cardiology, 2018. **71**(5): p. 527-542, doi: https://doi.org/10.1016/j.jacc.2017.11.055.
126. Lameijer, M., et al., *Efficacy and safety assessment of a TRAF6-targeted nanoimmunotherapy in atherosclerotic mice and non-human primates.* Nature Biomedical Engineering, 2018. **2**(5): p. 279-292, doi: https://doi.org/10.1038/s41551-018-0221-2.
127. Bosch, L., et al., *Small molecule-mediated inhibition of CD40-TRAF6 reduces adverse cardiac remodelling in pressure overload induced heart failure.* International Journal of Cardiology, 2019. **279**: p. 141-144, doi: https://doi.org/10.1016/j.ijcard.2018.12.076.
128. Kim, H., et al., *Mouse Cre-LoxP system: general principles to determine tissue-specific roles of target genes.* lar, 2018. **34**(4): p. 147-159, doi: https://doi.org/10.5625/lar.2018.34.4.147.
129. Muessig, J.M., et al., *A Model of Blood Component–Heart Interaction in Cardiac Ischemia–Reperfusion Injury using a Langendorff-Based Ex Vivo Assay.* Journal of Cardiovascular

Pharmacology and Therapeutics, 2020. **25**(2): p. 164-173, doi: https://doi.org/10.1177/1074248419874348.
130. Taniuchi, I., *CD4 Helper and CD8 Cytotoxic T Cell Differentiation.* Annual Review of Immunology, 2018. **36**(1): p. 579-601, doi: https://doi.org/10.1146/annurev-immunol-042617-053411.
131. Simões, F.C. and P.R. Riley, *Immune cells in cardiac repair and regeneration.* Development, 2022. **149**(8): p. dev199906, doi: https://doi.org/10.1242/dev.199906.
132. Nahrendorf, M., et al., *The healing myocardium sequentially mobilizes two monocyte subsets with divergent and complementary functions.* Journal of Experimental Medicine, 2007. **204**(12): p. 3037-3047, doi: https://doi.org/10.1084/jem.20070885.
133. Swirski, F.K. and M. Nahrendorf, *Cardioimmunology: the immune system in cardiac homeostasis and disease.* Nature Reviews Immunology, 2018. **18**(12): p. 733-744, doi: https://doi.org/10.1038/s41577-018-0065-8.
134. Rusinkevich, V., et al., *Temporal dynamics of immune response following prolonged myocardial ischemia/reperfusion with and without cyclosporine A.* Acta Pharmacologica Sinica, 2019. **40**(9): p. 1168-1183, doi: https://doi.org/10.1038/s41401-018-0197-1.
135. Yang, F., et al., *Myocardial Infarction and Cardiac Remodelling in Mice.* Experimental Physiology, 2002. **87**(5): p. 547-555, doi: https://doi.org/10.1113/eph8702385.
136. Lancellotti, P., et al., *The use of echocardiography in acute cardiovascular care: Recommendations of the European Association of Cardiovascular Imaging and the Acute Cardiovascular Care Association.* European Heart Journal. Acute Cardiovascular Care, 2014, doi: https://doi.org/10.1177/2048872614568073.
137. Gao, X.-M., et al., *Serial echocardiographic assessment of left ventricular dimensions and function after myocardial infarction in mice.* Cardiovascular Research, 2000. **45**(2): p. 330-338, doi: https://doi.org/10.1016/S0008-6363(99)00274-6.
138. Peters, A.L., L.L. Stunz, and G.A. Bishop, *CD40 and autoimmunity: The dark side of a great activator.* Seminars in Immunology, 2009. **21**(5): p. 293-300, doi: https://doi.org/10.1016/j.smim.2009.05.012.
139. Zhang, B., et al., *The CD40/CD40L system: A new therapeutic target for disease.* Immunology Letters, 2013. **153**(1): p. 58-61, doi: https://doi.org/10.1016/j.imlet.2013.07.005.
140. Daub, S., et al. *CD40/CD40L and Related Signaling Pathways in Cardiovascular Health and Disease—The Pros and Cons for Cardioprotection*. International Journal of Molecular Sciences, 2020. **21**, DOI: https://doi.org/10.3390/ijms21228533.
141. Lutgens, E., et al., *CD40 and Its Ligand in Atherosclerosis.* Trends in Cardiovascular Medicine, 2007. **17**(4): p. 118-123, doi: https://doi.org/10.1016/j.tcm.2007.02.004.
142. Shami, A., et al., *CD40 levels in plasma are associated with cardiovascular disease and in carotid plaques with a vulnerable plaque phenotype and remodelling.* European Heart Journal, 2020. **41**(Supplement_2): p. ehaa946.3782, doi: https://doi.org/10.1093/ehjci/ehaa946.3782.
143. Verma, S., et al., *The relationship between soluble CD40 ligand levels and Framingham coronary heart disease risk score in healthy volunteers.* Atherosclerosis, 2005. **182**(2): p. 361-365, doi: https://doi.org/10.1016/j.atherosclerosis.2005.02.019.
144. Gergei, I., et al., *Association of soluble CD40L with short-term and long-term cardiovascular and all-cause mortality: The Ludwigshafen Risk and Cardiovascular Health (LURIC) study.* Atherosclerosis, 2019. **291**: p. 127-131, doi: https://doi.org/10.1016/j.atherosclerosis.2019.09.004.
145. Duncan, S.E., et al., *Macrophage Activities in Myocardial Infarction and Heart Failure.* Cardiology Research and Practice, 2020. **2020**: p. 4375127, doi: https://doi.org/10.1155/2020/4375127.
146. Jin, K., et al., *Single-Cell RNA Sequencing Reveals the Temporal Diversity and Dynamics of Cardiac Immunity after Myocardial Infarction.* Small Methods, 2022. **6**(3): p. 2100752, doi: https://doi.org/10.1002/smtd.202100752.

147. Zhuang, L., et al., *Global Characteristics and Dynamics of Single Immune Cells After Myocardial Infarction.* Journal of the American Heart Association, 2022. **11**(24): p. e027228, doi: https://doi.org/10.1161/JAHA.122.027228.
148. Ma, Y., A.J. Mouton, and M.L. Lindsey, *Cardiac macrophage biology in the steady-state heart, the aging heart, and following myocardial infarction.* Translational Research, 2018. **191**: p. 15-28, doi: https://doi.org/10.1016/j.trsl.2017.10.001.
149. Bell, R.M., M.M. Mocanu, and D.M. Yellon, *Retrograde heart perfusion: The Langendorff technique of isolated heart perfusion.* Journal of Molecular and Cellular Cardiology, 2011. **50**(6): p. 940-950, doi: https://doi.org/10.1016/j.yjmcc.2011.02.018.
150. Sutherland, F.J. and D.J. Hearse, *THE ISOLATED BLOOD AND PERFUSION FLUID PERFUSED HEART.* Pharmacological Research, 2000. **41**(6): p. 613-627, doi: https://doi.org/10.1006/phrs.1999.0653.
151. Sutton, M.G.S.J. and N. Sharpe, *Left Ventricular Remodeling After Myocardial Infarction.* Circulation, 2000. **101**(25): p. 2981-2988, doi: https://doi.org/10.1161/01.CIR.101.25.2981.
152. Li, T., et al., *Cardiac repair after myocardial infarction: A two-sided role of inflammation-mediated.* Frontiers in Cardiovascular Medicine, 2023. **9**, doi: https://doi.org/10.3389/fcvm.2022.1077290.
153. Fishbein, M.C., et al., *Early phase acute myocardial infarct size quantification: Validation of the triphenyl tetrazolium chloride tissue enzyme staining technique.* American Heart Journal, 1981. **101**(5): p. 593-600, doi: https://doi.org/10.1016/0002-8703(81)90226-X.
154. Klein, H.H., et al., *The mechanism of the tetrazolium reaction in identifying experimental myocardial infarction.* Virchows Archiv A, 1981. **393**(3): p. 287-297, doi: https://doi.org/10.1007/BF00430828.
155. Saxena, A., I. Russo, and N.G. Frangogiannis, *Inflammation as a therapeutic target in myocardial infarction: learning from past failures to meet future challenges.* Translational Research, 2016. **167**(1): p. 152-166, doi: https://doi.org/10.1016/j.trsl.2015.07.002.
156. Huang, S. and N.G. Frangogiannis, *Anti-inflammatory therapies in myocardial infarction: failures, hopes and challenges.* British Journal of Pharmacology, 2018. **175**(9): p. 1377-1400, doi: https://doi.org/10.1111/bph.14155.
157. DeBerge, M., et al., *Monocytes prime autoreactive T cells after myocardial infarction.* American Journal of Physiology-Heart and Circulatory Physiology, 2019. **318**(1): p. H116-H123, doi: https://doi.org/10.1152/ajpheart.00595.2019.
158. Zhuang, R., et al., *CD4+ FoxP3+ CD73+ regulatory T cell promotes cardiac healing post-myocardial infarction.* Theranostics, 2022. **12**(6): p. 2707-2721, doi: https://doi.org/10.7150/thno.68437.
159. Kubota, A., et al., *Inhibition of Interleukin-21 prolongs the survival through the promotion of wound healing after myocardial infarction.* Journal of Molecular and Cellular Cardiology, 2021. **159**: p. 48-61, doi: https://doi.org/10.1016/j.yjmcc.2021.06.006.
160. Boidin, M., et al., *Dynamic changes of monocytes subsets predict major adverse cardiovascular events and left ventricular function after STEMI.* Scientific Reports, 2023. **13**(1): p. 48, doi: https://doi.org/10.1038/s41598-022-26688-9.
161. Zhang, R.Y.K., et al., *Impact of Reperfusion on Temporal Immune Cell Dynamics After Myocardial Infarction.* Journal of the American Heart Association, 2023. **12**(4): p. e027600, doi: https://doi.org/10.1161/JAHA.122.027600.
162. Hess, A., et al., *Molecular imaging-guided repair after acute myocardial infarction by targeting the chemokine receptor CXCR4.* European Heart Journal, 2020. **41**(37): p. 3564-3575, doi: https://doi.org/10.1093/eurheartj/ehaa598.
163. Nicin, L., et al., *Fibroblast-mediated intercellular crosstalk in the healthy and diseased heart.* FEBS Letters, 2022. **596**(5): p. 638-654, doi: https://doi.org/10.1002/1873-3468.14234.
164. Daseke, M.J., et al., *Cardiac fibroblast activation during myocardial infarction wound healing: Fibroblast polarization after MI.* Matrix Biology, 2020. **91-92**: p. 109-116, doi: https://doi.org/10.1016/j.matbio.2020.03.010.

165. Le Bras, A., *Dynamics of fibroblast activation in the infarcted heart.* Nature Reviews Cardiology, 2018. **15**(7): p. 379-379, doi: https://doi.org/10.1038/s41569-018-0025-9.
166. Fries, K.M., et al., *CD40 Expression by human fibroblasts.* Clinical Immunology and Immunopathology, 1995. **77**(1): p. 42-51, doi: https://doi.org/10.1016/0090-1229(95)90135-3.
167. Olenchock, B.A., et al., *Lack of association between soluble CD40L and risk in a large cohort of patients with acute coronary syndrome in OPUS TIMI-16.* Journal of Thrombosis and Thrombolysis, 2008. **26**(2): p. 79-84, doi: https://doi.org/10.1007/s11239-007-0156-z.
168. Morrow, D.A., et al., *Concurrent evaluation of novel cardiac biomarkers in acute coronary syndrome: myeloperoxidase and soluble CD40 ligand and the risk of recurrent ischaemic events in TACTICS-TIMI 18.* European Heart Journal, 2008. **29**(9): p. 1096-1102, doi: https://doi.org/10.1093/eurheartj/ehn071.
169. Jinchuan, Y., et al., *Upregulation of CD40–CD40 ligand system in patients with diabetes mellitus.* Clinica Chimica Acta, 2004. **339**(1): p. 85-90, doi: https://doi.org/10.1016/j.cccn.2003.09.007.
170. Seijkens, T., et al., *CD40–CD40L: Linking pancreatic, adipose tissue and vascular inflammation in type 2 diabetes and its complications.* Diabetes and Vascular Disease Research, 2012. **10**(2): p. 115-122, doi: https://doi.org/10.1177/1479164112455817.
171. Rawshani, A., et al., *Risk Factors, Mortality, and Cardiovascular Outcomes in Patients with Type 2 Diabetes.* New England Journal of Medicine, 2018. **379**(7): p. 633-644, doi: https://doi.org/10.1056/NEJMoa1800256.
172. Murcia, A.M., et al., *Impact of Diabetes on Mortality in Patients With Myocardial Infarction and Left Ventricular Dysfunction.* Archives of Internal Medicine, 2004. **164**(20): p. 2273-2279, doi: https://doi.org/10.1001/archinte.164.20.2273.
173. Mauri, C., L.T. Mars, and M. Londei, *Therapeutic activity of agonistic monoclonal antibodies against CD40 in a chronic autoimmune inflammatory process.* Nature Medicine, 2000. **6**(6): p. 673-679, doi: https://doi.org/10.1038/76251.
174. Puliaev, R., et al., *CTL-Promoting Effects of CD40 Stimulation Outweigh B Cell-Stimulatory Effects Resulting in B Cell Elimination and Disease Improvement in a Murine Model of Lupus1.* The Journal of Immunology, 2008. **181**(1): p. 47-61, doi: https://doi.org/10.4049/jimmunol.181.1.47.
175. Salomon, R. and R. Dahan, *Next Generation CD40 Agonistic Antibodies for Cancer Immunotherapy.* Frontiers in Immunology, 2022. **13**, doi: https://doi.org/10.3389/fimmu.2022.940674.
176. Ingoglia, G., et al., *Line-selective macrophage activation with an anti-CD40 antibody drives a hemophagocytic syndrome in mice.* Blood Advances, 2020. **4**(12): p. 2751-2761, doi: https://doi.org/10.1182/bloodadvances.2020001624.
177. Gail, D.S., et al., *Differential phenotypes of memory CD4 and CD8 T cells in the spleen and peripheral tissues following immunostimulatory therapy.* Journal for ImmunoTherapy of Cancer, 2017. **5**(1): p. 33, doi: https://doi.org/10.1186/s40425-017-0235-4.
178. Hofmann, U., et al., *Activation of CD4+ T Lymphocytes Improves Wound Healing and Survival After Experimental Myocardial Infarction in Mice.* Circulation, 2012. **125**(13): p. 1652-1663, doi: https://doi.org/10.1161/CIRCULATIONAHA.111.044164.
179. Santos-Zas, I., et al., *Cytotoxic CD8+ T cells promote granzyme B-dependent adverse post-ischemic cardiac remodeling.* Nature Communications, 2021. **12**(1): p. 1483, doi: https://doi.org/10.1038/s41467-021-21737-9.
180. Tang, T.-T., et al., *Regulatory T cells ameliorate cardiac remodeling after myocardial infarction.* Basic Research in Cardiology, 2011. **107**(1): p. 232, doi: https://doi.org/10.1007/s00395-011-0232-6.
181. Steven, S., et al., *CD40L controls obesity-associated vascular inflammation, oxidative stress, and endothelial dysfunction in high fat diet-treated and db/db mice.* Cardiovascular Research, 2018. **114**(2): p. 312-323, doi: https://doi.org/10.1093/cvr/cvx197.

182. Puga, I., et al., *B cell–helper neutrophils stimulate the diversification and production of immunoglobulin in the marginal zone of the spleen.* Nature Immunology, 2012. **13**(2): p. 170-180, doi: https://doi.org/10.1038/ni.2194.
183. García-Rivas, G., et al., *The role of B cells in heart failure and implications for future immunomodulatory treatment strategies.* ESC Heart Failure, 2020. **7**(4): p. 1387-1399, doi: https://doi.org/10.1002/ehf2.12744.
184. Henn, V., et al., *CD40 ligand on activated platelets triggers an inflammatory reaction of endothelial cells.* Nature, 1998. **391**(6667): p. 591-594, doi: https://doi.org/10.1038/35393.
185. Elzey, B.D., et al., *Platelet-Mediated Modulation of Adaptive Immunity: A Communication Link between Innate and Adaptive Immune Compartments.* Immunity, 2003. **19**(1): p. 9-19, doi: https://doi.org/10.1016/S1074-7613(03)00177-8.
186. Henn, V., et al., *The inflammatory action of CD40 ligand (CD154) expressed on activated human platelets is temporally limited by coexpressed CD40.* Blood, 2001. **98**(4): p. 1047-1054, doi: https://doi.org/10.1182/blood.V98.4.1047.
187. Furman, M.I., et al., *Release of soluble CD40L from platelets is regulated by glycoprotein IIb/IIIa and actin polymerization.* Journal of the American College of Cardiology, 2004. **43**(12): p. 2319-2325, doi: https://doi.org/10.1016/j.jacc.2003.12.055.
188. Cognasse, F., et al., *Platelets as Key Factors in Inflammation: Focus on CD40L/CD40.* Frontiers in Immunology, 2022. **13**, doi: https://doi.org/10.3389/fimmu.2022.825892.
189. Napoleão, P., et al., *Changes of soluble CD40 ligand in the progression of acute myocardial infarction associate to endothelial nitric oxide synthase polymorphisms and vascular endothelial growth factor but not to platelet CD62P expression.* Translational Research, 2015. **166**(6): p. 650-659, doi: https://doi.org/10.1016/j.trsl.2015.07.006.

7 Acknowledgements

For me as a child of the Ruhr area, writing this dissertation was comparable to a long shift underground. At first, I went down into the unknown, where some smaller but also heavy boulders had to be cleared away and a few paths led into nowhere. However, over and over again, new tunnels opened up that brought promising discoveries to light, the results and findings, which are documented in this doctoral thesis. Now that this shift has come to an end, I would like to take the opportunity to thank everyone who accompanied and supported me during my doctoral thesis, for their help and guidance to finish my PhD.

First and foremost, I would like to express my sincere gratitude to my supervisor Prof. Dr. Norbert Gerdes for his advice, continuous support and patience during my PhD study. I am especially thankful for sharing your widespread knowledge, experience and ideas with me and I will always remember our lively discussions.

I would also like to thank Jun.-Prof. Dr. Mathias Beller as mentor for his feedback during my PhD thesis and as reviewer.

My gratitude extends to the director of the clinic for cardiology, Univ.-Prof. Dr. med. Malte Kelm, for giving me the opportunity to undertake my studies at the cardiovascular research laboratory. Furthermore, I am thankful for the funding provided by the “SFB 1116” and for offering a great graduate school that helped me to improve as scientist.

A special thanks to all the members of the cardiovascular research lab for their support and guidance. In particular, I would like to highlight the persons, who have contributed to this thesis with their work and analyses. First, I would like to thank Dr. Grace Ampem for accompanying my progress and for her help regarding echocardiography and qPCR analyses. Pia Fiegenbaum und Stefanie Becher, I would like to thank for performing the surgeries and the latter also for teaching me the Langendorff method. Thanks should also go to Dr. Alexander Lang for his advices, ideas and troubleshooting, as well as for his assistance during the sequencing experiments. I would like to extend my thanks to Ashley-Jane Duplessis and Christin Elster for providing a new histological staining method, which was thankfully carried out by Chiara Wernet. Many thanks to Dr. Susanne Pfeiler for her expertise and helping hand with a lot of administrative tasks. I am extremely grateful that some members of the lab became friends over the years and I appreciate that you were always there for me as moral support and made the last years much more enjoyable.

Finally, but most importantly I would like to thank my friends and family for their encouragement, patience, motivation and emotional support. Biggest thanks and love go out to my mom and dad, my grandparents and my brother. This endeavor would not have been possible without you.

I want to end and thank all of you with the phrase that miners use to say before and after every shift to wish each other luck and success: “Glück auf!”

Eidesstattliche Versicherung

Ich versichere an Eides Statt, dass die Dissertation von mir selbstständig und ohne unzulässige fremde Hilfe unter Beachtung der „Grundsätze zur Sicherung guter wissenschaftlicher Praxis an der Heinrich-Heine-Universität Düsseldorf“ erstellt worden ist.

Die aufgeführten Versuche wurden selbständig durchgeführt. Mit Ausnahme der folgenden Versuche und Ergebnisse, welche von Dritten bzw. in Kooperation mit Dritten erstellt wurden:

- Die IR-Operationen wurden von Stefanie Becher und Pia Fiegenbaum durchgeführt.
- Die Aufnahmen und Analysen der Echokardiographie wurde in Zusammenarbeit mit Dr. Grace Ampem erstellt.
- Koordination, Durchführung und Analysen der Einzelzell-Sequenzierung wurden von Dr. Alexander Lang begleitet.
- Die histologischen Analysen zur Narbengröße mittels Phalloidin und WGA wurden unter meiner Betreuung von Chiara Wernet durchgeführt.

Diese Dissertation wurde weder in gleicher noch in ähnlicher Form in einem anderen Prüfungsverfahren vorgelegt. Außerdem erkläre ich, dass ich bisher noch keine weiteren akademischen Grade erworben oder zu erwerben versucht habe.

Düsseldorf, den 14.12.2023

_____

Unterschrift